REPUBLIC OF TURKEY
YILDIZ TECHNICAL UNIVERSITY
GRADUATE SCHOOL OF NATURAL AND APPLIED SCIENCES

MODELLING AND CONTROL OF AUTONOMOUS UNDERWATER VEHICLES (AUVs)

ALPER YALMAN

MSc. THESIS
DEPARTMENT OF MECHATRONICS ENGINEERING
PROGRAM OF MECHATRONICS ENGINEERING

ADVISOR
ASSOC. PROF. AYDIN YEŞİLDİREK

İSTANBUL, 2017

REPUBLIC OF TURKEY

YILDIZ TECHNICAL UNIVERSITY

GRADUATE SCHOOL OF NATURAL AND APPLIED SCIENCES

MODELLING AND CONTROL OF AUTONOMOUS UNDERWATER VEHICLES (AUVs)

A thesis submitted by Alper YALMAN in partial fulfillment of the requirements for the degree of **MASTER OF SCIENCE** is approved by the committee on 14.06.2017 in Department of Mechatronics Engineering, Mechatronics Engineering Program.

Thesis Advisor

Assoc. Prof. Aydın YEŞİLDİREK

Yıldız Technical University

Approved By the Examining Committee

Assoc. Prof. Aydın YEŞİLDİREK

Yıldız Technical University

Asst. Prof. M. Selçuk ARSLAN

Yıldız Technical University

Assoc. Prof. H. Fatih UĞURDAĞ

Özyeğin University

ACKNOWLEDGEMENTS

I express my sincere gratitude to my thesis advisor Assoc. Prof. Aydın YEŞİLDİREK for his guidance, support, endless patience and immense knowledge throughout my thesis work. I am grateful for having the chance to work under his valuable supervision.

Besides my advisor, I would like to thank the rest of my thesis committee: Asst. Prof. M. Selçuk ARSLAN and Assoc. Prof. H. Fatih UĞURDAĞ, for their encouragement and insightful comments.

I am grateful to my young, innovative and talented colleagues in Servo and Stabilization Design Department in ASELSAN Inc. for their help and sincere friendship. I would like to thank to Mustafa Burak GÜRCAN, Evrim Onur ARI, Ercan ÇANDIR and Eyyüp SİNCAR for sharing their experience and supporting me through the tough times.

I would like to thank to my family for their continuous and unparalleled love, help and endless support. I am forever indebted to my parents for giving me the opportunities and experiences that have made me who I am.

Finally, special thanks goes to my fiancé, Özge, for providing me with unfailing support and continuous encouragement throughout my years of study and through the process of researching and writing this thesis. This accomplishment would not have been possible without her. Thank you my love.

June, 2017

Alper YALMAN

TABLE OF CONTENTS

Page

LIST OF SYMBOLS vi

LIST OF ABBREVIATIONS vii

LIST OF FIGURES viii

LIST OF TABLES ix

ABSTRACT x

ÖZET xi

CHAPTER 1

INTRODUCTION 1

1.1 Literature Review 1
1.2 Objective of the Thesis 8
1.3 Hypothesis 8

CHAPTER 2

MODELLING: KINEMATICS OF AUV 10

2.1 Kinematics of AUV 11
2.1.1 Linear Velocity Transformation 12
2.1.2 Angular Velocity Transformation 13

CHAPTER 3

MODELLING: DYNAMICS OF AUV 15

3.1 Rigid Body Dynamics 15
3.1.1 Translational Motion 17
3.1.2 Rotational Motion 17
3.1.3 6DOF Rigid Body Equations of Motion 19
3.2 External Forces and Moments 21
3.2.1 Hydrostatic Forces and Moments 21
3.2.2 Hydrodynamic Damping 23
3.2.3 Added Mass 24

3.2.4 Body Lift and Fin Lift 26
3.3 Total Forces and Moments 27
3.4 Equations of Motion 27

CHAPTER 4

DECOUPLED SURGE AND ROLL MOTION CONTROL 36

4.1 Forward Speed (Surge Speed) Control 37
4.1.1 Linearization of Forward Speed Dynamics and Proportional Control 37
4.1.2 Forward Speed Control Using Feedback Linearization 39
4.2 Roll Dynamics and Backstepping Control 41

CHAPTER 5

LONGITUDINAL DYNAMICS AND DEPTH CONTROL 46

5.1 Equations of Motion In Diving Plane 46
5.2 Depth Control Using Linearized Depth Plane Equations 47
5.2.1 Linearized Depth Plane Equations 48
5.2.2 Transfer Functions and Linear Controller Design 49
5.3 Nonlinear Switched Depth Control 53

CHAPTER 6

LATITUDINAL DYNAMICS AND HEADING CONTROL 59

6.1 Horizontal Plane Equations of Motion 59
6.2 Proportional Yaw Control Using Feedback Linearized Angular Velocity . 61
6.3 Single Input Multiple States (SIMS) Sliding Mode Control 63

CHAPTER 7

6-DOF SIMULATION WITH DECOUPLED CONTROLLERS 68

CHAPTER 8

CONCLUSION AND FUTURE WORK 73

REFERENCES 74

CURRICULUM VITAE 78

LIST OF SYMBOLS

x, y, z	x-y-z positions with respect to earth-fixed frame
ϕ, θ, ψ	Roll-pitch-yaw angles with respect to earth-fixed frame
u, v, w	Surge-sway-heave linear velocities with respect to body-fixed frame
p, q, r	Roll-pitch-yaw angular velocities with respect to body-fixed frame
$\boldsymbol{\eta}$	Position and attitude vector in earth-fixed frame
$\boldsymbol{\nu}$	Linear and angular velocity vector in body-fixed frame
m	Mass of the vehicle
W	Weight of the vehicle
B	Buoyancy force acting on the vehicle
I_x, I_y, I_z	Inertia values of the vehicle around x-y-z axes
∇	Total volume of the vehicle
g	Gravity
ρ_f	Seawater density
$\boldsymbol{r}_B$	Center of buoyancy vector with respect to body-fixed frame
$\boldsymbol{r}_G$	Center of gravity vector with respect to body-fixed frame
$\boldsymbol{C}_{x,\phi}$	Rotation matrix with angle ϕ about x-axis
X_u	Linear damping coefficient
$X_{u\|u\|}$	Quadratic damping coefficient
$X_{\dot{u}}$	Added mass coefficient
$\boldsymbol{\tau}_{HS}$	Hydrostatic forces and moments
$\boldsymbol{\tau}_A$	Added mass forces and moments
$\boldsymbol{\tau}_D$	Drag forces and moments
$\boldsymbol{\tau}_L$	Lift forces and moments
$\boldsymbol{\tau}_P$	Propulsion forces and moments
$\boldsymbol{M}_{RB}$	Rigid body inertia matrix
$\boldsymbol{M}_A$	Added mass inertia matrix
$\boldsymbol{C}_{RB}(\boldsymbol{\nu})$	Rigid body coriolis and centripetal matrix
$\boldsymbol{C}_{RB}(\boldsymbol{\nu})$	Added mass coriolis and centripetal matrix
$\boldsymbol{D}(\boldsymbol{\nu})$	Hydrodynamic damping matrix
$\boldsymbol{g}(\boldsymbol{\eta})$	Hydrostatic force and moment vector
δ_r	Rudder fin angle
δ_s	Stern fin angle

LIST OF ABBREVIATIONS

AUV	Autonomous Underwater Vehicle
CB	Center of buoyancy
CG	Center of gravity
DOF	Degree of freedom
PID	Proportional-Integral-Derivative
SIMS	Single Input Multiple States
SNAME	Society of Naval Architects and Marine Engineers
ROV	Remotely Operated Vehicle

LIST OF FIGURES

Page

Figure 1.1 The Epulard AUV by IFREMER 13
Figure 1.2 The HUGIN AUV 14
Figure 1.3 The ARIES AUV [7] 15
Figure 1.4 The Phoenix AUV [7] 15
Figure 1.5 The Odyssey IV 16
Figure 1.6 The Autonomous Benthic Explorer (ABE) 17
Figure 1.7 Pioneer REMUS-600 Autonomous Underwater Vehicle (AUV) 17
Figure 1.8 Nekton Research's miniature AUV prototype [8] 17
Figure 2.1 Earth-fixed and body-fixed coordinate frames 22
Figure 3.1 The inertial, earth-fixed non-rotating reference frame XYZ and the body-fixed rotating reference frame $X_0Y_0Z_0$. 27
Figure 3.2 REMUS AUV [25] 46
Figure 4.1 Forward speed step response and steady state error 49
Figure 4.2 Forward speed controller block diagram 51
Figure 4.3 Forward speed step response and steady state error 51
Figure 4.4 Roll motion control block diagram 55
Figure 4.5 Roll motion response to the initial condition $\phi_0 = 30°$ 55
Figure 5.1 Pitch angle open loop step response 61
Figure 5.2 Closed loop pitch control block diagram 62
Figure 5.3 Pitch angle closed loop step response 63
Figure 5.4 Closed loop depth control block diagram 63
Figure 5.5 Closed loop step response and stern fin angle ($z_d = 30$ m) 64
Figure 5.6 Nonlinear switched depth control step response, pitch angle and stern fin angle ($z_d = 30$ m) 68
Figure 5.7 Comparison between Linear and Nonlinear Depth Control of AUV 69
Figure 6.1 Cascaded heading position and velocity controllers 73
Figure 6.2 Angular velocity tracking response around z axis 73
Figure 6.3 Yaw position step response and rudder fin angle ($\psi_d = 30°$) 74
Figure 6.4 Heading Control System Block Diagram 76
Figure 6.5 SIMS yaw position control step response and corresponding rudder fin angle, ($\psi_d = 30°$) 76
Figure 6.6 Comparison between Cascaded and Sliding Mode Heading Control 77
Figure 7.1 6-DOF block diagram including decoupled controllers 79
Figure 7.2 Reference Values For Depth And Heading Angle 80
Figure 7.3 Roll position response in 6-DOF simulation 81
Figure 7.4 Heading angle response in 6-DOF simulation 81
Figure 7.5 Depth position response in 6-DOF simulation 82
Figure 7.6 6-DOF motion of AUV 82

LIST OF TABLES

Page

Table 2.1 Notation Used For Marine Vehicles 21
Table 3.1 Physical Parameters 44
Table 3.2 Added Mass Coefficients 45
Table 3.3 Hydrodynamic Damping Coefficients 45
Table 3.4 Control Fin Coefficients 45
Table 3.5 Body & Fin Lift and Moment Coefficients 46
Table 7.1 Selected Decoupled Controllers 80
Table 7.2 Reference Values For Depth And Heading Angle 80

ABSTRACT

MODELLING AND CONTROL OF AUTONOMOUS UNDERWATER VEHICLES (AUVs)

Alper YALMAN

Department of Mechatronics Engineering

MSc. Thesis

Adviser: Assoc. Prof. Aydın YEŞİLDİREK

The purpose of this study is to model a REMUS-like autonomous underwater vehicle (AUV) and control the vehicle in each decoupled subsystems. First, the kinematic equations are obtained using transformations between body and inertial reference frames and dynamic equations of motion are derived by considering the hydrostatics and hydrodynamics effects. After modelling, the equations of motion are decoupled and various controllers are applied in order to control forward speed, roll position/velocity, depth positon and yaw angle by using independent control variables. Proportional control and feedback linearization are used to reach the desired forward speed. In many applications, the roll states are generally neglected or used as constant but in this study the roll states are controlled by backstepping method to stabilize the roll motion. Sliding mode control, nonlinear switched control and cascaded PID control are applied in order to control the depth and heading of the AUV. Finally, the simulation results are demonstrated and future works are presented.

Key words: autonomous underwater vehicle, mathematical modelling, decoupled control, nonlinear control, cascaded control.

ÖZET

OTONOM SUALTI ARACININ MODELLENMESİ VE KONTROLÜ

Alper YALMAN

Mekatronik Mühendisliği Anabilim Dalı

Yüksek Lisans Tezi

Tez Danışmanı: Doç Dr. Aydın YEŞİLDİREK

Bu çalışmada REMUS benzeri sualtı araçlarının modellenmesi ve elde edilen model denkelmelerinin ayrıştırılarak birbirinden bağımsız şekilde kontrol edilmesi amaçlanmaktadır. İlk olarak ataletsel koordinat takımı ve gövde ekseni koordinat takımı arasındaki dönüşümlerden faydalanarak aracın kinematik denklemleri elde edilmektedir. Hidrostatik ve hidrodinamik etkiler göz önünde bulundurularak aracın dinamik modeli elde türetilmektedir. Modelleme tamamlandıktan sonra elde edilen denklemler farklı altsistemlere ayrıştırılarak hız, dönme, derinlik ve sapma açısı durumları için çeşitli kontrol yöntemlerinin uygulamaları yapılmaktadır. Aracın ileri yöndeki hız kontrolü için lineer oransal kontrol ve geribesleme ile doğrusallaştırma yöntremleri kullanılmıştır. Pek çok uygulamada aracın kendi ekseni etrafındaki dönme hareketi ihmal edilmekte veya sabit olarak kabul edilmektedir. Ancak bu çalışmada dönme hareketi için geri adımlama yöntemi ile kontrolcü tasarımı yapılmıştır. Aracın sapma açısı ve derinlik kontrolü için kayan kipli kontrol, kaskat PID kontrol, doğrusal olmayan anahtarlamalı kontrol gibi yöntemler kullnılmıştır. Son olarak simülasyon sonuçları gösterilmiş ve gelecekte hedeflenen çalışmalardan söz edilmiştir.

Anahtar Kelimeler: otonom sualtı aracı, matematiksel modelleme, ayrıştırılmış kontrol, doğrusal olmayan kontrol, kaskat kontrol.

CHAPTER 1

INTRODUCTION

1.1 Literature Review

About 70% of the Earth's surface is covered with water which is like an empire of natural resources. Underwater vehicles are developed so as to utilize these resources [1]. The possibility of submersible vehicles started quite a while back.

Robert Whitehead is believed to be the designer of the first Torpedo which is called Whitehead Automobile "Fish" Torpedo in Austria, 1866. Whitehead's first torpedo, which was driven by compressed air and carried an explosive charge, reached a speed of over 3 m/s and ran for 700 m. It may be thought the first AUV if one ignores the fact that it carried an explosive charge.

Applied Physics Laboratory of the University of Washington started development of what may have been first "true" AUV in the late 1950's since oceanographic data must be gathered along precise trajectories. The work led to the development and operation of The Self Propelled Underwater Research Vehicle(s) (SPURV). SPURV I was 480 kg, and could reach velocity at 2.2 m/s for 5.5 hours at depths to 3 km. The acoustically controlled vehicle could autonomously run at a constant depth. The vehicle was used to make CT measurements along isobaric lines in support of internal wave modeling [2] and it could track the dye plume 66 hours after the dye was released [3].

Epulard, which was designed in 1976 by IFREMER, was an acoustically controlled vehicle and it was the first 6 km rated AUV. The vehicle was capable to provide a constant depth above the bottom using a cable. Epulard achieved 300 dives between 1970 and 1990 [4].

Figure 1.1 The Epulard AUV by IFREMER

There are different sorts of underwater vehicles that can be classified into two categories called manned and unmanned systems. In manned system, there are military submarines and non-military submersibles managed for underwater explorations and appraisal. Unmanned submersibles can also be classified into various categories. The least complex and most effortlessly described are those submersibles that are towed behind a ship. They act as platforms for different sensor suites attached to the vehicle frame. Second type is a tethered vehicle which is called Remotely Operated Vehicle (ROV). ROVs have been utilized in the offshore industry since the late 1960s and are well established for underwater missions. However, they have limited use due to the constraints such as requirement for a tether to communicate and a control platform. Communication and power are supplied by the tether and the ROV is controlled directly by a remote operator. Third type is an Unmanned Untethered Vehicle (UUV). These vehicles have their own onboard power but are controlled by a remote operator via a communication link.

The requirement for autonomy in vehicles is increasingly becoming a significant subject in many environments and circumstances worldwide. One of the primary factor that makes the autonomous motion important is the lack of the ability to communicate between the vehicle and operator. Underwater is one of the environments in which

communication is very constrained. Autonomous underwater vehicles have a crucial role in discovery of underwater environment and allow people to find out unreachable depths.

Autonomous underwater vehicles (AUVs) have been developed for the underwater discovery in order to achieve the inadequacies of ROVs. An Autonomous Underwater Vehicle (AUV) is an untethered, autonomous undersea system that has its own power and controlled by an integrated computer while doing a pre-defined task [5] [6] [7].

In 1970s, the first AUVs were improved and put into commercial use in the 1990s. Today, they are generally used for scientific applications, military applications and research objectives [6]. The HUGIN series, which is considered as the most commercially successful AUV series on the today's world market, is developed in collaboration between the Norwegian Defense Research Establishment and Kongsberg [1]. AUVs are also widely used in the mining and oil industries [8]. Many countries have intensive AUV R&D programs which is an indication of the increasing significance of AUVs.

Figure 1.2 The HUGIN AUV

Bluefin Robotics is a company that was developed from the AUV laboratory at Massachusetts Institute of Technology (MIT) and is a world leader in underwater vehicle development. It started building AUVs in 1989 and its success in this area has led to the deployment of these vehicles all over the world [9].

The Naval Postgraduate School of California is an institute with its own AUV department and is currently going on intensive research in control, navigation, fault detection, computer simulations and different areas for AUVs. The department has two main AUVs as shown in Figure 1.3 and Figure 1.4. The ARIES is being utilized to test and improve navigation systems in underwater while the Phoenix is used as an underwater test vehicle for control studies [10].

Figure 1.3 The ARIES AUV [10]

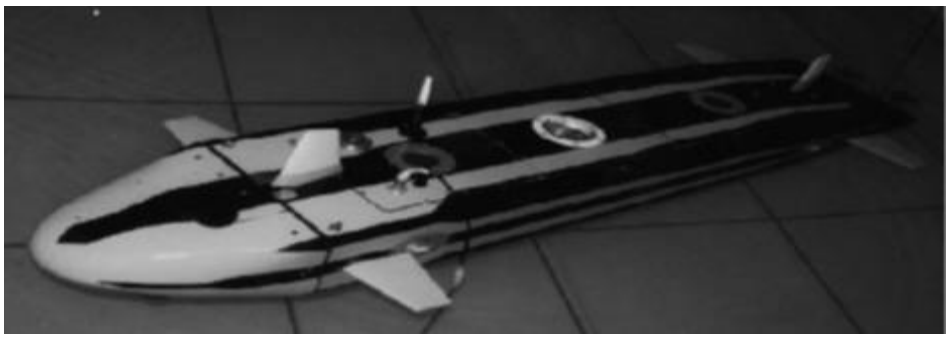

Figure 1.4 The Phoenix AUV [10]

The Defense Advanced Research Projects Agency of the United States began an AUV program in the late 1980s specifically oriented toward military applications. The vehicles

built by the agency are the largest and more versatile of any AUVs created anywhere else at present. They have been used in testing advanced submerged technologies and systems, and have proven instrumental in advancing developments in underwater vehicles worldwide.

There was an increasing interest in academic research about AUV's during the 90's. Six Odyssey vehicles were developed by the The Massachusetts Institute of Technology's Sea Grant AUV lab during the early 90's. These vehicles were 160 kg, had 1.5 m/s operating speed and were rated to 6 km. In 1994, Odyssey vehicles were operated under ice and to a depth of 1.4 km for 3 hours in the open ocean in 1995 [11].

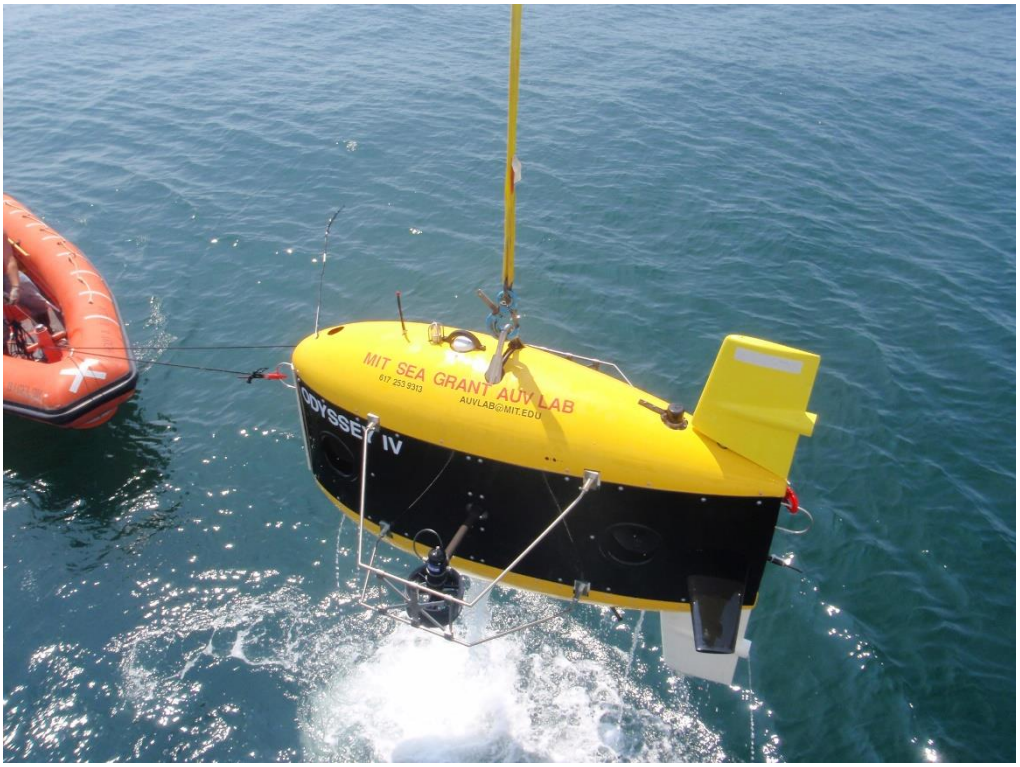

Figure 1.5 The Odyssey IV

Autonomous Benthic Explorer (ABE) was created by WHOI in early 90's. ABE accomplished its first scientific mission in 1994. ABE displaces 680 kg and has operating speed about 0.75 m/s. ABE is a highly maneuverable vehicle in since it has six thrusters. ABE has completed over 80 dives; one dive lasted for 30 hours at 2.2 km. Its deepest dive to date was to 4 km [12].

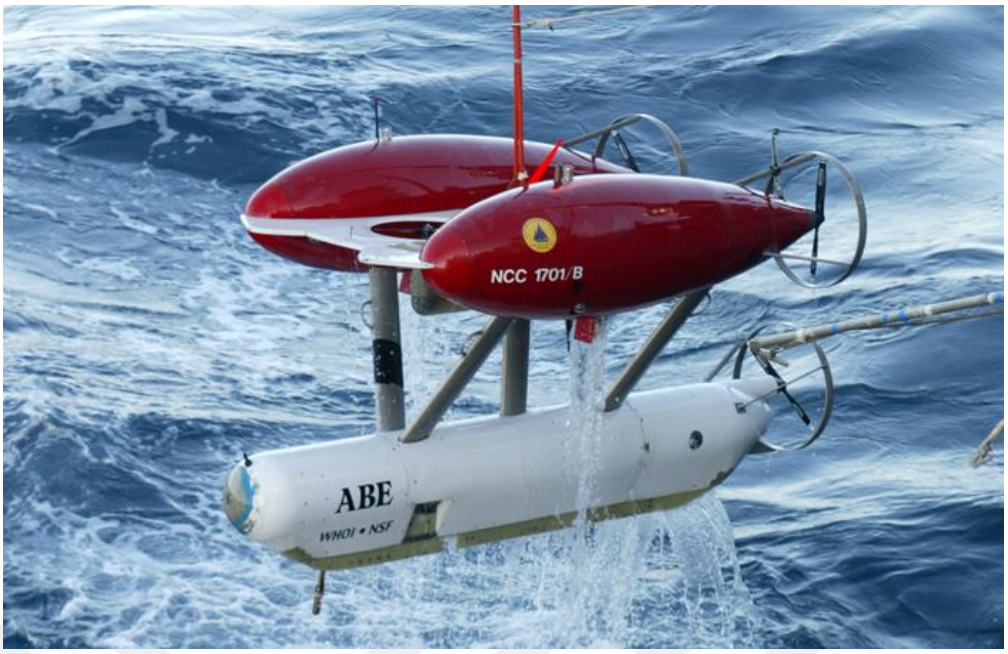

Figure 1.6 The Autonomous Benthic Explorer (ABE)

In the late 90's, REMUS AUV was developed by WHOI to contribute scientific studies at LEO-15 observatory in Tuckerton. The first mission was completed in 1967. The vehicle has operating velocity about 1.5 m/s and has ability to dive up to 100 m for 20 hours. Since there many REMUS vehicles in many different configurations, it is not possible to know how many missions have been performed by REMUS vehicles. However, it is known that the longest REMUS mission lasted 17 hours while traveling 60 km at 1.75 m/s at a maximum depth of 20 m off the coast of NJ at the LEO-15 observatory [13].

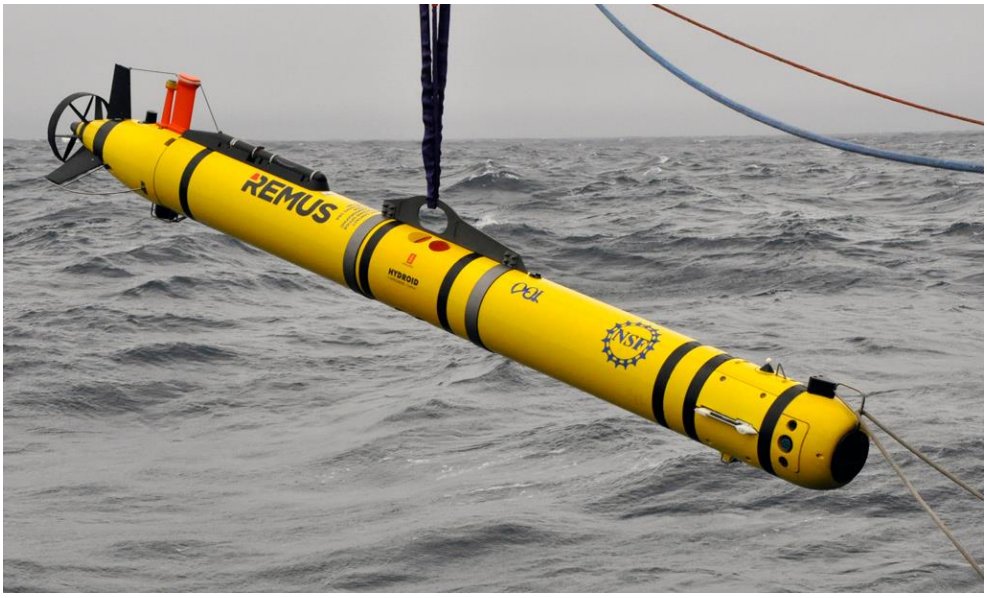

Figure 1.7 Pioneer REMUS-600 Autonomous Underwater Vehicle (AUV)

Presently, the difficulties for AUV address the navigation, communication, autonomy, and endurance issues. Being autonomous is the fundamental property of AUVs which is related to the electronics and control system design.

Numerous new submerged technologies are being investigated and applied to AUVs. For instance, hybrid underwater vehicles utilizing both ROV and AUV technologies are currently being used by The Monterey Bay Aquarium Research Institute of California. MIT is working on fish tail propulsion systems to use on their vehicles while institutes such as Nekton Research have been developing miniature AUVs (Figure 1.8) that can travel in groups, communicate with each other and provide researchers with simultaneous data over a large volume of water [14]. AUV research and technology is definitely on an upward curve.

Figure 1.8 Nekton Research's miniature AUV prototype [8]

The AUV basically utilizes an integrated computer system, power packs and vehicle payloads to perform the guidance, navigation and control objectives. They can be outfitted with various sensors to measure the environmental effects, or specialized biochemical payloads to identify underwater life when in motion. In many developments today, AUVs have been utilized in a semi-autonomous mode under human control that requires them to be tracked, observed, or even stopped through an objective in order to alter the mission plan. However, there have been successful developments at the achievement of autonomous operation [15].

After modelling and system identification, a control system can be designed for AUVs. An AUV may experience various maneuvering scenarios while performing any task especially in target tracking [16]. Different control methods are utilized for different operations. The vehicle speed is generally controller by thrusters attached to the vehicle aft. Pitch and depth controller is used to keep the AUV at a specific depth and heading angle of the vehicle is controlled using the different number of control surfaces on AUV. Roll motion is passively stabilized thanks to the mechanical properties of the vehicle or actively controlled with different kind of elements such as control surfaces, internal rotating mass and counter-rotating propellers. Control systems provide required commands to the controlled actuators in order to reach the desired position and/or velocity states for the vehicle. Controlling AUVs has many difficulties due to the effects of underwater environment. Thus, designing control systems for AUVs has been an extensive research area that include various techniques having been studied in the literature to provide autonomous motion [17],[18],[19],[20]. Current technology is focused on using intelligent and adaptive controllers to provide AUVs with outstanding control capabilities over ROVs.

1.2 Objective of the Thesis

The scope of thesis includes

- Kinematic and dynamic analysis of an AUV,
- Decoupled control systems design,
- Implementation of dynamic model and controllers in MATLAB/Simulink environment

In second and third chapters, the kinematic and dynamic equations of motion are derived. Chapter 4 discusses the decoupled controllers for the surge speed and roll motion of the AUV. In Chapter 5, decoupled equations for diving system are derived, linear and nonlinear controllers are applied and simulated. In Chapter 6, dynamic model for the horizontal plane is given and various control methods are applied in order to reach the desired heading angle. The last chapter discusses the results and suggests future work.

1.3 Hypothesis

In this study, the kinematic and dynamic model of the REMUS like AUVs are obtained and the dynamic model is implemented using MATLAB/Simulink. In addition to 6-DOF

model, the decoupled subsystems are separately implemented and design of controllers are performed using these decoupled equations. In the literature, the effect of roll motion is generally neglected. Contrary to the studies in the literature, the effect of roll motion is included here and roll controller is designed in order to stabilize the vehicle around *x-axis*. Outputs of this study will be implemented and tested on TORK system, an anti-torpedo torpedo system developed by ASELSAN Inc., Turkey.

CHAPTER 2

MODELLING: KINEMATICS OF AUV

In this section, the 6 degrees of freedom (DOF) motion of AUV is presented. In order to determine the position and orientation of a rigid body, six independent coordinates are required. Linear motion which describes the position of the vehicle along *x*, *y* and *z* axes is defined in first three coordinates while the last three coordinates are used to define the rotational motion which describes the orientation of the vehicle [21].

In general, the six different motion components are given for marine vehicles as *surge, sway, heave, roll, pitch* and *yaw*. The SNAME (1950) notation is generally used to define these components as shown in Table 2.1 [22].

Table 2.1 Notation Used For Marine Vehicles

DOF	Forces and moments	Linear and angular velocities	Positions and Euler angles
Motion along *x*-direction (surge)	X	u	x
Motion along *y*-direction (sway)	Y	v	y
Motion along *z*-direction (heave)	Z	w	z
Rotation about *x*-axis (roll)	K	p	ϕ
Rotation about *y*-axis (pitch)	M	q	θ
Rotation about *z*-axis (yaw)	N	r	ψ

2.1 Kinematics of AUV

It is appropriate to define two coordinate frames as given in Figure 2.1 while studying the 6-DOF motion of AUVs [21].

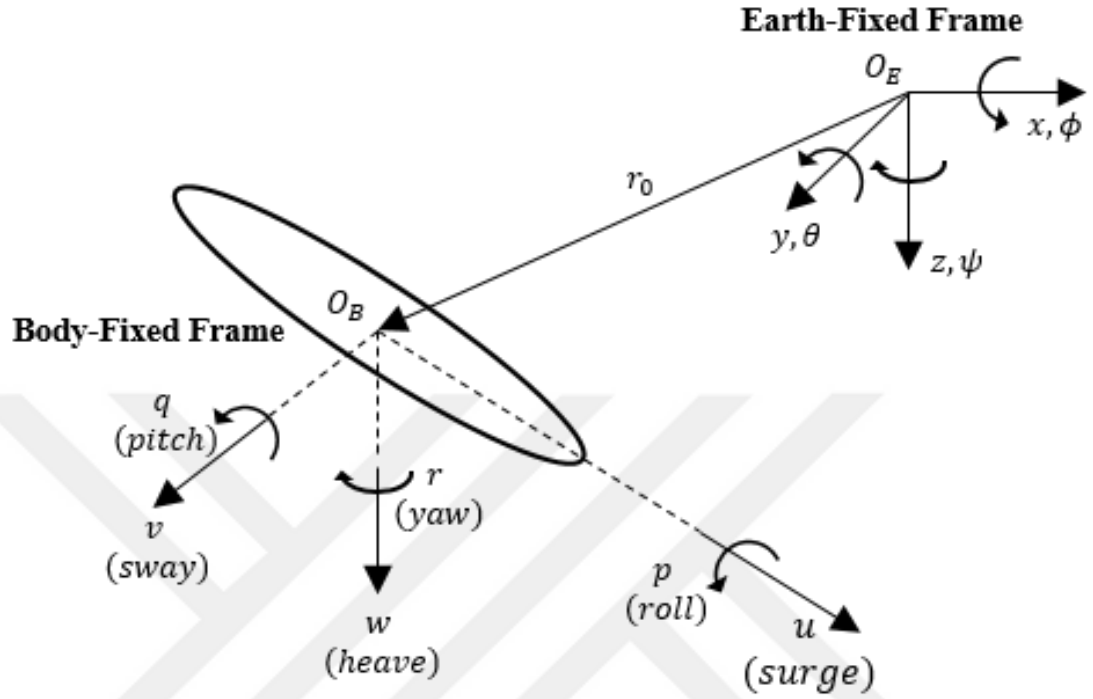

Figure 2.1 Earth-fixed and body-fixed coordinate frames

The moving coordinate frame $X_0Y_0Z_0$ is attached to the vehicle body and is called the body-fixed frame. The origin O_B of the body-fixed frame is mostly selected to make the dynamic equations simpler.

For underwater vehicles, the body axes X_0, Y_0 and Z_0 are defined as follows:

- X_0 – longitudinal axis (directed from aft to fore)
- Y_0 – transverse axis (directed to starboard)
- Z_0 – normal axis (directed from top to bottom)

The motion of the body-fixed frame is described relative to and inertial reference frame. It is assumed that the acceleration of a point on the surface of the Earth can be neglected and earth-fixed reference frame *XYZ* can be considered to be inertial. Based on SNAME notation given in Table 2.1, the general motion of the vehicle in 6 DOF can be described by:

$$\boldsymbol{\eta} = \begin{bmatrix} \boldsymbol{\eta}_1 \\ \boldsymbol{\eta}_2 \end{bmatrix}; \quad \boldsymbol{\eta}_1 = [x \quad y \quad z]^T; \qquad \boldsymbol{\eta}_2 = [\phi \quad \theta \quad \psi]^T$$

$$\boldsymbol{\nu} = \begin{bmatrix} \boldsymbol{\nu}_1 \\ \boldsymbol{\nu}_2 \end{bmatrix}; \quad \boldsymbol{\nu}_1 = [u \quad v \quad w]^T; \qquad \boldsymbol{\nu}_2 = [p \quad q \quad r]^T$$

$$\boldsymbol{\tau} = \begin{bmatrix} \boldsymbol{\tau}_1 \\ \boldsymbol{\tau}_2 \end{bmatrix}; \quad \boldsymbol{\tau}_1 = [X \quad Y \quad Z]^T; \qquad \boldsymbol{\tau}_2 = [K \quad M \quad N]^T$$

where

- $\boldsymbol{\eta}$: positions and orientations in earth-fixed frame
- $\boldsymbol{\nu}$: linear and angular velocities in body-fixed frame
- $\boldsymbol{\tau}$: forces and moments acting on the vehicle in body-fixed frame

The vehicle's velocity vector relative to the earth-fixed frame is expressed by the velocity transformation.

$$\dot{\boldsymbol{\eta}}_1 = \boldsymbol{J}_1(\boldsymbol{\eta}_2)\boldsymbol{\nu}_1 \tag{2.1}$$

where $\boldsymbol{J}_1(\boldsymbol{\eta}_2)$ is transformation matrix which is function of roll (ϕ), pitch (θ) and yaw (ψ) angles. In order to find the transformation matrix, three basic rotation matrices are defined for x, y and z axes.

$$\boldsymbol{C}_{x,\phi} = \begin{bmatrix} 1 & 0 & 0 \\ 0 & c\phi & s\phi \\ 0 & -s\phi & c\phi \end{bmatrix}; \quad \boldsymbol{C}_{y,\theta} = \begin{bmatrix} c\theta & 0 & -s\theta \\ 0 & 1 & 0 \\ s\theta & 0 & c\theta \end{bmatrix}; \quad \boldsymbol{C}_{z,\psi} = \begin{bmatrix} c\psi & s\psi & 0 \\ -s\psi & c\psi & 0 \\ 0 & 0 & 1 \end{bmatrix} \tag{2.2}$$

where $s\cdot = \sin(\cdot)$ and $c\cdot = \cos(\cdot)$. The notation $\boldsymbol{C}_{i,\alpha}$ represents a rotation angle α about the *i*-axis. All $\boldsymbol{C}_{i,\alpha}$ have the following properties:

- $\boldsymbol{C}$ is orthogonal.
- $\boldsymbol{C}\boldsymbol{C}^T = \boldsymbol{C}^T\boldsymbol{C} = \boldsymbol{I}$; $\det \boldsymbol{C} = \mathbf{1}$
- $\boldsymbol{C}^{-1} = \boldsymbol{C}^T$

2.1.1 Linear Velocity Transformation

Let $X_3Y_3Z_3$ be the coordinate system attained by translating the earth-fixed coordinate frame XYZ parallel to itself until its origin coincides with the origin of the body-fixed coordinate frame. Then, the following rotational operations are applied one by one [21].

- $X_3Y_3Z_3$ is rotated a *yaw* angle ψ about Z_3 axis and this yields the coordinate system $X_2Y_2Z_2$.

- $X_2Y_2Z_2$ is rotated a *pitch* angle θ about Y_2 axis and this yields the coordinate system $X_1Y_1Z_1$.
- $X_1Y_1Z_1$ is rotated a *roll* angle ϕ about X_1 axis and this yields the body coordinate system $X_0Y_0Z_0$.

$$\boldsymbol{J}_1(\boldsymbol{\eta}_2) = \boldsymbol{C}_{z,\psi}^T \boldsymbol{C}_{y,\theta}^T \boldsymbol{C}_{z,\phi}^T \tag{2.3}$$

The inverse transformation can also be written as:

$$\boldsymbol{J}_1^{-1}(\boldsymbol{\eta}_2) = \boldsymbol{J}_1^T(\boldsymbol{\eta}_2) = \boldsymbol{C}_{x,\phi} \boldsymbol{C}_{y,\theta} \boldsymbol{C}_{z,\psi} \tag{2.4}$$

Expanding expression (2.3) yields:

$$\boldsymbol{J}_1(\boldsymbol{\eta}_2) = \begin{bmatrix} c\psi c\theta & -s\psi c\phi + c\psi s\theta s\phi & s\psi s\phi + c\psi c\phi s\theta \\ s\psi c\theta & c\psi c\phi + s\phi s\theta s\psi & -c\psi s\phi + s\theta s\psi c\phi \\ -s\theta & c\theta s\phi & c\theta c\phi \end{bmatrix} \tag{2.5}$$

2.1.2 Angular Velocity Transformation

The body-fixed angular velocity vector and the Euler rate vector are related through a transformation matrix $\boldsymbol{J}_2(\boldsymbol{\eta}_2)$ according to:

$$\dot{\boldsymbol{\eta}}_2 = \boldsymbol{J}_2(\boldsymbol{\eta}_2)\boldsymbol{\nu}_2 \tag{2.6}$$

The angular body velocity vector $\boldsymbol{\nu}_2 = [p \quad q \quad r]^T$ cannot be integrated directly to obtain actual angular coordinates [23]. This is because $\int_o^t \boldsymbol{\nu}_2(\tau)d\tau$ does not have any physical meaning. However, the vector $\boldsymbol{\eta}_2 = [\phi \quad \theta \quad \psi]^{\boldsymbol{T}}$ will represent convenient generalized coordinates. The orientation of the body-fixed reference frame with respect to the inertial reference frame is given by:

$$\boldsymbol{\nu}_2 = \begin{bmatrix} \dot{\phi} \\ 0 \\ 0 \end{bmatrix} + \boldsymbol{C}_{x,\phi} \begin{bmatrix} 0 \\ \dot{\theta} \\ 0 \end{bmatrix} + \boldsymbol{C}_{x,\phi} \boldsymbol{C}_{y,\theta} \begin{bmatrix} 0 \\ 0 \\ \dot{\psi} \end{bmatrix} = \boldsymbol{J}_2^{-1}(\boldsymbol{\eta}_2)\dot{\boldsymbol{\eta}}_2 \tag{2.7}$$

Expanding (2.7) yields:

$$\boldsymbol{J}_2^{-1}(\boldsymbol{\eta}_2) = \begin{bmatrix} 1 & 0 & -s\theta \\ 0 & c\phi & c\theta s\phi \\ 0 & -s\phi & c\theta c\phi \end{bmatrix} \rightarrow \quad \boldsymbol{J}_2(\boldsymbol{\eta}_2) = \begin{bmatrix} 1 & s\phi t\theta & c\phi t\theta \\ 0 & c\phi & -s\phi \\ 0 & s\phi/c\theta & c\phi/c\theta \end{bmatrix} \tag{2.8}$$

where $s\cdot = \sin(\cdot)$, $c\cdot = \cos(\cdot)$ and $t\cdot = \tan(\cdot)$

It is seen from the (2.8) that $\boldsymbol{J}_2(\boldsymbol{\eta}_2)$ is undefined for $\theta = \pm 90°$ and $\boldsymbol{J}_2^{-1}(\boldsymbol{\eta}_2) \neq \boldsymbol{J}_2^T(\boldsymbol{\eta}_2)$.

Finally, the kinematic equations can be written in vector form as given below.

$$\begin{bmatrix} \dot{\boldsymbol{\eta}}_1 \\ \dot{\boldsymbol{\eta}}_2 \end{bmatrix} = \begin{bmatrix} \boldsymbol{J}_1(\boldsymbol{\eta}_2) & \mathbf{0}_{3x3} \\ \mathbf{0}_{3x3} & \boldsymbol{J}_2(\boldsymbol{\eta}_2) \end{bmatrix} \begin{bmatrix} \boldsymbol{\nu}_1 \\ \boldsymbol{\nu}_2 \end{bmatrix} \rightarrow \dot{\boldsymbol{\eta}} = \boldsymbol{J}(\boldsymbol{\eta})\boldsymbol{\nu} \tag{2.9}$$

CHAPTER 3

MODELLING: DYNAMICS OF AUV

3.1 Rigid Body Dynamics

In this section the rigid body equations of motion are derived using Newtonian Mechanics. When deriving the equations of motion the following assumption are made.

- The vehicle is rigid
- The earth-fixed reference frame is inertial

The 6 DOF nonlinear dynamic equations of motion can be expressed as:

$$\boldsymbol{M}_{RB}\dot{\boldsymbol{\nu}} + \boldsymbol{C}_{RB}(\boldsymbol{\nu})\boldsymbol{\nu} = \boldsymbol{\tau} \tag{3.1}$$

where

- $\boldsymbol{M}_{RB}$: Rigid body inertia matrix
- $\boldsymbol{C}_{RB}(\boldsymbol{\nu})$: Matrix of Coriolis and centripetal terms (including added mass)
- $\boldsymbol{\tau}$: Total external forces acting on the vehicle

The *Newton-Euler formulation* is based on *Newton's Second Law* which relates mass *m*, acceleration $\dot{\boldsymbol{v}}_C$ and force $\boldsymbol{f}_C$ according to:

$$m\dot{\boldsymbol{v}}_C = \boldsymbol{f}_C \tag{3.2}$$

Newton's Second Law is expressed in terms of conservation of linear momentum $\boldsymbol{p}_C$ and angular momentum $\boldsymbol{h}_C$ [24]**.** These results are known as *Euler's First and Second Axioms* as given below:

$$\dot{\boldsymbol{p}}_C \triangleq \boldsymbol{f}_C; \qquad \boldsymbol{p}_C \triangleq m\boldsymbol{v}_C; \tag{3.3}$$

$$\dot{\boldsymbol{h}}_C \triangleq \boldsymbol{m}_C; \qquad \boldsymbol{h}_C \triangleq \boldsymbol{I}_C\boldsymbol{\omega}; \tag{3.4}$$

where $\boldsymbol{f}_C$ and $\boldsymbol{m}_C$ are the forces and moments referred to the vehicle's center of gravity (CG), $\boldsymbol{\omega}$ is the angular velocity vector and $\boldsymbol{I}_C$ is the inertia tensor about the CG.

Let us consider a body-fixed coordinate system $X_0Y_0Z_0$ rotating with an angular velocity $\boldsymbol{\omega} = [\omega_1 \quad \omega_2 \quad \omega_3]^T$ about an earth-fixed coordinate system XYZ as shown in Figure 3.1.

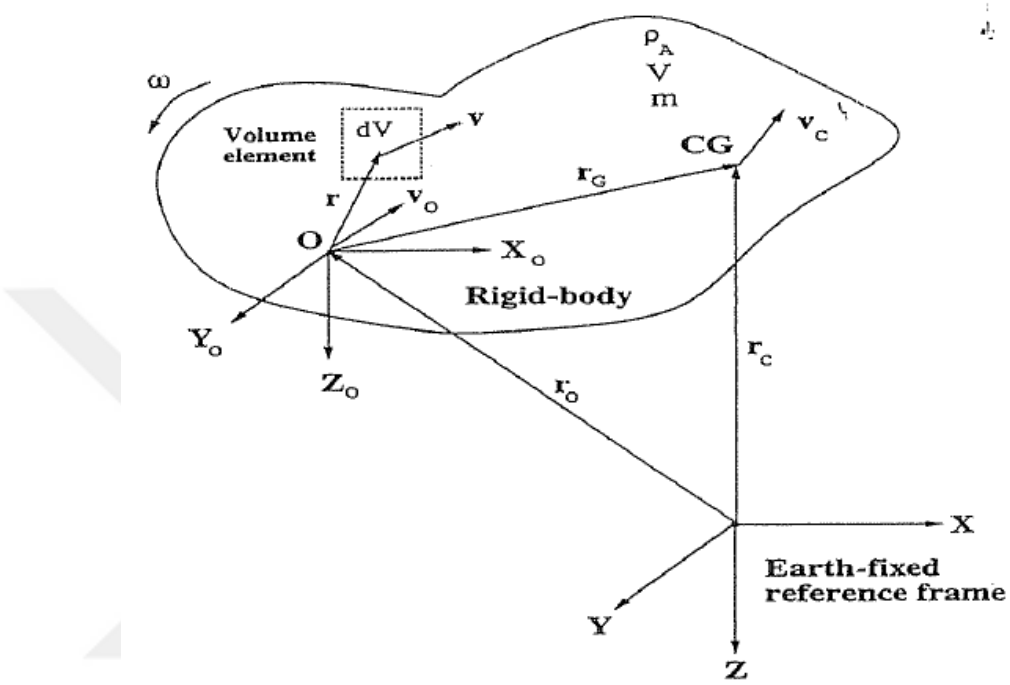

Figure 3.1 The inertial, earth-fixed non-rotating reference frame XYZ and the body-fixed rotating reference frame $X_0Y_0Z_0$ [21].

The inertia tensor $\boldsymbol{I}_0$ referred to an arbitrary body-fixed coordinate system $X_0Y_0Z_0$ with origin O in the body-fixed frame is defined as:

$$\boldsymbol{I}_0 \triangleq \begin{bmatrix} I_x & -I_{xy} & -I_{xz} \\ -I_{yx} & I_y & -I_{yz} \\ -I_{zx} & -I_{zy} & I_z \end{bmatrix};\ \boldsymbol{I}_0 = \boldsymbol{I}_0^T > 0 \tag{3.5}$$

The time derivatives of an arbitrary vector $\boldsymbol{c}$ in XYZ is given as:

$$\dot{\boldsymbol{c}} = \overset{o}{\boldsymbol{c}} + \boldsymbol{\omega} \times \boldsymbol{c} \tag{3.6}$$

Where $\dot{\boldsymbol{c}}$ is the time derivative in frame XYZ and $\overset{o}{\boldsymbol{c}}$ is the time derivative in the moving frame $X_0Y_0Z_0$. It is easily seen that the angular acceleration is equal in $X_0Y_0Z_0$ and XYZ by using (3.6) as:

$$\dot{\boldsymbol{\omega}} = \overset{o}{\boldsymbol{\omega}} + \boldsymbol{\omega} \times \boldsymbol{\omega} = \overset{o}{\boldsymbol{\omega}} \tag{3.7}$$

3.1.1 Translational Motion

From Figure 3.1 it can be written that:

$$\boldsymbol{r}_C = \boldsymbol{r}_O + \boldsymbol{r}_G \tag{3.8}$$

The velocity of the center of gravity is:

$$\boldsymbol{v}_C = \dot{\boldsymbol{r}}_C = \dot{\boldsymbol{r}}_O + \dot{\boldsymbol{r}}_G \tag{3.9}$$

The time derivative of $\boldsymbol{r}_G$ can be written as:

$$\dot{\boldsymbol{r}}_G = \overset{o}{\boldsymbol{r}}_G + \boldsymbol{\omega} \text{ x } \boldsymbol{r}_G \tag{3.10}$$

We can write $\boldsymbol{v}_0 = \dot{\boldsymbol{r}}_O$ and $\overset{o}{\boldsymbol{r}}_G = 0$ for a rigid body,

$$\boldsymbol{v}_C = \boldsymbol{v}_0 + \overset{o}{\boldsymbol{r}}_G + \boldsymbol{\omega} \text{ x } \boldsymbol{r}_G = \boldsymbol{v}_0 + \boldsymbol{\omega} \text{ x } \boldsymbol{r}_G \tag{3.11}$$

By taking the derivative of (3.11) the acceleration vector can be found as:

$$\dot{\boldsymbol{v}}_c = \dot{\boldsymbol{v}}_0 + \dot{\boldsymbol{\omega}} \text{ x } \boldsymbol{r}_G + \boldsymbol{\omega} \text{ x } \dot{\boldsymbol{r}}_G \tag{3.12}$$

Since $\dot{\boldsymbol{v}}_0 = \overset{o}{\boldsymbol{v}}_0 + \boldsymbol{\omega} \text{ x } \boldsymbol{v}_0$, $\dot{\boldsymbol{\omega}} = \overset{o}{\boldsymbol{\omega}}$ and $\dot{\boldsymbol{r}}_G = \boldsymbol{\omega} \text{ x } \boldsymbol{r}_G$ the (3.12) yields

$$\dot{\boldsymbol{v}}_c = \overset{o}{\boldsymbol{v}}_0 + \boldsymbol{\omega} \text{ x } \boldsymbol{v}_0 + \overset{o}{\boldsymbol{\omega}} \text{ x } \boldsymbol{r}_G + \boldsymbol{\omega} \text{ x } (\boldsymbol{\omega} \text{ x } \boldsymbol{r}_G) \tag{3.13}$$

Substituting (3.13) into (3.3) finally yields

$$m\left(\overset{o}{\boldsymbol{v}}_0 + \boldsymbol{\omega} \text{ x } \boldsymbol{v}_0 + \overset{o}{\boldsymbol{\omega}} \text{ x } \boldsymbol{r}_G + \boldsymbol{\omega} \text{ x } (\boldsymbol{\omega} \text{ x } \boldsymbol{r}_G)\right) = \boldsymbol{f}_0 \tag{3.14}$$

If the origin of the $X_0Y_0Z_0$ is chosen to coincide with the vehicle's center of gravity, $\boldsymbol{r}_G = [0 \quad 0 \quad 0]^T$, $\boldsymbol{f}_0 = \boldsymbol{f}_C$ and $\boldsymbol{v}_0 = \boldsymbol{v}_C$ yields:

$$m\left(\overset{o}{\boldsymbol{v}}_C + \boldsymbol{\omega} \text{ x } \boldsymbol{v}_C\right) = \boldsymbol{f}_C \tag{3.15}$$

3.1.2 Rotational Motion

The absolute angular momentum in [21] about O is defined as:

$$\boldsymbol{h}_0 \triangleq \int_V \boldsymbol{r} \text{ x } \boldsymbol{v}\, \rho_A dV \tag{3.16}$$

Differentiating (3.16) with respect to time yields:

$$\dot{\boldsymbol{h}}_0 = \int_V \boldsymbol{r} \text{ x } \dot{\boldsymbol{v}}\, \rho_A dV + \int_V \dot{\boldsymbol{r}} \text{ x } \boldsymbol{v}\, \rho_A dV \tag{3.17}$$

The first term on the right-hand side is the moment vector:

$$\boldsymbol{m}_0 \triangleq \int_V \boldsymbol{r} \times \dot{\boldsymbol{v}}\, \rho_A dV \tag{3.18}$$

From Figure 3.1 it is seen that:

$$\boldsymbol{v} = \dot{\boldsymbol{r}}_0 + \dot{\boldsymbol{r}} \;\rightarrow\; \dot{\boldsymbol{r}} = \boldsymbol{v} - \boldsymbol{v}_0 \tag{3.19}$$

Substituting (3.19) into (3.18) for $\dot{\boldsymbol{h}}_0$ and $\boldsymbol{v} \times \boldsymbol{v} = 0$,

$$\dot{\boldsymbol{h}}_0 = \boldsymbol{m}_0 + \int_V (\boldsymbol{v} - \boldsymbol{v}_0) \times \boldsymbol{v}\, \rho_A dV = \boldsymbol{m}_0 + \int_V \boldsymbol{v} \times \boldsymbol{v}\, \rho_A dV - \int_V \boldsymbol{v_0} \times \boldsymbol{v}\, \rho_A dV \tag{3.20}$$

$$\dot{\boldsymbol{h}}_0 = \boldsymbol{m}_0 - \boldsymbol{v}_0 \times \int_V \boldsymbol{v}\, \rho_A dV \tag{3.21}$$

or equivalently

$$\dot{\boldsymbol{h}}_0 = \boldsymbol{m}_0 - \boldsymbol{v}_0 \times \int_V (\boldsymbol{v}_0 + \dot{\boldsymbol{r}}) \rho_A dV = \boldsymbol{m}_0 - \boldsymbol{v}_0 \times \int_V \dot{\boldsymbol{r}}\, \rho_A dV \tag{3.22}$$

Expression (3.22) can be written by differentiating the vehicle's center of gravity which can be defines as:

$$\boldsymbol{r}_G = \frac{1}{m} \int_V \boldsymbol{r}\, \rho_A dV \tag{3.23}$$

Differentiating (3.23) yields

$$m\dot{\boldsymbol{r}}_G = \int_V \dot{\boldsymbol{r}}\, \rho_A dV \tag{3.24}$$

Since $\dot{\boldsymbol{r}}_G = \boldsymbol{\omega} \times \boldsymbol{r}_G$, (3.24) can be written as

$$\int_V \dot{\boldsymbol{r}}\, \rho_A dV = m(\boldsymbol{\omega} \times \boldsymbol{r}_G) \tag{3.25}$$

Substituting (3.25) into the (23.22) yields

$$\dot{\boldsymbol{h}}_0 = \boldsymbol{m}_0 - m\boldsymbol{v}_0 \times (\boldsymbol{\omega} \times \boldsymbol{r}_G) \tag{3.26}$$

The absolute angular momentum (3.16) is written as

$$\boldsymbol{h}_0 \triangleq \int_V \boldsymbol{r} \times \boldsymbol{v}\, \rho_A dV = \int_V \boldsymbol{r} \times \boldsymbol{v}_0\, \rho_A dV + \int_V \boldsymbol{r} \times (\boldsymbol{\omega} \times \boldsymbol{r})\, \rho_A dV \tag{3.27}$$

The first term on the right-hand side of (3.27) can be written by using (3.23).

$$\int_V \boldsymbol{r} \times \boldsymbol{v}_0 \, \rho_A dV = \left(\int_V \boldsymbol{r} \, \rho_A dV \right) \times \boldsymbol{v}_0 = m\boldsymbol{r}_G \times \boldsymbol{v}_0 \tag{3.28}$$

The second term in (3.27) is recognized as the definition of inertia tensor which can be written as

$$\boldsymbol{I}_0\boldsymbol{\omega} = \int_V \boldsymbol{r} \times (\boldsymbol{\omega} \times \boldsymbol{r}) \, \rho_A dV \tag{3.29}$$

Thus, the expression (3.27) reduces to:

$$\boldsymbol{h}_0 = \boldsymbol{I}_0\boldsymbol{\omega} + m\boldsymbol{r}_G \times \boldsymbol{v}_0 \tag{3.30}$$

Differentiating expression (3.30) assuming that $\boldsymbol{I}_0$ is constant with respect to time yields

$$\dot{\boldsymbol{h}}_0 = \boldsymbol{I}_0\overset{o}{\boldsymbol{\omega}} + \boldsymbol{\omega} \times (\boldsymbol{I}_0\boldsymbol{\omega}) + m(\boldsymbol{\omega} \times \boldsymbol{r}_G) \times \boldsymbol{v}_0 + m\boldsymbol{r}_G \times (\overset{o}{\boldsymbol{v}}_0 + \boldsymbol{\omega} \times \boldsymbol{v}_0) \tag{3.31}$$

Using the vector product property $(\boldsymbol{\omega} \times \boldsymbol{r}_G) \times \boldsymbol{v}_0 = -\boldsymbol{v}_0 \times (\boldsymbol{\omega} \times \boldsymbol{r}_G)$ and eliminating $\dot{\boldsymbol{h}}_0$ from (3.26) and (3.31) finally yields

$$\boldsymbol{I}_0\overset{o}{\boldsymbol{\omega}} + \boldsymbol{\omega} \times (\boldsymbol{I}_0\boldsymbol{\omega}) + m\boldsymbol{r}_G \times (\overset{o}{\boldsymbol{v}}_0 + \boldsymbol{\omega} \times \boldsymbol{v}_0) = \boldsymbol{m}_0 \tag{3.32}$$

If the origin O of the body-fixed $X_0Y_0Z_0$ is chosen to coincide with the vehicle's center of gravity, (3.32) is simplified to:

$$\boldsymbol{I}_C\overset{o}{\boldsymbol{\omega}} + \boldsymbol{\omega} \times (\boldsymbol{I}_C\boldsymbol{\omega}) = \boldsymbol{m}_C \tag{3.33}$$

3.1.3 6DOF Rigid Body Equations of Motion

Equations (3.14) and (3.32) are written in component according to SNAME (1950) notation as follows:

- $\boldsymbol{f}_0 = \boldsymbol{\tau}_1 = [X \quad Y \quad Z]^T$ external forces
- $\boldsymbol{m}_0 = \boldsymbol{\tau}_2 = [K \quad M \quad N]^T$ moments of external forces about O
- $\boldsymbol{v}_0 = \boldsymbol{\nu}_1 = [u \quad v \quad w]^T$ linear velocity of $X_0Y_0Z_0$
- $\boldsymbol{\omega} = \boldsymbol{\nu}_2 = [p \quad q \quad r]^T$ angular velocity of $X_0Y_0Z_0$
- $\boldsymbol{r}_G = [x_G \quad y_G \quad z_G]^T$ center of gravity

Applying the notation to equations (3.14) and (3.32) yields:

$$\begin{aligned}
m[\dot{u} - vr + wq - x_G(q^2 + r^2) + y_G(pq - \dot{r}) + z_G(pr + \dot{q})] &= X \\
m[\dot{v} - wp + ur - y_G(r^2 + p^2) + z_G(qr - \dot{p}) + x_G(qp + \dot{r})] &= Y \\
m[\dot{w} - uq + vp - z_G(p^2 + q^2) + x_G(rp - \dot{q}) + y_G(rq + \dot{p})] &= Z
\end{aligned} \tag{3.34}$$

$$I_x\dot{p} + (I_z - I_y)qr - (\dot{r} + pq)I_{xz} + (r^2 - q^2)I_{yz} + (pr - \dot{q})I_{xy} + m[y_G(\dot{w} - uq + vp) - z_G(\dot{v} - wp + ur)] = K$$

$$I_y\dot{q} + (I_x - I_z)rp - (\dot{p} + qr)I_{xy} + (p^2 - r^2)I_{zx} + (qp - \dot{r})I_{yz} + m[z_G(\dot{u} - vr + wq) - x_G(\dot{w} - uq + vp)] = M$$

$$I_z\dot{r} + (I_y - I_x)pq - (\dot{q} + rp)I_{yz} + (q^2 - p^2)I_{xy} + (rq - \dot{p})I_{zx} + m[x_G(\dot{v} - wp + ur) - y_G(\dot{u} - vr + wq)] = N$$

These equations can be written in vectorial form as:

$$\boldsymbol{M}_{RB}\dot{\boldsymbol{\nu}} + \boldsymbol{C}_{RB}(\boldsymbol{\nu})\boldsymbol{\nu} = \boldsymbol{\tau} \tag{3.35}$$

where $\boldsymbol{\nu} = [u \quad v \quad w \quad p \quad q \quad r]^T$ is the body-fixed linear and angular velocity vector and $\boldsymbol{\tau} = [X \quad Y \quad Z \quad K \quad M \quad N]^T$ is generalized vector of external forces and moments.

The rigid-body inertia matrix $\boldsymbol{M}_{RB}$ satisfies following properties:

- $\boldsymbol{M}_{RB} = \boldsymbol{M}_{RB}^T > 0$
- $\dot{\boldsymbol{M}}_{RB} = 0$

where

$$\boldsymbol{M}_{RB} = \begin{bmatrix} m\boldsymbol{I}_{3x3} & -m\boldsymbol{S}(\boldsymbol{r}_G) \\ m\boldsymbol{S}(\boldsymbol{r}_G) & \boldsymbol{I}_0 \end{bmatrix} = \begin{bmatrix} m & 0 & 0 & 0 & mz_G & -my_G \\ 0 & m & 0 & -mz_G & 0 & mx_G \\ 0 & 0 & m & my_G & -mx_G & 0 \\ 0 & -mz_G & my_G & I_x & -I_{xy} & -I_{xz} \\ mz_G & 0 & -mx_G & -I_{yx} & I_y & -I_{yz} \\ -my_G & mx_G & 0 & -I_{zx} & -I_{zy} & I_z \end{bmatrix} \tag{3.36}$$

$\boldsymbol{I}_{3x3}$ is the idendity matrix, $\boldsymbol{I}_0 = \boldsymbol{I}_0^T > 0$ is the inertia tensor with respect to O and $\boldsymbol{S}(\boldsymbol{r}_G)$ is skew-symmetric matrix which is generally defined as follows:

$$\boldsymbol{S}(\boldsymbol{\lambda}) = \begin{bmatrix} 0 & -\lambda_3 & \lambda_2 \\ \lambda_3 & 0 & -\lambda_1 \\ -\lambda_2 & \lambda_1 & 0 \end{bmatrix}; \quad \boldsymbol{\lambda} = [\lambda_1 \quad \lambda_2 \quad \lambda_3]^T \tag{3.37}$$

The 6x6 inertia matrix $\boldsymbol{M}_{RB}$ can be written as:

$$\boldsymbol{M}_{RB} = \begin{bmatrix} \boldsymbol{M}_{11} & \boldsymbol{M}_{12} \\ \boldsymbol{M}_{21} & \boldsymbol{M}_{22} \end{bmatrix} \tag{3.38}$$

The coriolis and centripetal matrix $\boldsymbol{C}_{RB}(\boldsymbol{\nu})$ is found by using inertia matrix.

$$\boldsymbol{C}_{RB}(\boldsymbol{\nu}) = \begin{bmatrix} \boldsymbol{0}_{3x3} & -\boldsymbol{S}(\boldsymbol{M}_{11}\boldsymbol{\nu}_1 + \boldsymbol{M}_{12}\boldsymbol{\nu}_2) \\ -\boldsymbol{S}(\boldsymbol{M}_{11}\boldsymbol{\nu}_1 + \boldsymbol{M}_{12}\boldsymbol{\nu}_2) & -\boldsymbol{S}(\boldsymbol{M}_{21}\boldsymbol{\nu}_1 + \boldsymbol{M}_{22}\boldsymbol{\nu}_2) \end{bmatrix} \tag{3.39}$$

Since the $\boldsymbol{M}_{ij}$ matrices are know from the (3.36), the coriolis and centripetal matrix $\boldsymbol{C}_{RB}(\boldsymbol{\nu})$ is found by expanding (3.39).

$$\boldsymbol{C}_{RB}(\boldsymbol{\nu}) = \begin{bmatrix} 0 & 0 & 0 \\ 0 & 0 & 0 \\ 0 & 0 & 0 \\ -m(y_G q + z_G r) & m(y_G p + w) & m(z_G p - v) \\ m(x_G q - w) & -m(z_G r + x_G p) & m(z_G q + u) \\ m(x_G r + v) & m(y_G r - u) & -m(x_G p + y_G q) \end{bmatrix}$$

$$\begin{bmatrix} m(y_G q + z_G r) & -m(x_G q - w) & -m(x_G r + v) \\ -m(y_G p + w) & m(z_G r + x_G p) & -m(y_G r - u) \\ -m(z_G p - v) & -m(z_G q + u) & m(x_G p + y_G q) \\ 0 & -I_{yz} q - I_{xz} p + I_z r & I_{yz} r + I_{xy} p - I_y q \\ I_{yz} q + I_{xz} p - I_z r & 0 & -I_{xz} r - I_{xy} q + I_x p \\ -I_{yz} r - I_{xy} p + I_y q & I_{xz} r + I_{xy} q - I_x p & 0 \end{bmatrix} \tag{3.40}$$

3.2 External Forces and Moments

It is assumed that environmental effects such as waves and water current are neglected and do not affect the motion of underwater vehicle. The total forces and moments acting on the vehicle can be written in terms of hydrostatics, hydrodynamics and actuator forces [25].

$$\boldsymbol{\tau} = \boldsymbol{\tau}_{HS} + \boldsymbol{\tau}_A + + \boldsymbol{\tau}_D + \boldsymbol{\tau}_L + \boldsymbol{\tau}_P \tag{3.41}$$

where

- $\boldsymbol{\tau}_{HS}$ **:** Hydrostatic forces and moments
- $\boldsymbol{\tau}_A$ **:** Added mass forces and moments
- $\boldsymbol{\tau}_D$ **:** Drag forces and moments
- $\boldsymbol{\tau}_L$ **:** Lift forces and moments
- $\boldsymbol{\tau}_P$ **:** Propulsion forces and moments

Following sections describes these forces and moments.

3.2.1 Hydrostatic Forces and Moments

The hydrostatic forces and moments are acting on the vehicle due to the effects of vehicle weight and buoyancy [21]. Let m be the mass of the vehicle and g is the acceleration of gravity, the weight of the vehicle is $W = m\mathrm{g}$. The buoyancy force is expressed as $B = \rho_f \nabla \mathrm{g}$, where the ρ_f is the fluid density and ∇ is the total volume of the vehicle.

The center of gravity is given in the previous sections as $\boldsymbol{r}_G = [x_G \quad y_G \quad z_G]^T$. Let the coordinates of center of buoyancy be $\boldsymbol{r}_B = [x_B \quad y_B \quad z_B]^T$. The gravitational force $\boldsymbol{f}_G$

will act through the $\boldsymbol{r}_G$ and the buoyancy force $\boldsymbol{f}_B$ will act through the $\boldsymbol{r}_B$. Gravitational and buoyancy forces can be expressed in body-fixed coordinate system using transformation matrices derived in kinematic analysis as given below:

$$\boldsymbol{f}_G(\boldsymbol{\eta}_2) = \boldsymbol{J}_1^{-1}(\boldsymbol{\eta}_2)\begin{bmatrix}0\\0\\W\end{bmatrix}; \qquad \boldsymbol{f}_B(\boldsymbol{\eta}_2) = \boldsymbol{J}_1^{-1}(\boldsymbol{\eta}_2)\begin{bmatrix}0\\0\\B\end{bmatrix}; \tag{3.42}$$

The hydrostatics forces and moments on the vehicle can be defined as:

$$\begin{aligned}\boldsymbol{F}_{HS} &= \boldsymbol{f}_G - \boldsymbol{f}_B\\ \boldsymbol{M}_{HS} &= \boldsymbol{r}_G \; x \; \boldsymbol{f}_G - \boldsymbol{r}_B \; x \; \boldsymbol{f}_B\end{aligned} \tag{3.43}$$

Equations in (3.43) are expanded to yield the nonlinear equations for hydrostatic forces and moments:

$$\begin{aligned}X_{HS} &= -(W-B)s\theta\\ Y_{HS} &= (W-B)c\theta s\phi\\ Z_{HS} &= (W-B)c\theta c\phi\\ K_{HS} &= (y_G W - y_B B)c\theta c\phi - (z_G W - z_B B)c\theta s\phi\\ M_{HS} &= -(z_G W - z_B B)s\theta - (x_G W - x_B B)c\theta c\phi\\ N_{HS} &= (x_G W - x_B B)c\theta s\phi + (y_G W - y_B B)s\theta\end{aligned} \tag{3.44}$$

Let us write the hydrostatic forces and moments in vector form:

$$\boldsymbol{\tau}_{HS} = -\boldsymbol{g}(\boldsymbol{\eta_2}) = \begin{bmatrix}\boldsymbol{F}_{HS}\\ \boldsymbol{M}_{HS}\end{bmatrix} = \begin{bmatrix}X_{HS}\\ Y_{HS}\\ Z_{HS}\\ K_{HS}\\ M_{HS}\\ N_{HS}\end{bmatrix}$$

$$\boldsymbol{g}(\boldsymbol{\eta_2}) = \begin{bmatrix}(W-B)s\theta\\ -(W-B)c\theta s\phi\\ -(W-B)c\theta c\phi\\ -(y_G W - y_B B)c\theta c\phi + (z_G W - z_B B)c\theta s\phi\\ (z_G W - z_B B)s\theta + (x_G W - x_B B)c\theta c\phi\\ -(x_G W - x_B B)c\theta s\phi - (y_G W - y_B B)s\theta\end{bmatrix} \tag{3.45}$$

3.2.2 Hydrodynamic Damping

Let use write hydrodynamic damping forces and moments $\boldsymbol{\tau}_D$ as:

$$\boldsymbol{\tau}_D = -\boldsymbol{D}(\boldsymbol{\nu})\boldsymbol{\nu}; \quad \boldsymbol{D}(\boldsymbol{\nu})\text{: Hydrodynamic damping matrix} \tag{3.46}$$

The hydrodynamic damping matrix $\boldsymbol{D}(\boldsymbol{\nu})$ will be real, non-symmetrical and strictly positive matrix. In general, higher order terms in damping matrix $\boldsymbol{D}(\boldsymbol{\nu})$ are neglected [26]. Thus, the damping matrix that includes linear and quadratic terms is written as:

$$\begin{aligned}\boldsymbol{D}(\boldsymbol{\nu}) = &-\begin{bmatrix} X_u & X_v & X_w & X_p & X_q & X_r \\ Y_u & Y_v & Y_w & Y_p & Y_q & Y_r \\ Z_u & Z_v & Z_w & Z_p & Z_q & Z_r \\ K_u & K_v & K_w & K_p & K_q & K_r \\ M_u & M_v & M_w & M_p & M_q & M_r \\ N_u & N_v & N_w & N_p & N_q & N_r \end{bmatrix} \\ &-\begin{bmatrix} X_{u|u|}|u| & X_{v|v|}|v| & X_{w|w|}|w| & X_{p|p|}|p| & X_{q|q|}|q| & X_{r|r|}|r| \\ Y_{u|u|}|u| & Y_{v|v|}|v| & Y_{w|w|}|w| & Y_{p|p|}|p| & Y_{q|q|}|q| & Y_{r|r|}|r| \\ Z_{u|u|}|u| & Z_{v|v|}|v| & Z_{w|w|}|w| & Z_{p|p|}|p| & Z_{q|q|}|q| & Z_{r|r|}|r| \\ K_{u|u|}|u| & K_{v|v|}|v| & K_{w|w|}|w| & K_{p|p|}|p| & K_{q|q|}|q| & K_{r|r|}|r| \\ M_{u|u|}|u| & M_{v|v|}|v| & M_{w|w|}|w| & M_{p|p|}|p| & M_{q|q|}|q| & M_{r|r|}|r| \\ N_{u|u|}|u| & N_{v|v|}|v| & N_{w|w|}|w| & N_{p|p|}|p| & N_{q|q|}|q| & N_{r|r|}|r| \end{bmatrix}\end{aligned} \tag{3.47}$$

Since the vehicle has *xy* and *xz* symmetry, the damping matrix in (3.47) is reduced to following expression:

$$\begin{aligned}\boldsymbol{D}(\boldsymbol{\nu}) = &-\begin{bmatrix} X_u & 0 & 0 & 0 & 0 & 0 \\ 0 & Y_v & 0 & 0 & 0 & Y_r \\ 0 & 0 & Z_w & 0 & Z_q & 0 \\ 0 & 0 & 0 & K_p & 0 & 0 \\ 0 & 0 & M_w & 0 & M_q & 0 \\ 0 & N_v & 0 & 0 & 0 & N_r \end{bmatrix} \\ &-\begin{bmatrix} X_{u|u|}|u| & 0 & 0 & 0 & 0 & 0 \\ 0| & Y_{v|v|}|v| & 0 & 0 & 0 & Y_{r|r|}|r| \\ 0 & 0 & Z_{w|w|}|w| & 0 & Z_{q|q|}|q| & 0 \\ 0 & 0 & 0 & K_{p|p|}|p| & 0 & 0 \\ 0 & 0 & M_{w|w|}|w| & 0 & M_{q|q|}|q| & 0 \\ 0 & N_{v|v|}|v| & 0 & 0 & 0 & N_{r|r|}|r| \end{bmatrix}\end{aligned} \tag{3.48}$$

Finally, drag forces and moment can be written using (3.46), and (3.48):

$$
\begin{aligned}
X_d &= X_u u + X_{u|u|} u|u| \\
Y_d &= Y_v v + Y_r r + Y_{v|v|} v|v| + Y_{r|r|} r|r| \\
Z_d &= Z_w w + Z_q q + Z_{w|w|} w|w| + Z_{q|q|} q|q| \\
K_d &= K_p p + K_{p|p|} p|p| \\
M_d &= M_w w + M_q q + M_{w|w|} w|w| + M_{q|q|} q|q| \\
N_d &= N_v v + N_r r + N_{v|v|} v|v| + N_{r|r|} r|r|
\end{aligned}
\tag{3.49}
$$

3.2.3 Added Mass

Added mass is a measure of the mass of the moving water when the vehicle accelerates [27]. The forces and moments $\boldsymbol{\tau}_A$ due to the added mass can be written in following form:

$$
\boldsymbol{\tau}_A = -\boldsymbol{M}_A \dot{\boldsymbol{\nu}} - \boldsymbol{C}_A(\boldsymbol{\nu})\boldsymbol{\nu} \tag{3.50}
$$

where $\boldsymbol{M}_A$ is the added inertia matrix and $\boldsymbol{C}_A(\boldsymbol{\nu})$ the hydrodynamic Coriolis and centripetal matrix [25].

The 6x6 added inertia matrix $\boldsymbol{M}_A$ is given as:

$$
\boldsymbol{M}_A = \begin{bmatrix} \boldsymbol{A}_{11} & \boldsymbol{A}_{12} \\ \boldsymbol{A}_{21} & \boldsymbol{A}_{22} \end{bmatrix} \triangleq -\begin{bmatrix} X_{\dot{u}} & X_{\dot{v}} & X_{\dot{w}} & X_{\dot{p}} & X_{\dot{q}} & X_{\dot{r}} \\ Y_{\dot{u}} & Y_{\dot{v}} & Y_{\dot{w}} & Y_{\dot{p}} & Y_{\dot{q}} & Y_{\dot{r}} \\ Z_{\dot{u}} & Z_{\dot{v}} & Z_{\dot{w}} & Z_{\dot{p}} & Z_{\dot{q}} & Z_{\dot{r}} \\ K_{\dot{u}} & K_{\dot{v}} & K_{\dot{w}} & K_{\dot{p}} & K_{\dot{q}} & K_{\dot{r}} \\ M_{\dot{u}} & M_{\dot{v}} & M_{\dot{w}} & M_{\dot{p}} & M_{\dot{q}} & M_{\dot{r}} \\ N_{\dot{u}} & N_{\dot{v}} & N_{\dot{w}} & N_{\dot{p}} & N_{\dot{q}} & N_{\dot{r}} \end{bmatrix} \tag{3.51}
$$

The SNAME notation is used in (3.51); for instance the $Y_{\dot{u}}$ is the hydrodynamic added mass along the *y-axis* due to an acceleration $\dot{u}$ in the *x*-direction.

Hydrodynamic Coriolis and centripetal matrix $\boldsymbol{C}_A(\boldsymbol{\nu})$ is skew-symmetric and defined as:

$$
\boldsymbol{C}_A(\boldsymbol{\nu}) = \begin{bmatrix} \boldsymbol{0}_{3x3} & -\boldsymbol{S}(\boldsymbol{A}_{11}\boldsymbol{\nu}_1 + \boldsymbol{A}_{12}\boldsymbol{\nu}_2) \\ -\boldsymbol{S}(\boldsymbol{A}_{11}\boldsymbol{\nu}_1 + \boldsymbol{A}_{12}\boldsymbol{\nu}_2) & -\boldsymbol{S}(\boldsymbol{A}_{21}\boldsymbol{\nu}_1 + \boldsymbol{A}_{22}\boldsymbol{\nu}_2) \end{bmatrix};\ \boldsymbol{C}_A(\boldsymbol{\nu}) = -\boldsymbol{C}_A^T(\boldsymbol{\nu}) \tag{3.52}
$$

Substituting $\boldsymbol{A}_{ij}$ from (3.51) into (3.52) yields the following expression for $\boldsymbol{C}_A(\boldsymbol{\nu})$.

$$\boldsymbol{C}_A(\boldsymbol{\nu}) = \begin{bmatrix} 0 & 0 & 0 & 0 & -a_3 & a_2 \\ 0 & 0 & 0 & a_3 & 0 & -a_1 \\ 0 & 0 & 0 & -a_2 & a_1 & 0 \\ 0 & -a_3 & a_2 & 0 & -b_3 & b_2 \\ a_3 & 0 & -a_1 & b_3 & 0 & -b_1 \\ -a_2 & a_1 & 0 & -b_2 & b_1 & 0 \end{bmatrix} \tag{3.53}$$

where

$$\begin{aligned} a_1 &= X_{\dot{u}}u + X_{\dot{v}}v + X_{\dot{w}}w + X_{\dot{p}}p + X_{\dot{q}}q + X_{\dot{r}}r \\ a_2 &= X_{\dot{v}}u + Y_{\dot{v}}v + Y_{\dot{w}}w + Y_{\dot{p}}p + Y_{\dot{q}}q + Y_{\dot{r}}r \\ a_3 &= X_{\dot{w}}u + Y_{\dot{w}}v + Z_{\dot{w}}w + Z_{\dot{p}}p + Z_{\dot{q}}q + Z_{\dot{r}}r \\ b_1 &= X_{\dot{p}}u + Y_{\dot{p}}v + Z_{\dot{p}}w + K_{\dot{p}}p + K_{\dot{q}}q + K_{\dot{r}}r \\ b_2 &= X_{\dot{q}}u + Y_{\dot{q}}v + Z_{\dot{q}}w + K_{\dot{q}}p + M_{\dot{q}}q + M_{\dot{r}}r \\ b_3 &= X_{\dot{r}}u + Y_{\dot{r}}v + Z_{\dot{r}}w + K_{\dot{r}}p + M_{\dot{r}}q + N_{\dot{r}}r \end{aligned} \tag{3.54}$$

Due to the *xy* and *xz* symmetry of the vehicle, the added inertia matrix given in (3.51) reduces to following expression:

$$\boldsymbol{M}_A = -\begin{bmatrix} X_{\dot{u}} & 0 & 0 & 0 & 0 & 0 \\ 0 & Y_{\dot{v}} & 0 & 0 & 0 & Y_{\dot{r}} \\ 0 & 0 & Z_{\dot{w}} & 0 & Z_{\dot{q}} & 0 \\ 0 & 0 & 0 & K_{\dot{p}} & 0 & 0 \\ 0 & 0 & M_{\dot{w}} & 0 & M_{\dot{q}} & 0 \\ 0 & N_{\dot{v}} & 0 & 0 & 0 & N_{\dot{r}} \end{bmatrix} \tag{3.55}$$

Using the simplified expression in (3.55), the hydrodynamic Coriolis and centripetal matrix $\boldsymbol{C}(\boldsymbol{\nu})$ can be written as:

$$\boldsymbol{C}_A(\boldsymbol{\nu}) = \begin{bmatrix} 0 & 0 & 0 & 0 & -(Z_{\dot{w}}w + Z_{\dot{q}}q) & Y_{\dot{v}}v + Y_{\dot{r}}r \\ 0 & 0 & 0 & Z_{\dot{w}}w + Z_{\dot{q}}q & 0 & -X_{\dot{u}}u \\ 0 & 0 & 0 & -(Y_{\dot{v}}v + Y_{\dot{r}}r) & X_{\dot{u}}u & 0 \\ 0 & -(Z_{\dot{w}}w + Z_{\dot{q}}q) & Y_{\dot{v}}v + Y_{\dot{r}}r & 0 & -(Y_{\dot{r}}v + N_{\dot{r}}r) & Z_{\dot{q}}w + M_{\dot{q}}q \\ Z_{\dot{w}}w + Z_{\dot{q}}q & 0 & -X_{\dot{u}}u & Y_{\dot{r}}v + N_{\dot{r}}r & 0 & -K_{\dot{p}}p \\ -(Y_{\dot{v}}v + Y_{\dot{r}}r) & X_{\dot{u}}u & 0 & -(Z_{\dot{q}}w + M_{\dot{q}}q) & K_{\dot{p}}p & 0 \end{bmatrix} \tag{3.56}$$

Substituting the matrices (3.55) and (3.56) into the (3.50) gives the forces and moment due to the added mass.

$$\begin{aligned} X_A &= X_{\dot{u}}\dot{u} + Z_{\dot{w}}wq + Z_{\dot{q}}q^2 - Y_{\dot{v}}vr - Y_{\dot{r}}r^2 \\ Y_A &= Y_{\dot{v}}\dot{v} + Y_{\dot{r}}\dot{r} - Z_{\dot{w}}wp - Z_{\dot{q}}pq + X_{\dot{u}}ur \\ Z_A &= Z_{\dot{w}}\dot{w} + Z_{\dot{q}}\dot{q} + Y_{\dot{v}}vp + Y_{\dot{r}}pr - X_{\dot{u}}uq \end{aligned} \tag{3.57}$$

$$K_A = K_{\dot{p}}\dot{p} + (Z_{\dot{w}} - Y_{\dot{v}})vw + (Z_{\dot{q}} + Y_{\dot{r}})vq - (Y_{\dot{r}} + Z_{\dot{q}})wr + (N_{\dot{r}} - M_{\dot{q}})qr$$

$$M_A = M_{\dot{w}}\dot{w} + M_{\dot{q}}\dot{q} + (X_{\dot{u}} - Z_{\dot{w}})uw - Z_{\dot{q}}uq - Y_{\dot{r}}vp + (K_{\dot{p}} - N_{\dot{r}})pr$$

$$N_A = N_{\dot{v}}\dot{v} + N_{\dot{r}}\dot{r} + (Y_{\dot{v}} - X_{\dot{u}})uv + Y_{\dot{r}}ur + Z_{\dot{q}}wp + (M_{\dot{q}} - K_{\dot{p}})pq$$

3.2.4 Body Lift and Fin Lift

The lift forces and moments $\boldsymbol{\tau}_L$ can be separated into the two parts as:

$$\boldsymbol{\tau}_L = \boldsymbol{\tau}_{L_B} + \boldsymbol{\tau}_{L_F} \tag{3.58}$$

where the $\boldsymbol{\tau}_{L_B}$ defines the body lift and $\boldsymbol{\tau}_{L_F}$ defines the fin lift forces and moments.

Vehicle body lift results from the vehicle moving through the water at an angle of attack, causing flow separation and a subsequent drop in pressure along aft, upper section of the vehicle hull. This pressure drop is modeled as a point force applied at the center of pressure. As this center pressure does not line up with the origin of the vehicle-fixed coordinate system, this force also lead to a pitching moment about the origin [25]. Body lift forces and moments are defined as:

$$\boldsymbol{\tau}_{L_B} = \begin{bmatrix} 0 \\ Y_{uvl}uv \\ Z_{uwl}uw \\ 0 \\ M_{uwl}uw \\ N_{uvl}uv \end{bmatrix} \tag{3.59}$$

where the Y_{uvl}, Z_{uwl}, M_{uwl} and N_{uvl} are called the body lift coefficients and theoretical expressions for these coefficients can be found in [25].

The attitude of the underwater vehicle is controlled by two horizontal fins, or stern planes, and two vertical fins, or rudders. It is known that the pairs of fins move together. The fin lift forces and moments is given as:

$$\boldsymbol{\tau}_{L_F} = \begin{bmatrix} 0 \\ Y_{uvf}uv + Y_{urf}ur + Y_{uu\delta_r}u^2\delta_r \\ Z_{uwf}uw + Z_{uqf}uq + Z_{uu\delta_s}u^2\delta_s \\ 0 \\ M_{uwf}uw + M_{uqf}uq + M_{uu\delta_s}u^2\delta_s \\ N_{uvf}uv + N_{urf}ur + N_{uu\delta_r}u^2\delta_r \end{bmatrix} \tag{3.60}$$

The total lift forces and moments are obtained substituting (3.59) and (3.60) into the (3.58) as given below:

$$\boldsymbol{\tau}_L = \begin{bmatrix} 0 \\ Y_{uvl}uv + Y_{uvf}uv + Y_{urf}ur + Y_{uu\delta_r}u^2\delta_r \\ Z_{uwl}uw + Z_{uwf}uw + Z_{uqf}uq + Z_{uu\delta_s}u^2\delta_s \\ 0 \\ M_{uwl}uw + M_{uwf}uw + M_{uqf}uq + M_{uu\delta_s}u^2\delta_s \\ N_{uvl}uv + N_{uvf}uv + N_{urf}ur + N_{uu\delta_r}u^2\delta_r \end{bmatrix} \tag{3.61}$$

3.3 Total Forces and Moments

Substituting the equations obtained in the previous sections into the (3.41) gives us the total forces and moments acting on the vehicle as given below:

$$\boldsymbol{\tau} = \boldsymbol{\tau}_{HS} + \boldsymbol{\tau}_L + \boldsymbol{\tau}_D + \boldsymbol{\tau}_A + \boldsymbol{\tau}_P = \begin{bmatrix} X \\ Y \\ Z \\ K \\ M \\ N \end{bmatrix}$$

$$\begin{aligned}
X = {} & -(W-B)s\theta + X_{\dot{u}}\dot{u} + Z_{\dot{w}}wq + Z_{\dot{q}}q^2 - Y_{\dot{v}}vr - Y_{\dot{r}}r^2 + X_u u \\
& + X_{u|u|}u|u| + X_{prop} \\
Y = {} & (W-B)c\theta s\phi + Y_{\dot{v}}\dot{v} + Y_{\dot{r}}\dot{r} - Z_{\dot{w}}wp - Z_{\dot{q}}pq + X_{\dot{u}}ur \\
& + Y_v v + Y_r r + Y_{v|v|}v|v| + Y_{r|r|}r|r| + Y_{uvl}uv + Y_{uvf}uv \\
& + Y_{urf}ur + Y_{uu\delta_r}u^2\delta_r \\
Z = {} & (W-B)c\theta c\phi + Z_{\dot{w}}\dot{w} + Z_{\dot{q}}\dot{q} + Y_{\dot{v}}vp + Y_{\dot{r}}pr - X_{\dot{u}}uq + Z_w w + Z_q q \\
& + Z_{w|w|}w|w| + Z_{q|q|}q|q| + Z_{uwl}uw + Z_{uwf}uw + Z_{uqf}uq \\
& + Z_{uu\delta_s}u^2\delta_s \\
K = {} & (y_G W - y_B B)c\theta c\phi - (z_G W - z_B B)c\theta s\phi + K_{\dot{p}}\dot{p} + (Z_{\dot{w}} - Y_{\dot{v}})vw + (Z_{\dot{q}} \\
& + Y_{\dot{r}})vq - (Y_{\dot{r}} + Z_{\dot{q}})wr + (N_{\dot{r}} - M_{\dot{q}})qr + K_p p + K_{p|p|}p|p| \\
& + K_{prop} \\
M = {} & -(z_G W - z_B B)s\theta - (x_G W - x_B B)c\theta c\phi + M_{\dot{w}}\dot{w} + M_{\dot{q}}\dot{q} + (X_{\dot{u}} \\
& - Z_{\dot{w}})uw - Z_{\dot{q}}uq - Y_{\dot{r}}vp + (K_{\dot{p}} - N_{\dot{r}})pr + M_w w + M_q q \\
& + M_{w|w|}w|w| + M_{q|q|}q|q| + M_{uwl}uw + M_{uwf}uw + M_{uqf}uq \\
& + M_{uu\delta_s}u^2\delta_s \\
N = {} & (x_G W - x_B B)c\theta s\phi + (y_G W - y_B B)s\theta + N_{\dot{v}}\dot{v} + N_{\dot{r}}\dot{r} + (Y_{\dot{v}} - X_{\dot{u}})uv \\
& + Y_{\dot{r}}ur + Z_{\dot{q}}wp + (M_{\dot{q}} - K_{\dot{p}})pq + N_v v + N_r r + N_{v|v|}v|v| \\
& + N_{r|r|}r|r| + N_{uvl}uv + N_{uvf}uv + N_{urf}ur + N_{uu\delta_r}u^2\delta_r
\end{aligned} \tag{3.62}$$

3.4 Equations of Motion

In (3.35) the dynamic equations are defines as

$$\boldsymbol{M}_{RB}\dot{\boldsymbol{\nu}} + \boldsymbol{C}_{RB}(\boldsymbol{\nu})\boldsymbol{\nu} = \boldsymbol{\tau}$$

Here $\boldsymbol{\tau}$ consists all forces acting on the vehicle's body and can be written as sum of three components as given in (3.41), that is:

$$\boldsymbol{\tau} = \boldsymbol{\tau}_{HS} + \boldsymbol{\tau}_A + \boldsymbol{\tau}_D + \boldsymbol{\tau}_L + \boldsymbol{\tau}_P$$

where $\boldsymbol{\tau}_{HS}$ is hydrostatic forces and moments and moments defined in (3.45), $\boldsymbol{\tau}_A$ the forces and moments due to the *added mass* defined in (3.57), $\boldsymbol{\tau}_D$ the hydrodynamic damping defined in (3.49), $\boldsymbol{\tau}_L$ the body and fin lift forces and moments defined in (3.58) and $\boldsymbol{\tau}_C$ propulsion forces and moments.

Substituting the equations (3.46), (3.46) and (3.50) into the (3.41) yields the following expression:

$$\boldsymbol{M}_{RB}\dot{\boldsymbol{\nu}} + \boldsymbol{C}_{RB}(\boldsymbol{\nu})\boldsymbol{\nu} = -\boldsymbol{g}(\boldsymbol{\eta}_2) - \boldsymbol{M}_A\dot{\boldsymbol{\nu}} - \boldsymbol{C}_A(\boldsymbol{\nu})\boldsymbol{\nu} - \boldsymbol{D}(\boldsymbol{\nu})\boldsymbol{\nu} + \boldsymbol{\tau}_L + \boldsymbol{\tau}_P \tag{3.63}$$

The (3.63) can be written in general form as:

$$\boldsymbol{M}\dot{\boldsymbol{\nu}} + \boldsymbol{C}(\boldsymbol{\nu})\boldsymbol{\nu} + \boldsymbol{D}(\boldsymbol{\nu})\boldsymbol{\nu} + \boldsymbol{g}(\boldsymbol{\eta}) = \boldsymbol{\tau}_L + \boldsymbol{\tau}_P \tag{3.64}$$

where

- $\boldsymbol{M}$ **:** Inertia matrix including added mass, $\boldsymbol{M} \triangleq \boldsymbol{M}_{RB} + \boldsymbol{M}_A$
- $\boldsymbol{C}(\boldsymbol{\nu})$ **:** Coriolis and centripetal terms including added mass, $\boldsymbol{C}(\boldsymbol{\nu}) \triangleq \boldsymbol{C}_{RB}(\boldsymbol{\nu}) + \boldsymbol{C}_A(\boldsymbol{\nu})$
- $\boldsymbol{D}(\boldsymbol{\nu})$ **:** Hydrodynamic damping matrix
- $\boldsymbol{g}(\boldsymbol{\eta})$ **:** Hydrostatic forces and moments
- $\boldsymbol{\tau}_L$ **:** Forces and moments due to the body and fin lift
- $\boldsymbol{\tau}_P$ **:** Propulsion force and moment

The body-fixed frame is chosen in order to coincide with the center of buoyancy. Thus, the position vector of the CB implies that $\boldsymbol{r}_B = [0 \quad 0 \quad 0]^T$ and inertia tensor becomes $\boldsymbol{I}_0 = diag\{I_x, I_y, I_z\}$ [28].

Rigid-body inertia matrix can be written in simpler as given below.

$$\boldsymbol{M}_{RB} = \begin{bmatrix} m & 0 & 0 & 0 & mz_G & -my_G \\ 0 & m & 0 & -mz_G & 0 & mx_G \\ 0 & 0 & m & my_G & -mx_G & 0 \\ 0 & -mz_G & my_G & I_x & 0 & 0 \\ mz_G & 0 & -mx_G & 0 & I_y & 0 \\ -my_G & mx_G & 0 & 0 & 0 & I_z \end{bmatrix} \tag{3.65}$$

The inertia matrix $\boldsymbol{M}$ is written as sum of rigid body inertia matrix $\boldsymbol{M}_{RB}$ and added mass matrix $\boldsymbol{M}_A$ as follows:

$$\boldsymbol{M} = \begin{bmatrix} m - X_{\dot{u}} & 0 & 0 & 0 & mz_G & -my_G \\ 0 & m - Y_{\dot{v}} & 0 & -mz_G & 0 & mx_G - Y_{\dot{r}} \\ 0 & 0 & m - Z_{\dot{w}} & my_G & -mx_G - Z_{\dot{q}} & 0 \\ 0 & -mz_G & my_G & I_x - K_{\dot{p}} & 0 & 0 \\ mz_G & 0 & -mx_G - M_{\dot{w}} & 0 & I_y - M_{\dot{q}} & 0 \\ -my_G & mx_G - N_{\dot{v}} & 0 & 0 & 0 & I_z - N_{\dot{r}} \end{bmatrix} \tag{3.66}$$

The rigid-body Coriolis and centripetal matrix $\boldsymbol{C}_{RB}(\boldsymbol{\nu})$ defined in (3.40) is simplified as:

$$\boldsymbol{C}_{RB}(\boldsymbol{\nu}) = \begin{bmatrix} 0 & 0 & 0 \\ 0 & 0 & 0 \\ 0 & 0 & 0 \\ -m(y_G q + z_G r) & m(y_G p + w) & m(z_G p - v) \\ m(x_G q - w) & -m(z_G r + x_G p) & m(z_G q + u) \\ m(x_G r + v) & m(y_G r - u) & -m(x_G p + y_G q) \end{bmatrix}$$
$$\begin{bmatrix} m(y_G q + z_G r) & -m(x_G q - w) & -m(x_G r + v) \\ -m(y_G p + w) & m(z_G r + x_G p) & -m(y_G r - u) \\ -m(z_G p - v) & -m(z_G q + u) & m(x_G p + y_G q) \\ 0 & I_z r & -I_y q \\ -I_z r & 0 & I_x p \\ I_y q & -I_x p & 0 \end{bmatrix} \tag{3.67}$$

The Coriolis and centripetal matrix $\boldsymbol{C}(\boldsymbol{\nu})$ can be written as sum of $\boldsymbol{C}_{RB}(\boldsymbol{\nu})$ defined in (2.67) and $\boldsymbol{C}_A(\boldsymbol{\nu})$ defined in (2.68).

$$\boldsymbol{C}(\boldsymbol{\nu}) = \boldsymbol{C}_{RB}(\boldsymbol{\nu}) + \boldsymbol{C}_A(\boldsymbol{\nu})$$

$$\boldsymbol{C}(\boldsymbol{\nu}) = \begin{bmatrix} 0 & 0 & 0 \\ 0 & 0 & 0 \\ 0 & 0 & 0 \\ -m(y_G q + z_G r) & m(y_G p + w) - (Z_{\dot{w}} w + Z_{\dot{q}} q) & m(z_G p - v) + Y_{\dot{v}} v + Y_{\dot{r}} r \\ m(x_G q - w) + Z_{\dot{w}} w + Z_{\dot{q}} q & -m(z_G r + x_G p) & m(z_G q + u) - X_{\dot{u}} u \\ m(x_G r + v) - (Y_{\dot{v}} v + Y_{\dot{r}} r) & m(y_G r - u) + X_{\dot{u}} u & -m(x_G p + y_G q) \end{bmatrix}$$
$$\begin{bmatrix} m(y_G q + z_G r) & -m(x_G q - w) - (Z_{\dot{w}} w + Z_{\dot{q}} q) & -m(x_G r + v) + Y_{\dot{v}} v + Y_{\dot{r}} r \\ -m(y_G p + w) + Z_{\dot{w}} w + Z_{\dot{q}} q & m(z_G r + x_G p) & -m(y_G r - u) - X_{\dot{u}} u \\ -m(z_G p - v) - (Y_{\dot{v}} v + Y_{\dot{r}} r) & -m(z_G q + u) + X_{\dot{u}} u & m(x_G p + y_G q) \\ 0 & I_z r - (Y_{\dot{r}} v + N_{\dot{r}} r) & -I_y q + Z_{\dot{q}} w + M_{\dot{q}} q \\ -I_z r + Y_{\dot{r}} v + N_{\dot{r}} r & 0 & I_x p - K_{\dot{p}} p \\ I_y q - (Z_{\dot{q}} w + M_{\dot{q}} q) & -I_x p + K_{\dot{p}} p & 0 \end{bmatrix} \tag{3.68}$$

The simplified form of the hydrodynamic damping matrix $\boldsymbol{D}(\boldsymbol{\nu})$ in (3.48) due to the plane symmetry properties of the vehicle is used in the implementations.

The restoring forces and moments $\boldsymbol{g}(\boldsymbol{\eta})$ can be reduced since $\boldsymbol{r}_B = [0 \quad 0 \quad 0]^T$.

$$\boldsymbol{g}(\boldsymbol{\eta_2}) = \begin{bmatrix} (W-B)s\theta \\ -(W-B)c\theta s\phi \\ -(W-B)c\theta c\phi \\ -(y_G W)c\theta c\phi + (z_G W)c\theta s\phi \\ (z_G W)s\theta + (x_G W)c\theta c\phi \\ -(x_G W)c\theta s\phi - (y_G W)s\theta \end{bmatrix} \tag{3.68}$$

Let us write the lift forces and moments defined as (3.58) in following form:

$$\boldsymbol{\tau}_L = -\boldsymbol{L}(\boldsymbol{\nu})\boldsymbol{\nu} + \boldsymbol{\tau}_{fin} = \begin{bmatrix} 0 \\ Y_{uvl}uv + Y_{uvf}uv + Y_{urf}ur \\ Z_{uwl}uw + Z_{uwf}uw + Z_{uqf}uq \\ 0 \\ M_{uwl}uw + M_{uwf}uw + M_{uqf}uq \\ N_{uvl}uv + N_{uvf}uv + N_{urf}ur \end{bmatrix} + \begin{bmatrix} 0 \\ Y_{uu\delta_r}u^2\delta_r \\ Z_{uu\delta_s}u^2\delta_s \\ 0 \\ M_{uu\delta_s}u^2\delta_s \\ N_{uu\delta_r}u^2\delta_r \end{bmatrix}$$

$$\boldsymbol{L}(\boldsymbol{\nu})\boldsymbol{\nu} = -\begin{bmatrix} 0 & 0 & 0 & 0 & 0 & 0 \\ 0 & Y_{uv}u & 0 & 0 & 0 & Y_{ur}u \\ 0 & 0 & Z_{uw}u & 0 & Z_{uq}u & 0 \\ 0 & 0 & 0 & 0 & 0 & 0 \\ 0 & 0 & M_{uw}u & 0 & M_{uq}u & 0 \\ 0 & N_{uv}u & 0 & 0 & 0 & N_{ur}u \end{bmatrix} \begin{bmatrix} u \\ v \\ w \\ p \\ q \\ r \end{bmatrix} \tag{3.69}$$

where

$Y_{uv} = Y_{uvl} + Y_{uvf}; \quad Y_{ur} = Y_{urf}$

$Z_{uw} = Z_{uwl} + Z_{uwf}; \quad Z_{uq} = Z_{uqf};$

$M_{uw} = M_{uwl} + M_{uwf}; \quad M_{uq} = M_{uqf};$

$N_{uv} = N_{uvl} + N_{uvf}; \quad N_{ur} = N_{urf};$

The fin deflections δ_s and δ_r will be used as the control variables for the system. There are four identical control fins as control surfaces, two in xy plane and two in xy plane. The pair of fins in a plane works together.

When we look at the $\boldsymbol{\tau}_P$, the thrust and rolling moment produced by propellers can be considered as inputs along *x-axis* and around *x-axis*, and can be denoted as X_{prop} and K_{prop}. These quantities depend on the many parameters such as, torque coefficients, propeller diameter, number of blades, blade pitch angle etc. The $\boldsymbol{\tau}_P$ vector can be written as:

$$\boldsymbol{\tau}_P = [X_{prop} \quad 0 \quad 0 \quad K_{prop} \quad 0 \quad 0]^T \tag{3.70}$$

Substituting the equations (3.69) and (3.70) into the (3.64) yields:

$$\boldsymbol{M}\dot{\boldsymbol{\nu}} + \boldsymbol{C}(\boldsymbol{\nu})\boldsymbol{\nu} + \boldsymbol{D}(\boldsymbol{\nu})\boldsymbol{\nu} + \boldsymbol{g}(\boldsymbol{\eta}) = -\boldsymbol{L}(\boldsymbol{\nu})\boldsymbol{\nu} + \boldsymbol{\tau}_{fin} + \boldsymbol{\tau}_P \tag{3.71}$$

$$\boldsymbol{M\dot{\nu}} + \boldsymbol{C(\nu)\nu} + \boldsymbol{D(\nu)\nu} + \boldsymbol{L(\nu)\nu} + \boldsymbol{g(\eta)} = \begin{bmatrix} 0 \\ Y_{uu\delta_r} u^2 \delta_r \\ Z_{uu\delta_s} u^2 \delta_s \\ 0 \\ M_{uu\delta_s} u^2 \delta_s \\ N_{uu\delta_r} u^2 \delta_r \end{bmatrix} + \begin{bmatrix} X_{prop} \\ 0 \\ 0 \\ K_{prop} \\ 0 \\ 0 \end{bmatrix}$$

Let us define $\boldsymbol{\Gamma}$ as control input for the system which includes propulsion force and moment and fin deflections.

$$\boldsymbol{\Gamma} = \begin{bmatrix} X_{prop} \\ K_{prop} \\ \delta_s \\ \delta_r \end{bmatrix} \tag{3.72}$$

Then the (3.71) is transformed into the following representation using $\boldsymbol{u_C}$.

$$\boldsymbol{M\dot{\nu}} + \boldsymbol{C(\nu)\nu} + \boldsymbol{D(\nu)\nu} + \boldsymbol{L(\nu)\nu} + \boldsymbol{g(\eta)} = \boldsymbol{T u_C}$$

$$\boldsymbol{T} = \begin{bmatrix} 1 & 0 & 0 & 0 \\ 0 & 0 & 0 & Y_{uu\delta_r} u^2 \\ 0 & 0 & Z_{uu\delta_s} u^2 & 0 \\ 0 & 1 & 0 & 0 \\ 0 & 0 & M_{uu\delta_s} u^2 & 0 \\ 0 & 0 & 0 & N_{uu\delta_r} u^2 \end{bmatrix} \tag{3.73}$$

The following relations exist for the fin lift coefficients in matrix $\boldsymbol{T}$:

$$\left.\begin{aligned} Y_{uu\delta_r} &= -Z_{uu\delta_s} \\ M_{uu\delta_s} &= -x_{fin} Z_{uu\delta_s} \\ N_{uu\delta_r} &= x_{fin} Y_{uu\delta_r} \end{aligned}\right\} M_{uu\delta_s} = N_{uu\delta_r} \tag{3.74}$$

where the parameter x_{fin} is the axial position of the fin post in body-referenced coordinate system.

Finally, the all equations of motion of the system can be written as follows:

$$\begin{aligned} &\boldsymbol{\dot{\eta}} = \boldsymbol{J(\eta)\nu} \\ &\boldsymbol{M\dot{\nu}} + \boldsymbol{C(\nu)\nu} + \boldsymbol{D(\nu)\nu} + \boldsymbol{L(\nu)\nu} + \boldsymbol{g(\eta)} = \boldsymbol{\tau_{fin}} + \boldsymbol{\tau_P} = \boldsymbol{T\Gamma} \\ &\boldsymbol{J(\eta)} = \begin{bmatrix} \boldsymbol{J_1(\eta_2)} & \boldsymbol{0_{3x3}} \\ \boldsymbol{0_{3x3}} & \boldsymbol{J_2(\eta_2)} \end{bmatrix} \end{aligned} \tag{3.75}$$

$$\boldsymbol{J}_1(\boldsymbol{\eta}_2) = \begin{bmatrix} c\psi c\theta & -s\psi c\phi + c\psi s\theta s\phi & s\psi s\phi + c\psi c\phi s\theta \\ s\psi c\theta & c\psi c\phi + s\phi s\theta s\psi & -c\psi s\phi + s\theta s\psi c\phi \\ -s\theta & c\theta s\phi & c\theta c\phi \end{bmatrix}$$

$$\boldsymbol{J}_2(\boldsymbol{\eta}_2) = \begin{bmatrix} 1 & s\phi t\theta & c\phi t\theta \\ 0 & c\phi & -s\phi \\ 0 & s\phi/c\theta & c\phi/c\theta \end{bmatrix}$$

$\boldsymbol{M} = \boldsymbol{M}_{RB} + \boldsymbol{M}_A$;

$$\boldsymbol{M} = \begin{bmatrix} m - X_{\dot{u}} & 0 & 0 & 0 & mz_G & -my_G \\ 0 & m - Y_{\dot{v}} & 0 & -mz_G & 0 & mx_G - Y_{\dot{r}} \\ 0 & 0 & m - Z_{\dot{w}} & my_G & -mx_G - Z_{\dot{q}} & 0 \\ 0 & -mz_G & my_G & I_x - K_{\dot{p}} & 0 & 0 \\ mz_G & 0 & -mx_G - M_{\dot{w}} & 0 & I_y - M_{\dot{q}} & 0 \\ -my_G & mx_G - N_{\dot{v}} & 0 & 0 & 0 & I_z - N_{\dot{r}} \end{bmatrix}$$

$$\boldsymbol{C}(\boldsymbol{\nu}) = \boldsymbol{C}_{RB}(\boldsymbol{\nu}) + \boldsymbol{C}_A(\boldsymbol{\nu})$$

$$\boldsymbol{C}(\boldsymbol{\nu}) = \begin{bmatrix} 0 & 0 & 0 \\ 0 & 0 & 0 \\ 0 & 0 & 0 \\ -m(y_G q + z_G r) & m(y_G p + w) - (Z_{\dot{w}} w + Z_{\dot{q}} q) & m(z_G p - v) + Y_{\dot{v}} v + Y_{\dot{r}} r \\ m(x_G q - w) + Z_{\dot{w}} w + Z_{\dot{q}} q & -m(z_G r + x_G p) & m(z_G q + u) - X_{\dot{u}} u \\ m(x_G r + v) - (Y_{\dot{v}} v + Y_{\dot{r}} r) & m(y_G r - u) + X_{\dot{u}} u & -m(x_G p + y_G q) \end{bmatrix}$$

$$\begin{bmatrix} m(y_G q + z_G r) & -m(x_G q - w) - (Z_{\dot{w}} w + Z_{\dot{q}} q) & -m(x_G r + v) + Y_{\dot{v}} v + Y_{\dot{r}} r \\ -m(y_G p + w) + Z_{\dot{w}} w + Z_{\dot{q}} q & m(z_G r + x_G p) & -m(y_G r - u) - X_{\dot{u}} u \\ -m(z_G p - v) - (Y_{\dot{v}} v + Y_{\dot{r}} r) & -m(z_G q + u) + X_{\dot{u}} u & m(x_G p + y_G q) \\ 0 & I_z r - (Y_{\dot{r}} v + N_{\dot{r}} r) & -I_y q + Z_{\dot{q}} w + M_{\dot{q}} q \\ -I_z r + Y_{\dot{r}} v + N_{\dot{r}} r & 0 & I_x p - K_{\dot{p}} p \\ I_y q - (Z_{\dot{q}} w + M_{\dot{q}} q) & -I_x p + K_{\dot{p}} p & 0 \end{bmatrix}$$

$$\boldsymbol{D}(\boldsymbol{\nu}) = -\begin{bmatrix} X_u & 0 & 0 & 0 & 0 & 0 \\ 0 & Y_v & 0 & 0 & 0 & Y_r \\ 0 & 0 & Z_w & 0 & Z_q & 0 \\ 0 & 0 & 0 & K_p & 0 & 0 \\ 0 & 0 & M_w & 0 & M_q & 0 \\ 0 & N_v & 0 & 0 & 0 & N_r \end{bmatrix}$$

$$-\begin{bmatrix} X_{u|u|}|u| & 0 & 0 & 0 & 0 & 0 \\ 0| & Y_{v|v|}|v| & 0 & 0 & 0 & Y_{r|r|}|r| \\ 0 & 0 & Z_{w|w|}|w| & 0 & Z_{q|q|}|q| & 0 \\ 0 & 0 & 0 & K_{p|p|}|p| & 0 & 0 \\ 0 & 0 & M_{w|w|}|w| & 0 & M_{q|q|}|q| & 0 \\ 0 & N_{v|v|}|v| & 0 & 0 & 0 & N_{r|r|}|r| \end{bmatrix}$$

$$\boldsymbol{L}(\boldsymbol{\nu}) = -\begin{bmatrix} 0 & 0 & 0 & 0 & 0 & 0 \\ 0 & Y_{uv}u & 0 & 0 & 0 & Y_{ur}u \\ 0 & 0 & Z_{uw}u & 0 & Z_{uq}u & 0 \\ 0 & 0 & 0 & 0 & 0 & 0 \\ 0 & 0 & M_{uw}u & 0 & M_{uq}u & 0 \\ 0 & N_{uv}u & 0 & 0 & 0 & N_{ur}u \end{bmatrix}$$

$$\boldsymbol{g}(\boldsymbol{\eta}) = \begin{bmatrix} (W-B)s\theta \\ -(W-B)c\theta s\phi \\ -(W-B)c\theta c\phi \\ -(y_G W)c\theta c\phi + (z_G W)c\theta s\phi \\ (z_G W)s\theta + (x_G W)c\theta c\phi \\ -(x_G W)c\theta s\phi - (y_G W)s\theta \end{bmatrix}$$

$$\boldsymbol{\tau}_{fin} = \begin{bmatrix} 0 \\ Y_{uu\delta_r}u^2\delta_r \\ Z_{uu\delta_s}u^2\delta_s \\ 0 \\ M_{uu\delta_s}u^2\delta_s \\ N_{uu\delta_r}u^2\delta_r \end{bmatrix}; \quad \boldsymbol{\tau}_P = \begin{bmatrix} X_{prop} \\ 0 \\ 0 \\ K_{prop} \\ 0 \\ 0 \end{bmatrix}$$

$$\boldsymbol{T} = \begin{bmatrix} 1 & 0 & 0 & 0 \\ 0 & 0 & 0 & Y_{uu\delta_r}u^2 \\ 0 & 0 & Z_{uu\delta_s}u^2 & 0 \\ 0 & 1 & 0 & 0 \\ 0 & 0 & M_{uu\delta_s}u^2 & 0 \\ 0 & 0 & 0 & N_{uu\delta_r}u^2 \end{bmatrix}; \quad \boldsymbol{\Gamma} = \begin{bmatrix} X_{prop} \\ K_{prop} \\ \delta_s \\ \delta_r \end{bmatrix}$$

The following parameters of REMUS vehicle [25] are used in order to perform the vehicle simulation using the equations in (3.75).

Table 3.1 Physical Parameters

Parameter	Value	Units
m	$+3.05e+001$	kg
$W = B$	$+2.99e+002$	N
I_x	$+1.77e-001$	$kg \cdot m^2$
I_y	$+3.45e+000$	$kg \cdot m^2$
I_z	$+3.45e+000$	$kg \cdot m^2$
ρ_f	$+1.03e+003$	kg/m^3
x_G	$+0.00e+000$	m
y_G	$+0.00e+000$	m
z_G	$+1.96e-002$	m

Table 3.2 Added Mass Coefficients

Parameter	Value	Units
$X_{\dot{u}}$	$-9.30e-001$	kg
$Y_{\dot{v}}$	$-3.55e+001$	kg
$Y_{\dot{r}}$	$+1.93e+000$	$kg \cdot m/rad$
$Z_{\dot{w}}$	$-3.55e+001$	kg
$Z_{\dot{q}}$	$-1.93e+000$	$kg \cdot m/rad$
$K_{\dot{p}}$	$-7.04e-002$	$kg \cdot m^2/rad$
$M_{\dot{w}}$	$-1.93e+000$	$kg \cdot m$
$M_{\dot{q}}$	$-4.88e+000$	$kg \cdot m^2/rad$
$N_{\dot{v}}$	$+1.93e+000$	$kg \cdot m$
$N_{\dot{r}}$	$-4.88e+000$	$kg \cdot m^2/rad$

Table 3.3 Hydrodynamic Damping Coefficients

Parameter	Value	Units
$X_{u\|u\|}$	$-1.62e+000$	kg/m
$Y_{v\|v\|}$	$-1.31e+003$	kg/m
$Y_{r\|r\|}$	$+6.32e-001$	$kg \cdot m/rad^2$
$Z_{w\|w\|}$	$-1.31e+002$	kg/m
$Z_{q\|q\|}$	$-6.32e-001$	$kg \cdot m/rad^2$
$K_{p\|p\|}$	$-1.30e-001$	$kg \cdot m^2/rad^2$
$M_{w\|w\|}$	$+3.18e+000$	kg
$M_{q\|q\|}$	$-1.88e+002$	$kg \cdot m^2/rad^2$
$N_{v\|v\|}$	$-3.18e+000$	kg
$N_{r\|r\|}$	$-9.40e+001$	$kg \cdot m^2/rad^2$

Table 3.4 Control Fin Coefficients

Parameter	Value	Units
$Y_{uu\delta_r}$	$+9.64e+000$	$kg/(m \cdot rad)$
$Z_{uu\delta_s}$	$-9.64e+000$	$kg/(m \cdot rad)$
$M_{uu\delta_s}$	$-6.15e+000$	kg/rad
$N_{uu\delta_r}$	$-6.15e+000$	kg/rad

Table 3.5 Body & Fin Lift and Moment Coefficients

Parameter	Value	Units
Y_{uv}	$-2.86e+001$	kg/m
Y_{ur}	$+6.15e+000$	kg/rad
Z_{uw}	$-2.86e+001$	kg/m
Z_{uq}	$-6.15e+000$	kg/rad
M_{uw}	$-1.06e+001$	kg
M_{uq}	$-3.93e+000$	$kg \cdot m/rad$
N_{uv}	$+1.06e+001$	kg
N_{ur}	$-3.93e+000$	$kg \cdot m/rad$

The detailed information about derivation of the parameters and calculations can be found in [25].

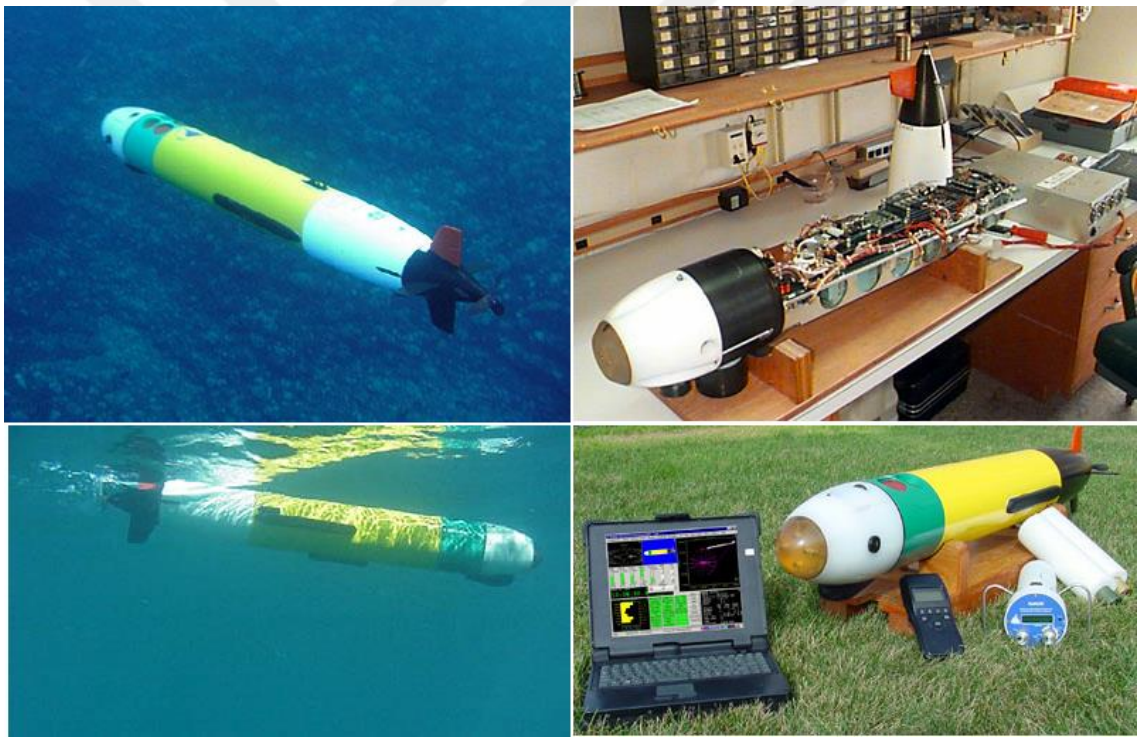

Figure 3.2 REMUS AUV [25]

CHAPTER 4

DECOUPLED SURGE AND ROLL MOTION CONTROL

It is suggested that the equations of motion in 6DOF can be divided into non-interacting (or lightly interacting) subsystems [21].

Starting from this chapter, the equations of motion derived in the previous section are decoupled in order to design control systems for different subsystems and simulated using MATLAB/Simulink. The parameters of REMUS vehicle given in the previous section are used in order to perform the vehicle simulation and controller implementation. Following assumptions are made while decoupling the equations and designing controllers.

- The system is neutrally buoyant which means the buoyancy force acting on the vehicle is equal to the vehicle's weight, $W = B$.
- The body fixed inertia frame is selected to coincide with the center of buoyancy, $\boldsymbol{r}_B = [x_B \quad y_B \quad z_B]^T = [0 \quad 0 \quad 0]^T$
- The inertia tensor is diagonal, $\boldsymbol{I}_0 = diag\{I_x, I_y, I_z\}$
- The vehicle is top-bottom ($xy - plane$) and port-starboard ($xz - plane$) symmetric. These symmetry properties cancel most terms in matrices expressed in vehicle dynamics.
- Any damping terms greater than second-order are neglected.

In this chapter, forward speed dynamics (surge) of the vehicle along *x-axis* will be derived. In addition to surge dynamics, the effect of roll motion around *x-axis*, which is generally neglected in literature, will also be calculated. Linear and non-linear controllers will be designed in accordance with the surge and roll dynamics. The dynamic equations

and controllers will be implemented using MATLAB/Simulink and simulation results will be shown.

4.1 Forward Speed (Surge Speed) Control

In forward speed control, the decoupled surge model is used. By neglecting the other dynamics of the system, the decupled surge model can be obtained as follows.

$$\begin{bmatrix} m - X_{\dot{u}} \\ 0 \\ 0 \\ 0 \\ mz_G \\ -my_G \end{bmatrix} \dot{u} + \begin{bmatrix} -X_{u|u|}|u| \\ 0 \\ 0 \\ 0 \\ 0 \\ 0 \end{bmatrix} u + \begin{bmatrix} 0 \\ 0 \\ (B - W) \\ -Wy_G \\ Wx_G \\ 0 \end{bmatrix} = \begin{bmatrix} X_{prop} \\ 0 \\ 0 \\ 0 \\ 0 \\ 0 \end{bmatrix} \tag{4.1}$$

In (4.1), most of the terms will be zero since $B = W, x_G = y_G = 0$ as given in Table 3.1. In this chapter and following chapters, the equations will be given symbolically as given in (4.1). The (4.1) is written in simpler form as follows.

$$\boldsymbol{M}_u \dot{u} + \boldsymbol{N}_u u + \boldsymbol{g}_u = \boldsymbol{\Gamma}_u \tag{4.2}$$

Finally, the decoupled surge state equation is obtained.

$$\dot{u} = (\boldsymbol{M}_u^T \boldsymbol{M}_u)^{-1} \boldsymbol{M}_u^T (-\boldsymbol{N}_u u - \boldsymbol{g}_u + \boldsymbol{\Gamma}_u) = f_u + b_u X_{prop} \tag{4.3}$$

where

$$f_u = \frac{(m - X_{\dot{u}}) X_{u|u|} u|u| - m x_G z_G W}{(m - X_{\dot{u}})^2 + m^2 (y_G^2 + z_G^2)} \quad ; \quad b_u = \frac{(m - X_{\dot{u}})}{(m - X_{\dot{u}})^2 + m^2 (y_G^2 + z_G^2)}$$

4.1.1 Linearization of Forward Speed Dynamics and Proportional Control

The nonlinear forward speed dynamics in (4.3) can be linearized around operating speed $u_0 \cong 1.5\ m/s$ and following linear state equation can be obtained.

$$\dot{u} = f_{u_L} u + b_{u_L} X_{prop} \tag{4.4}$$

where

$$f_{u_L} = \frac{(m - X_{\dot{u}}) X_u}{(m - X_{\dot{u}})^2 + m^2 (y_G^2 + z_G^2)} \quad ; \quad b_{u_L} = \frac{(m - X_{\dot{u}})}{(m - X_{\dot{u}})^2 + m^2 (y_G^2 + z_G^2)}$$

The transfer function of the forward speed system is

$$G_u(s) = \frac{U(s)}{X_{prop}(s)} = \frac{b_{u_L}}{s - f_{u_L}} \tag{4.5}$$

It is seen from the transfer function that the system is Type 0 which means the system has a constant steady-state error e_{ss} for the step reference input [29].

$$e_{ss} = \frac{1}{1 + \lim_{s \to 0} G_u(s)} = \frac{b_{u_L}}{-f_{u_L}} \cong 0.0741$$

The steady state error calculated above is very small and acceptable value for the forward speed of the vehicle. Based on the transfer function in (4.5), a proportional (P) controller can be designed.

$$\frac{X_{prop}(s)}{e_u(s)} = K_{P_u}\,; \quad e_u = u_d - u \tag{4.6}$$

The proportional controller has been applied to the nonlinear forward speed system using MATLAB/Simulink [45] and the value of K_{P_u} is chosen to achieve an acceptable level of performance. Figure 4.1 shows the step response and steady state error for the surge speed.

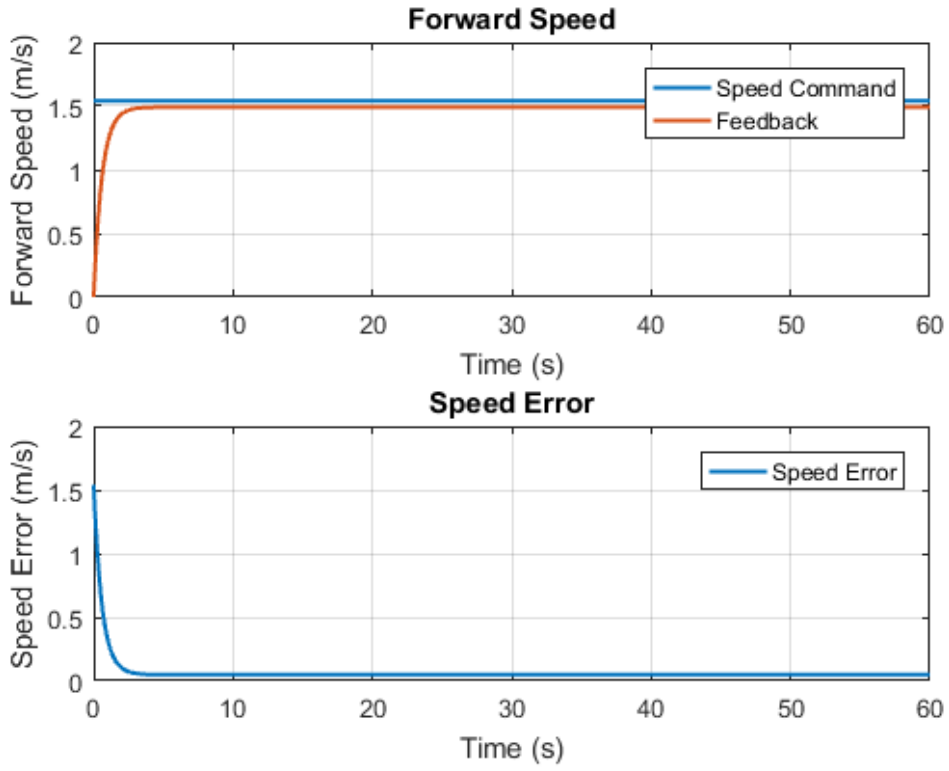

Figure 4.1 Forward speed step response and steady state error

Figure 4.2 indicates that forward speed can be controlled with a small steady state error using linearized model with proportional control. The steady state error can be reduced by increasing the proportional gain and/or adding an integrator to the controller. Increasing proportional gain is not an efficient solution since the system has limits due to the actuator dynamics in real life applications. Thus, adding an integrator to the controller will be better solution to remove the steady state error. In following section, a nonlinear controller will be designed in order to control forward speed and proportional-integral terms will be used in error dynamics.

4.1.2 Forward Speed Control Using Feedback Linearization

By considering the surge dynamics, it is easy to apply feedback linearization method to control the forward speed [30]. The surge dynamics is given in (4.4)

$$\dot{u} = f_u + b_u X_{prop}$$

where

$$f_u = \frac{(m - X_{\dot{u}})X_{u|u|}u|u| - mx_G z_G W}{(X_{\dot{u}} - m)^2 + m^2(y_G^2 + z_G^2)} \quad ; \quad b_u = \frac{(m - X_{\dot{u}})}{(X_{\dot{u}} - m)^2 + m^2(y_G^2 + z_G^2)}$$

Let us define and differentiate the speed error.

$$e_u = u - u_d \;\rightarrow\; \dot{e}_u = \dot{u} - \dot{u}_d$$

Substituting the error dynamics into the forward speed equation yields

$$\dot{e}_u + \dot{u}_d = f_u + b_u X_{prop} \tag{4.7}$$

The control variable X_{prop} can be selected as

$$X_{prop} = \frac{1}{b_u}\left(-f_u + \dot{u}_d - K_{p_u} e_u - K_{i_u}\int_0^t e_u(t)dt\right) \tag{4.8}$$

Selecting the X_{prop} as given above and substituting (4.8) into the (4.7) yields the following error dynamics.

$$\ddot{e}_u + K_{p_u}\dot{e}_u + K_{i_u} e_u = 0$$

Controller gains K_{p_u} and K_{i_u} are appropriately selected using second order system properties $K_{p_u} = 2\zeta\omega_n$ and $K_{i_u} = \omega_n^2$ while considering the dynamic performance of the

vehicle and actuator limits [31]. The block diagram for the surge speed control is given in Figure 4.2 and the response to the step input is shown in the next figure.

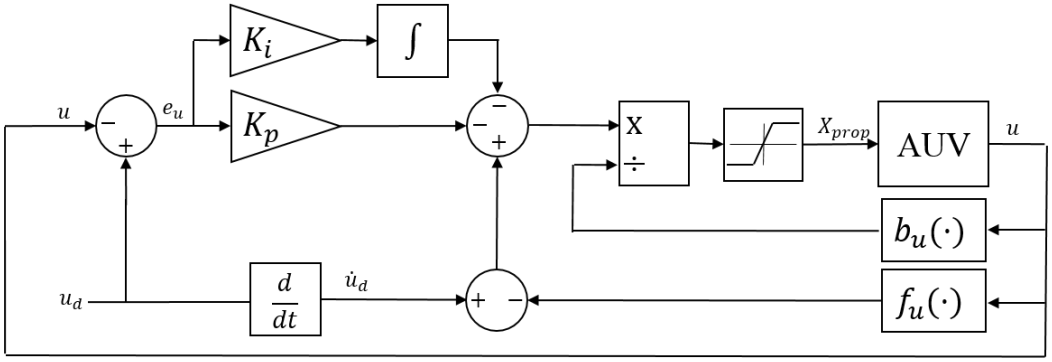

Figure 4.2 Forward speed controller block diagram

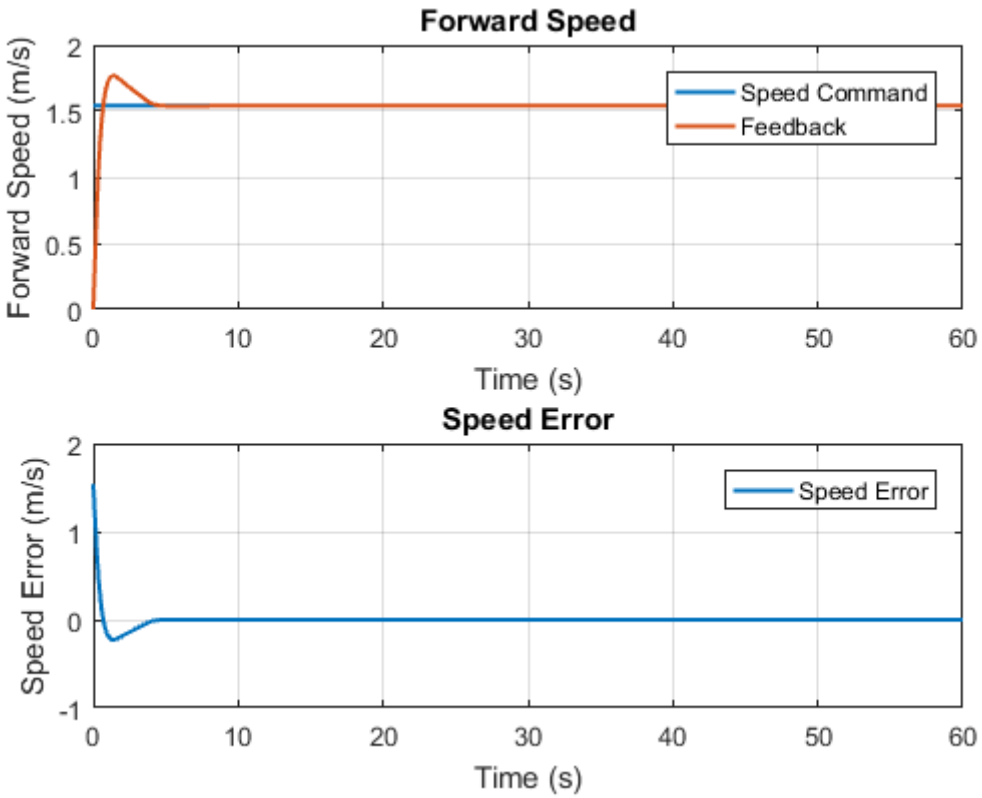

Figure 4.3 Forward speed step response and steady state error

It is seen from Figure 4.3 that the forward speed of the vehicle can be controlled using feedback linearization method with adjustable parameters K_{p_u} and K_{i_u}. Using the speed state error e_u and selecting the X_{prop} as given in (4.8) the 2^{nd} order linear error dynamics is obtained. Controller gains are selected by considering the desired system performance

and actuator limits and appropriate gain values can be found using Simulink Response Optimization tool.

In this and the previous sections, proportional control method with a linearized dynamics and feedback linearization control method with nonlinear dynamics have been applied. Both methods are easy to design and implement in real applications. The first method uses linearized dynamics so nonlinear terms are converted into the linear terms or neglected. The speed of the vehicle can be controlled just using a proportional gain and integrator if it is required. In feedback linearization method, the obtained control rule includes nonlinear terms and then provides linear error dynamics. There are two adjustable gain that is used to achieve desired performance specs. Feedback linearization method has an advantage since the nonlinearity is considered in control rule and a linear dynamics is obtained at the end of the derivations. However, if there are too much nonlinearities which are difficult to identify in the system, the linearization can be a better choice and PID-like controllers are easily designed and tuned.

4.2 Roll Dynamics and Backstepping Control

In general, the roll position and velocity are neglected in control system design or passively stabilized due to the mechanical properties of the AUV [32],[33],[34]. However, the roll effect can be actively controlled using fins, internal mass, counter rotating propellers and etc. [35],[36]. Depending on the system properties, the thruster force and moment, X_{prop} and K_{prop}, can be related to each other. For example, the revolution speed of the counter rotating propellers has effects on both X_{prop} and K_{prop}. On the contrary, the internal mass just affects the rolling moment K_{prop}. Here, the control system is designed for roll subsystem by assuming that the vehicle has independent control input $\mathrm{K_{prop}}$ to stabilize the roll motion. It is also assumed that the vehicle has constant surge speed $u_0 = 1.54\ m/s$. It is easy to obtain the dynamic equation for the roll angle in earth-fixed frame.

$$\dot{\phi} = p + r\cos\phi\tan\theta + q\sin\phi\tan\theta \quad \text{where } \theta = r = q = 0;$$
$$\dot{\phi} = p \tag{4.9}$$

The roll velocity is derived similar to process in surge speed.

$$\begin{bmatrix} 0 \\ -mz_G \\ my_G \\ I_x - K_{\dot{p}} \\ 0 \\ 0 \end{bmatrix} \dot{p} + \begin{bmatrix} 0 \\ -my_G p \\ -mz_G p \\ -K_{p|p|}|p| \\ 0 \\ 0 \end{bmatrix} p + \begin{bmatrix} 0 \\ s\phi(B-W) \\ c\phi(B-W) \\ (s\phi z_G - c\phi y_G)W \\ x_G c\phi W \\ -x_G s\phi W \end{bmatrix} = \begin{bmatrix} 0 \\ 0 \\ 0 \\ K_{prop} \\ 0 \\ 0 \end{bmatrix} \tag{4.10}$$

Similar to the surge dynamics, the equation can be written in simpler form according to (4.10).

$$\boldsymbol{M}_p \dot{p} + \boldsymbol{N}_p p + \boldsymbol{g}_p = \boldsymbol{\Gamma}_p \tag{4.11}$$

Finally, the decoupled roll equations of motion is obtained.

$$\begin{aligned} \dot{\phi} &= p \\ \dot{p} &= \left(\boldsymbol{M}_p^T \boldsymbol{M}_p\right)^{-1} \boldsymbol{M}_p^T \left(-\boldsymbol{N}_p p - \boldsymbol{g}_p + \boldsymbol{\Gamma}_p\right) = f_p + b_p K_{prop} \end{aligned} \tag{4.12}$$

where

$$f_p = \frac{\left(I_x - K_{\dot{p}}\right)\left(K_{p|p|}p|p| + (y_G c\phi - z_G s\phi)W\right) + (B-W)(mz_G s\phi - my_G c\phi)}{\left(I_x - K_{\dot{p}}\right)^2 + m^2(y_G^2 + z_G^2)}$$

$$b_p = \frac{\left(I_x - K_{\dot{p}}\right)}{\left(I_x - K_{\dot{p}}\right)^2 + m^2(y_G^2 + z_G^2)}$$

Backstepping method can be applied to control the roll motion [37]. Let us consider the following equations of motion given in (4.12).

$$\dot{\phi} = p$$

$$\dot{p} = f_p + b_p K_{prop}$$

In the first equation, the p is considered as a virtual controller as follows:

$$\dot{\phi} = u_c \tag{4.13}$$

Let u_c be chosen as

$$u_c = -\lambda\phi\,; \quad \lambda > 0 \tag{4.14}$$

The state equation of roll position becomes

$$\dot{\phi} = -\lambda\phi \tag{4.15}$$

This equations means that the roll angle ϕ goes to zero with the required decay rate according to the value of λ. Lyapunov function can be selected as

$$V_1 = \frac{1}{2}\phi^2; \quad \dot{V}_1 = \phi\dot{\phi} = -\lambda\phi^2;$$

The second variable p is choosen to be equal to the virtual control u_c in order to ϕ to be asymptotically stable. The control K_{prop} can be designed to regulate the following output:

$$y_p = p - u_c = p + \lambda\phi \tag{4.16}$$

Differentiating the y_p yileds

$$\dot{y}_p = \dot{p} - \dot{u}_c = f_p + b_p K_{prop} - \dot{u}_c \tag{4.17}$$

where $\dot{u}_c = -\lambda\dot{\phi} = -\lambda p$. The Lyapunov function can be chosen as

$$V_2 = V_1 + \frac{1}{2}y_p^2 = \frac{1}{2}\phi^2 + \frac{1}{2}y_p^2 > 0 \ \ \forall \left(\phi, y_p\right) \neq (0,0);$$

$$\dot{V}_2 = \phi\dot{\phi} + y_p\dot{y}_p = -\lambda\phi^2 + y_p(f_p + b_p K_{prop} - \dot{u}_c);$$

Let us select the K_{prop} as

$$K_{prop} = \frac{1}{b_p}\left(\dot{u}_c - f_p - \alpha y_p\right) \tag{4.18}$$

Then the (4.17) becomes

$$\dot{y}_p = -\alpha y_p \ ; \quad \alpha > 0 \tag{4.19}$$

The derivative of final Lyapunov function is

$$\dot{V}_2 = \phi\dot{\phi} + y_p\dot{y}_p = -\lambda\phi^2 - \alpha y_p^2 < 0 \ \ \forall \left(\phi, y_p\right) \neq (0,0)$$

The y_p goes exponentially asymptotically zero as time goes to infinity. As y_p approach zero, then p goes to u_c. Finally the control law is obtained as

$$K_{prop} = \frac{1}{b_p}\Big(-\lambda p - f_{\,p} - \alpha(p + \lambda\phi)\Big) \tag{4.20}$$

The control parameters λ and α are need to be positive to satisfy stability criteria. The block diagram for the roll motion control is given in Figure 4.4 and the response to the given initial condition is shown in the next figure.

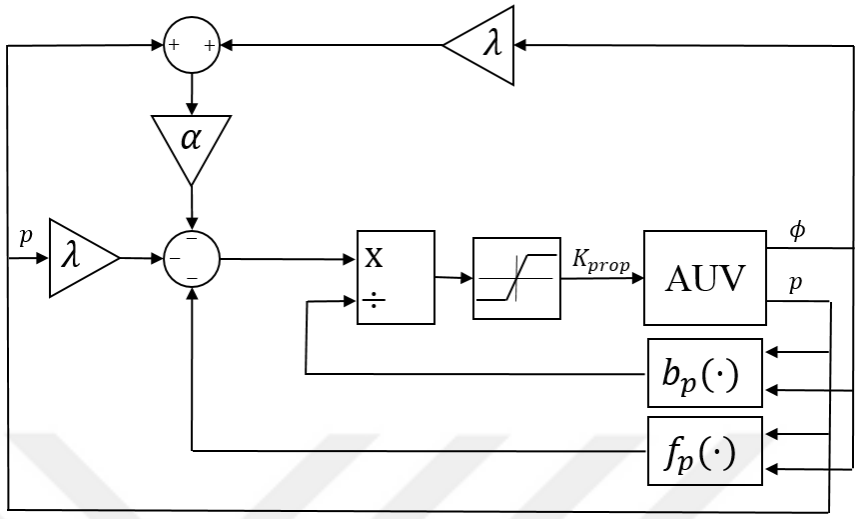

Figure 4.4 Roll motion control block diagram

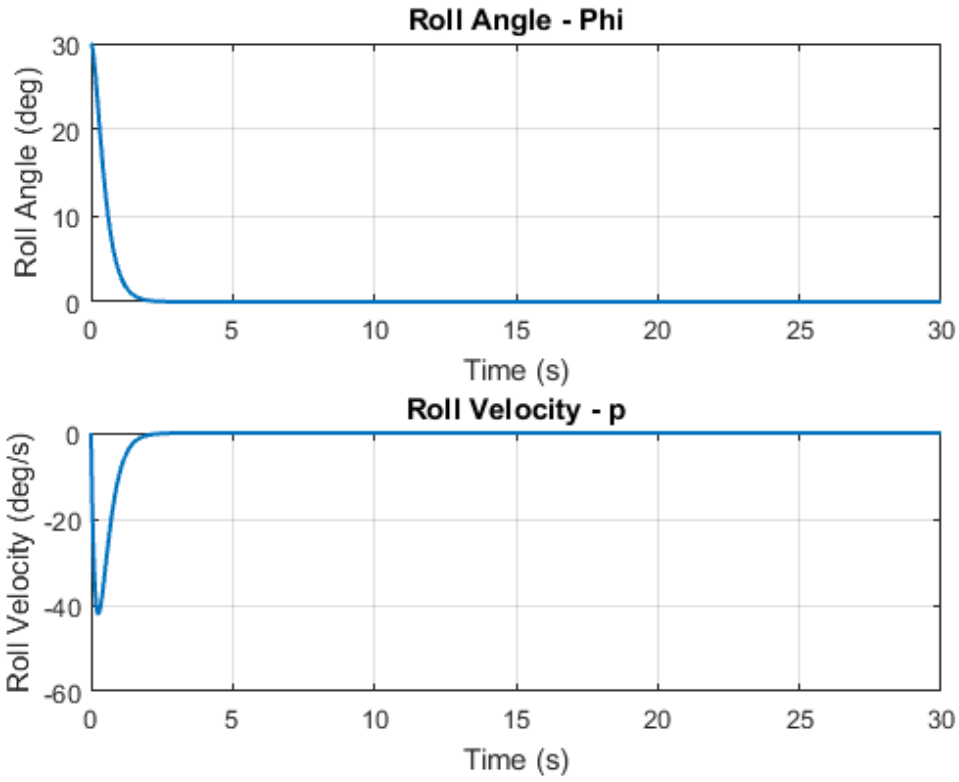

Figure 4.5 Roll motion response to the initial condition $\phi_0 = 30°$

Figure 4.5 shows that the roll dynamics goes to equilibrium point $[\phi, p] = [0,0]$ under the backstepping control for the given initial condition. Since only the roll motion has

been examined here, the initial condition has been given in order to see if the controller is working. On the other hand, the main task of the controller is to stabilize the roll angle and velocity due to the change of fin angles during vehicle motion. The controller gains λ and α can be arbitrarily selected using the simulation results or optimization algorithms can be used to find optimal parameters for desired performance criteria depending on the system.

The advantage of backstepping compared with other control methods lies in its design flexibility, due to its recursive use of Lyapunov functions. The key idea of the backstepping design is to select recursively some appropriate state variables as virtual inputs for lower dimension subsystems of the overall system and the Lyapunov functions are designed for each stable virtual controller [37]. Therefore, the designed final actual control law can guarantee the stability of the total control system.

CHAPTER 5

LONGITUDINAL DYNAMICS AND DEPTH CONTROL

Depth control is one of the significant part in AUVs since many practical application such as underwater pipeline checking and oceanographic mapping depends on the performance of the depth changing and depth keeping. Various control methods have been utilized for depth control of AUVs, such as PID control based on the linearized model [25], sliding mode control [38], etc. In this chapter, the decoupled equations of motion for depth plane are obtained similar to calculations in the previous sections. Linear and nonlinear controllers are designed and implemented using the obtained dynamic equations. Controlled systems are implemented and simulation results are shown using MATLAB/Simulink.

5.1 Equations of Motion In Diving Plane

The decoupled longitudinal dynamics of the AUVs is obtained assuming that the vehicle is neutrally buoyant and moving with constant surge speed u_0. The depth and pitch angle dynamics can be simply obtained by taking $\phi = \psi = v = p = r = 0$.

$$\begin{aligned} \dot{z} &= w\cos(\theta) - u\sin(\theta) \\ \dot{\theta} &= q \end{aligned} \tag{5.1}$$

Similar to the previous section, the longitudinal state equations of body velocity states would be derived as follows.

$$\boldsymbol{M}_{lon}\begin{bmatrix} \dot{w} \\ \dot{q} \end{bmatrix} + \boldsymbol{h}_{lon} = \boldsymbol{T}_{lon}\delta_s \tag{5.2}$$

where

$$\boldsymbol{M}_{lon} = \begin{bmatrix} 0 & mz_G \\ 0 & 0 \\ m - Z_{\dot{w}} & -mx_G - Z_{\dot{q}} \\ my_G & 0 \\ -mx_G - M_{\dot{w}} & I_y - M_{\dot{q}} \\ 0 & 0 \end{bmatrix}$$

$$\boldsymbol{h}_{lon} =$$

$$\begin{bmatrix} -q\left(Z_{\dot{q}}q + Z_{\dot{w}}w - m(w - x_G q)\right) - s\theta(B - W) - X_{u|u|}u|u| \\ 0 \\ c\theta(B - W) - q\left(Z_{uqf}u - X_{\dot{u}}u + Z_{q|q|}|q| + m(u + z_G q)\right) - w\left(Z_{w|w|}|w| + u(Z_{uwf} + Z_{uwl})\right) \\ -y_G(Wc\theta + muq) \\ u\left(Z_{\dot{q}}q + Z_{\dot{w}}w - m(w - x_G q)\right) - w\left(X_{\dot{u}}u + M_{w|w|}|w| + u(M_{uwf} + M_{uwl}) - m(u + z_G q)\right) - q(M_{uqf}u + M_{q|q|}|q|) + x_G Wc\theta + z_G Ws\theta \\ -y_G(Ws\theta + mwq) \end{bmatrix}$$

$$\boldsymbol{T}_{lon} = \begin{bmatrix} 0 \\ 0 \\ Z_{uu\delta_s}u^2 \\ 0 \\ M_{uu\delta_s}u^2 \\ 0 \end{bmatrix}$$

According to (5.2), the state equations is written as

$$\begin{bmatrix} \dot{w} \\ \dot{q} \end{bmatrix} = (\boldsymbol{M}_{lon}^T \boldsymbol{M}_{lon})^{-1} \boldsymbol{M}_{lon}^T (-\boldsymbol{h}_{lon}) + \left(\left(\left(\boldsymbol{M}_{lon}^T \boldsymbol{M}_{pitch}\right)^{-1} \boldsymbol{M}_{lon}^T\right) \boldsymbol{T}_{lon}\right) \delta_s \tag{5.3}$$

Since the calculations above include very long terms, the equations are given in following form and their values are calculated using MATLAB with parameters given in Chapter 3.

$$\begin{bmatrix} \dot{z} \\ \dot{\theta} \\ \dot{w} \\ \dot{q} \end{bmatrix} = \begin{bmatrix} wcos(\theta) - usin(\theta) \\ q \\ f_w \\ f_q \end{bmatrix} + \begin{bmatrix} 0 \\ 0 \\ b_w \\ b_q \end{bmatrix} \delta_s \tag{5.4}$$

where

$$\begin{bmatrix} f_w \\ f_q \end{bmatrix} = (\boldsymbol{M}_{lon}^T \boldsymbol{M}_{lon})^{-1} \boldsymbol{M}_{lon}^T (-\boldsymbol{h}_{lon})$$

$$\begin{bmatrix} b_w \\ b_q \end{bmatrix} = ((\boldsymbol{M}_{lon}^T \boldsymbol{M}_{lon})^{-1} \boldsymbol{M}_{lon}^T) \boldsymbol{T}_{lon}$$

5.2 Depth Control Using Linearized Depth Plane Equations

This section discusses the linearization of the depth plane equations of motion and linear control system design in order to reach the specific depth value.

5.2.1 Linearized Depth Plane Equations

It is assumed that the linear speed w is considered as very small when compared to angular speed q so linear speed w is set to be zero and depth plane equations are simplified [39].

$$\begin{aligned} \dot{z} &= -u_0 sin\theta \\ \dot{\theta} &= q \\ (I_y - M_{\dot{q}})\dot{q} - M_{q|q|}q|q| - M_{uq}uq + Wz_g sin\theta &= M_{uu\delta_s}u_0^2\delta_S \end{aligned} \tag{5.5}$$

The nonlinear terms in (5.5) are linearized and following equations of motion for depth plane are obtained.

$$\begin{aligned} \dot{z} &= -u_0\theta \\ \dot{\theta} &= q \\ (I_y - M_{\dot{q}})\dot{q} - M_q q + Wz_g\theta &= M_{\delta_s}\delta_S \end{aligned} \tag{5.6}$$

The linear equations can be rewritten in matrix form and given in generalized linear system representation as follows.

$$\begin{bmatrix} 1 & 0 & 0 \\ 0 & 1 & 0 \\ 0 & 0 & I_y - M_{\dot{q}} \end{bmatrix}\begin{bmatrix} \dot{z} \\ \dot{\theta} \\ \dot{q} \end{bmatrix} + \begin{bmatrix} 0 & u_0 & 0 \\ 0 & 0 & -1 \\ 0 & Wz_g & -M_q \end{bmatrix}\begin{bmatrix} z \\ \theta \\ q \end{bmatrix} = \begin{bmatrix} 0 \\ 0 \\ M_{\delta_s} \end{bmatrix}\delta_s$$
$$\dot{x} = Ax + Bu; \quad x = [z \quad \theta \quad q]^T; \; u = \delta_s \tag{5.7}$$

where

$$A = \begin{bmatrix} 1 & 0 & 0 \\ 0 & 1 & 0 \\ 0 & 0 & I_y - M_{\dot{q}} \end{bmatrix}^{-1}\begin{bmatrix} 0 & -u_0 & 0 \\ 0 & 0 & 1 \\ 0 & -Wz_g & M_q \end{bmatrix} = \begin{bmatrix} 0 & -1.54 & 0 \\ 0 & 0 & 1 \\ 0 & -0.6892 & -0.8247 \end{bmatrix};$$

$$B = \begin{bmatrix} 1 & 0 & 0 \\ 0 & 1 & 0 \\ 0 & 0 & I_y - M_{\dot{q}} \end{bmatrix}^{-1}\begin{bmatrix} 0 \\ 0 \\ M_{\delta_s} \end{bmatrix} = \begin{bmatrix} 0 \\ 0 \\ -4.1537 \end{bmatrix};$$

5.2.2 Transfer Functions and Linear Controller Design

In this section, a PID controller which consist of an inner proportional and derivative (PD) pitch loop and outer proportional depth loop will be designed using the transfer functions that will be obtained using state equations derived in the previous section.

The first step is to find the inner loop transfer function that defines the relation between the input stern angle δ_s and output pitch angle θ [25]. Taking derivative of θ yileds

$$\ddot{\theta} = \dot{q}$$
$$\left(I_y - M_{\dot{q}}\right)\ddot{\theta} - M_q\dot{\theta} + Wz_g\theta = M_{\delta_s}\delta_S \tag{5.8}$$

Taking Laplace transform of (5.8)

$$\left[\left(I_y - M_{\dot{q}}\right)s^2 - M_q s + Wz_g\right]\theta(s) = M_{\delta_s}\delta_s(s) \tag{5.9}$$

The open loop transfer function $G_\theta(s)$ is finally found as

$$G_\theta(s) = \frac{\theta(s)}{\delta_s(s)} = \frac{\frac{M_{\delta_s}}{I_y - M_{\dot{q}}}}{s^2 - \frac{M_q}{I_y - M_{\dot{q}}}s + \frac{Wz_g}{I_y - M_{\dot{q}}}} \tag{5.10}$$

Then the transfer function between the vehicle pitch angle θ and the vehicle depth position z is easily written such that

$$s\,Z(s) = -u_0\theta(s) \rightarrow\ G_z(s) = \frac{Z(s)}{\theta(s)} = -\frac{u_0}{s} \tag{5.11}$$

Let us now design the controller parameter for pitch and depth loops. Firstly, the pitch error is defined as

$$E_\theta(s) = \theta_d(s) - \ \theta(s)$$

where the θ_d is the desired pitch angle. The PD control law for inner pitch loop can be written as

$$\frac{\delta_s(s)}{E_\theta(s)} = K_{\theta_p}\left(\tau_{\theta_d}s + 1\right) = \ (K_{\theta_p} + K_{\theta_d}s) \tag{5.12}$$

where the K_{θ_p} is the proportional gain and τ_{θ_d} the derivative time constant.

Secondly, let us define the depth position error that is:

$$E_z(s) = Z_d(s) - Z(s)$$

Now the control law for the outer depth loop can be expressed as:

$$\frac{\theta(s)}{E_z(S)} = K_{p_z} \tag{5.13}$$

where the K_{p_z} is the proportional gain.

Substituting the linearized parameters into $G_\theta(s)$, the following transfer open-loop transfer function is found.

$$G_\theta(s) = \frac{-4.1537}{s^2 + 0.8247s + 0.6892} \; ; \quad s_{1,2} = -0.4123 \pm 0.7205i$$

The open loop step response for $G_\theta(s)$ is

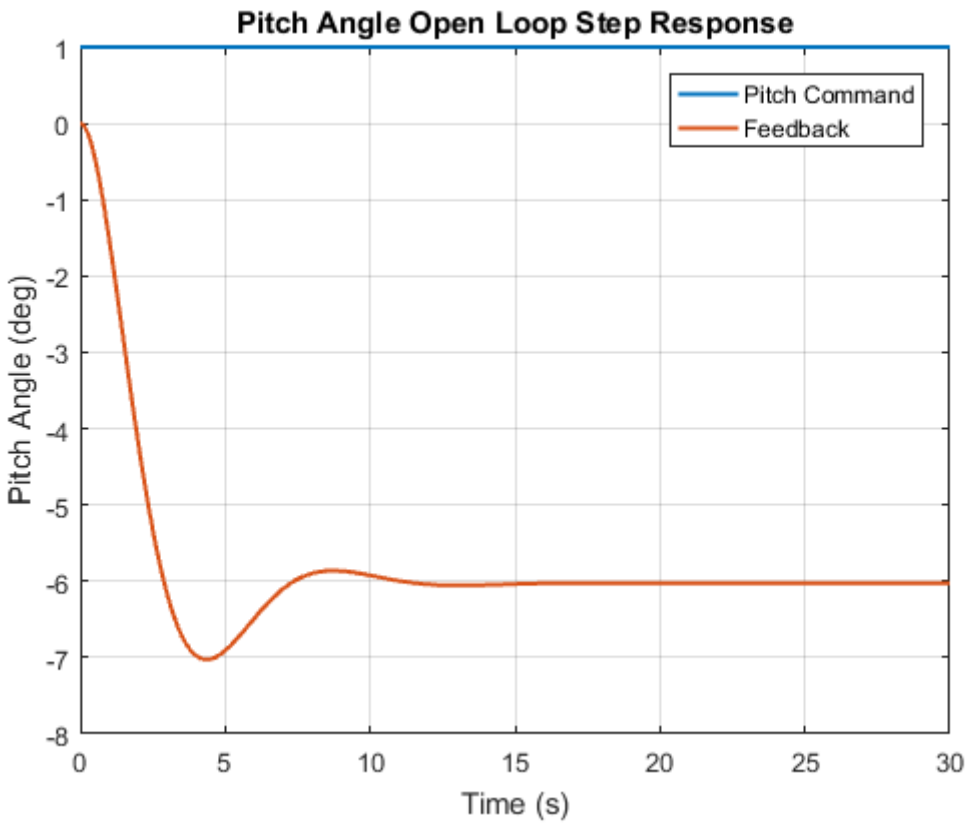

Figure 5.1 Pitch angle open loop step response

The desired specs for the pitch loop are selected as follows.

- $\%OS = 5;$
- $T_p = 0.7\ s$

The damping ratio for the given overshoot values is

$$\zeta = \frac{-\ln\left(\frac{\%OS}{100}\right)}{\sqrt{\pi^2 + \ln^2\left(\frac{\%OS}{100}\right)}} = \frac{-\ln(5)}{\sqrt{\pi^2 + \ln^2(5)}} \cong 0.6901$$

The natural frequency is

$$\omega_n = \frac{\pi}{T_p\sqrt{1-\zeta^2}} = \frac{\pi}{0.7\sqrt{1-0.6901^2}} = 6.2014\, rad/s$$

Desired poles for the closed loop controller system are

$$s_{d_{1,2}} = -\zeta\omega_n \pm \left(\omega_n\sqrt{1-\zeta^2}\right)i = -4.2796 \pm 4.4880i$$

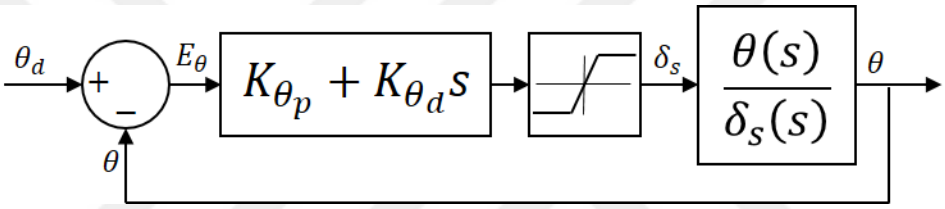

Figure 5.2 Closed loop pitch control block diagram

$$C_\theta(s) = \left(K_{\theta_p} + K_{\theta_d}s\right)$$

$$G_{\theta_{eq}}(s) = \frac{\omega_n^2}{s^2 + 2\zeta\omega_n s + \omega_n^2} = \frac{C_\theta(s)G_\theta(s)}{1 + C_\theta(s)G_\theta(s)}$$

Equalizing the characteristic equations yields

$$s^2 + 8.5592s + 38.4572 = s^2 + \left(0.8247 - 4.154K_{\theta_d}\right)s + (0.6892 - 1.154K_{\theta_p})$$

The pitch controller gains finally found as

$K_{\theta_p} = -9.0920$ and $K_{\theta_d} = -1.8619$

The pitch controller transfer function is

$$C_\theta(s) = K_{\theta_p} + K_{\theta_d}s = -9.0601 - 1.8947s = -9.0920(1 + 0.2091s)$$

Closed loop step response for the pitch is given below.

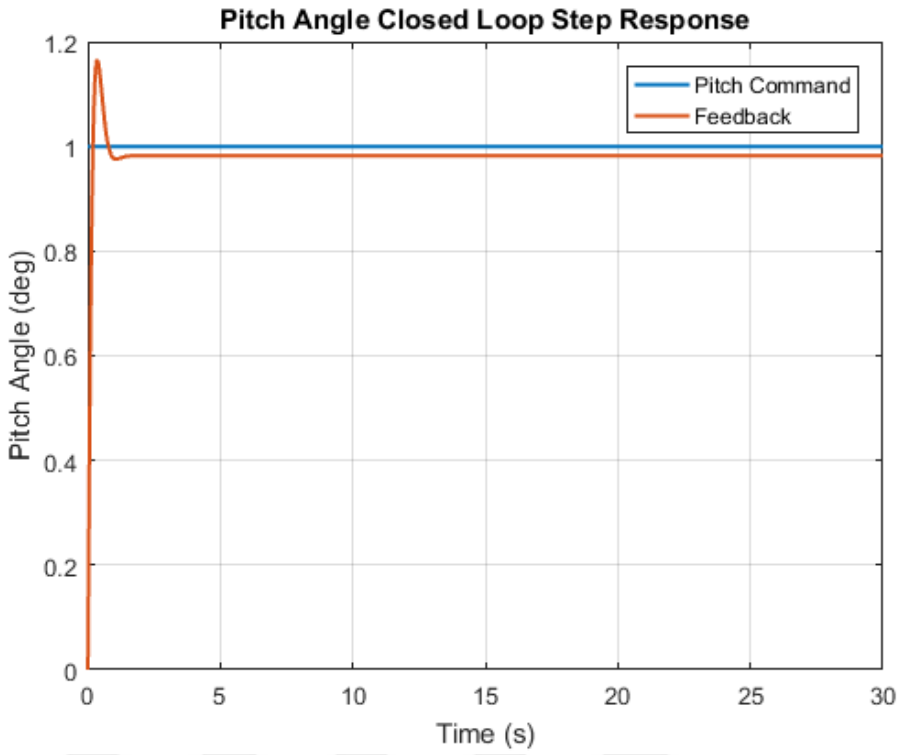

Figure 5.3 Pitch angle closed loop step response

There is approximately 2% steady state error which will be compensated when the outer loop is added. The integrator term can also be added to eliminate the steady state error.

Similar design procedure can be applied in order the find the depth controller gain. The pitch loop poles must be at least five time further away from the origin than the depth poles in order to ensure that the pitch loop response is sufficiently faster than the depth loop response.

The proportional depth gain and closed loop poles for depth response are selected as

$$K_{p_z} = -0.7;\ \ s_{CL_{1,2}} = -0.4124 + 1.8512i$$

The control system block diagram for depth control including the position and fin saturation limits is given below.

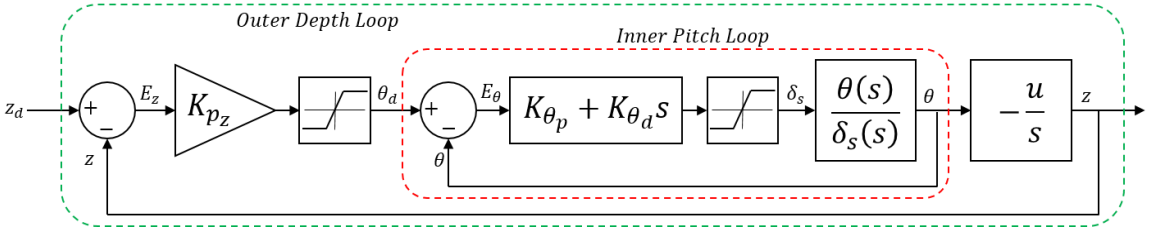

Figure 5.4 Closed loop depth control block diagram

The closed loop response to 30 meters reference depth and related fin angle are given below.

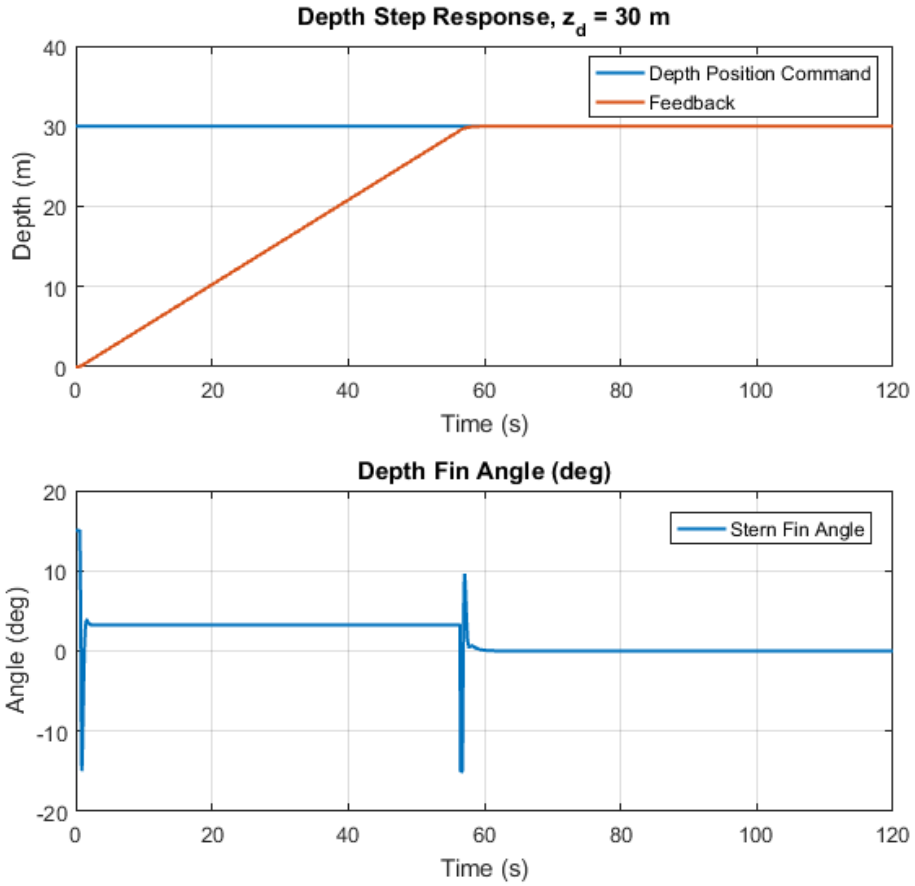

Figure 5.5 Closed loop step response and stern fin angle ($z_d = 30\ m$)

5.3 Nonlinear Switched Depth Control

In this section, nonlinear switched depth control is designed in order to drive the vehicle to dive as fast as possible to the reference depth value in the case of avoiding the appearance of stall.

It is assumed that the critical value for the pitch angle θ is $\bar{\theta}$. The pitch angle θ needs to satisfy the condition $|\theta| \leq \bar{\theta}$ in order to aovid the appearance of the stall. Let us consider the depth dynamics of the vehicle.

$$\dot{z} = -u\theta$$

$$\dot{\theta} = q$$

$$\dot{q} = f_q + b_q \delta_s$$

where

$f_q = -0.70465sin(\theta) - 0.50715q - 22.603q|q| - 0.018872q^2 - 0.033384;$

$b_q = -1.6733;$

We let z_d and z_s represent the desired depth and switch point respectively. The control strategy is divided into two part [40].

Case 1: $|z(0) - z_d| \leq z_s$

The design of δ_s can be given based on the backstepping method in three steps [37].

Step 1: Consider

$\dot{z} = -u\theta$

if taking $x_1 = z - z_d$ and $x_2 = \mu_1 x_1 - u\theta$

$$\dot{x}_1 = -\mu_1 x_1 + x_2 \tag{5.14}$$

where μ_1 is a positive design parameter. Let $V_1 = 0.5x_1^2$, then the derivative of V_1 with respect to time t along the trajectory of the system is:

$$\dot{V}_1 = -\mu_1 x_1^2 + x_1 x_2 \tag{5.15}$$

Step 2: Consider

$\dot{x}_1 = -\mu_1 x_1 + x_2$

$\dot{x}_2 = \mu_1 \dot{x}_1 - u\dot{\theta} = -\mu_1^2 x_1 + \mu_1 x_2 - uq$

Let $x_3 = (\mu_1 + \mu_2)x_2 - \mu_1^2 x_1 - uq$, we can get

$$\begin{aligned} \dot{x}_1 &= -\mu_1 x_1 + x_2 \\ \dot{x}_2 &= -\mu_2 x_2 + x_3 \end{aligned} \tag{5.16}$$

where μ_2 is a positive design parameter. Take Lyapunov function $V_2 = V_1 + 0.5x_2^2$, we can get

$$\dot{V}_2 = \dot{V}_1 + x_2 \dot{x}_2 = -\mu_1 x_1^2 + x_1 x_2 - \mu_2 x_2^2 + x_2 x_3 \tag{5.17}$$

Step 3: Consider

$\dot{x}_1 = -\mu_1 x_1 + x_2$

$$\dot{x}_2 = -\mu_2 x_2 + x_3$$

$$\dot{x}_3 = [\mu_1^3 x_1 - (\mu_1^2 + \mu_1\mu_2 + \mu_2^2)x_2 + (\mu_1 + \mu_2)x_3] - uf_q - ub_q\delta_s$$

if taking

$$\delta_s = \frac{1}{b_q u}\left([\mu_1^3 x_1 - (\mu_1^2 + \mu_1\mu_2 + \mu_2^2)x_2 + (\mu_1 + \mu_2 + \mu_3)x_3] - uf_q\right) \tag{5.18}$$

we can get

$$\begin{aligned}\dot{x}_1 &= -\mu_1 x_1 + x_2 \\ \dot{x}_2 &= -\mu_2 x_2 + x_3 \\ \dot{x}_3 &= -\mu_3 x_3\end{aligned} \tag{5.19}$$

where μ_3 is a positive design parameter.

We take Lyapunov function $V_3 = V_1 + V_2 + 0.5x_3^2$, then

$$\begin{aligned}\dot{V} &= -\mu_1 x_1^2 - x_1 x_2 + \mu_2 x_2^2 - x_2 x_3 + \mu_3 x_3^2 \\ &= -[x_1 \quad x_2 \quad x_3]\begin{bmatrix}\mu_1 & -\frac{1}{2} & 0 \\ -\frac{1}{2} & \mu_2 & -\frac{1}{2} \\ 0 & -\frac{1}{2} & \mu_3\end{bmatrix}\begin{bmatrix}x_1 \\ x_2 \\ x_3\end{bmatrix} = -[x_1 \quad x_2 \quad x_3]A\begin{bmatrix}x_1 \\ x_2 \\ x_3\end{bmatrix}\end{aligned} \tag{5.20}$$

where the matrix A can be made positive definite based on the choice of design parameters μ_i such that

$$\mu_1 > 0;\ \ \mu_1\mu_2 - \frac{1}{4} > 0; \mu_1\mu_2\mu_3 - \frac{1}{4}\mu_1 - \frac{1}{4}\mu_3 > 0 \tag{5.21}$$

Hence according to Lyapunov's stability theorem [41] we can get the equilibrium point $(0, 0, 0)^T$ of the system (5.19) with the control (5.18), hence the equilibrium point $(z_e, 0, 0)^T$ is asymptotic stable under the control input with the form

$$\delta_s = \frac{\left[(\mu_1\mu_2 + \mu_2\mu_3 + \mu_1\mu_3)u\theta - \mu_1\mu_2\mu_3(z - z_d) + (\mu_1 + \mu_2 + \mu_3)uq + f_q u\right]}{b_q u} \tag{5.22}$$

and design parameters μ_i satisfy condition (5.21).

Case 2: $|z(0) - z_d| > z_s$

In this case, the total diving process is divided into two stages to design controllers:

First, the control law is designed to drive the pitch angle to the desired point and then let the vehicle dive to the neighborhood $\{z : |z - z_d| \leq z_s\}$ of the desired depth with the desired pitch angle.

Step 1: Consider $\dot{\tilde{z}} = -u\theta$ with $\tilde{z} = z - z_d$, it is not difficult to get that the AUV is diving only if $\theta\dot{\tilde{z}}(0) > 0$. Hence if define the absolute value of desired pitch angle as θ_d, in order to drive the vehicle to desired depth z_d we need to drive its pitch angle to $sign\big(\tilde{z}(0)\big)\theta_d$.

Step 2: Consider $\dot{\theta} = q$, if taking $\tilde{x}_1 = \theta - sign\big(\tilde{z}(0)\big)\theta_d$ and $\tilde{x}_2 = q + \tilde{\mu}_1\tilde{x}_1$, we can get

$$\dot{\theta} = -\tilde{\mu}_1\tilde{x}_1 + \tilde{x}_2 \tag{5.23}$$

where $\tilde{\mu}_1 > 0$ is the design parameter. If let $\tilde{V}_1 = 0.5\tilde{x}_1^2$, we have $\dot{\tilde{V}} = -\tilde{\mu}_1\tilde{x}_1^2 + \tilde{x}_1\tilde{x}_2$.

Step 3: Consider

$\dot{\theta} = -\tilde{\mu}_1\tilde{x}_1 + \tilde{x}_2$

$\dot{\tilde{x}}_2 = \dot{q} + \tilde{\mu}_1\dot{\tilde{x}}_1 = f_q + b_q\delta_s - \tilde{\mu}_1^2\tilde{x}_1 + \tilde{\mu}_1\tilde{x}_2.$

If taking

$$\delta_s = \frac{\tilde{\mu}_1^2\tilde{x}_1 - \tilde{\mu}_1\tilde{x}_2 - f_q - \tilde{\mu}_2\tilde{x}_2}{b} = \frac{-\tilde{\mu}_1\tilde{\mu}_2\tilde{x}_1 - f_q - (\tilde{\mu}_1 + \tilde{\mu}_2)q}{b} \tag{5.24}$$

and $\tilde{V}_2 = \tilde{V}_1 + 0.5\tilde{x}_2^2$

$$\begin{aligned} \dot{\theta} &= -\tilde{\mu}_1\tilde{x}_1 + \tilde{x}_2 \\ \dot{\tilde{x}}_2 &= -\tilde{\mu}_2\tilde{x}_2 \end{aligned} \tag{5.25}$$

and $\dot{\tilde{V}}_2 = -\tilde{\mu}_1\tilde{x}_1^2 + \tilde{x}_1\tilde{x}_2 - \tilde{\mu}_2\tilde{x}_2^2$, where $\tilde{\mu}_2 > 0$ is a positive design parameter. We can make the right-hand side of above equation negative definite by selecting design parameters $\tilde{\mu}_1 > 0$ and $\tilde{\mu}_1\tilde{\mu}_2 > 0.25$ suitably. Figure 5.6 shows the depth step response of the system, corresponding pitch motion and fin angle.

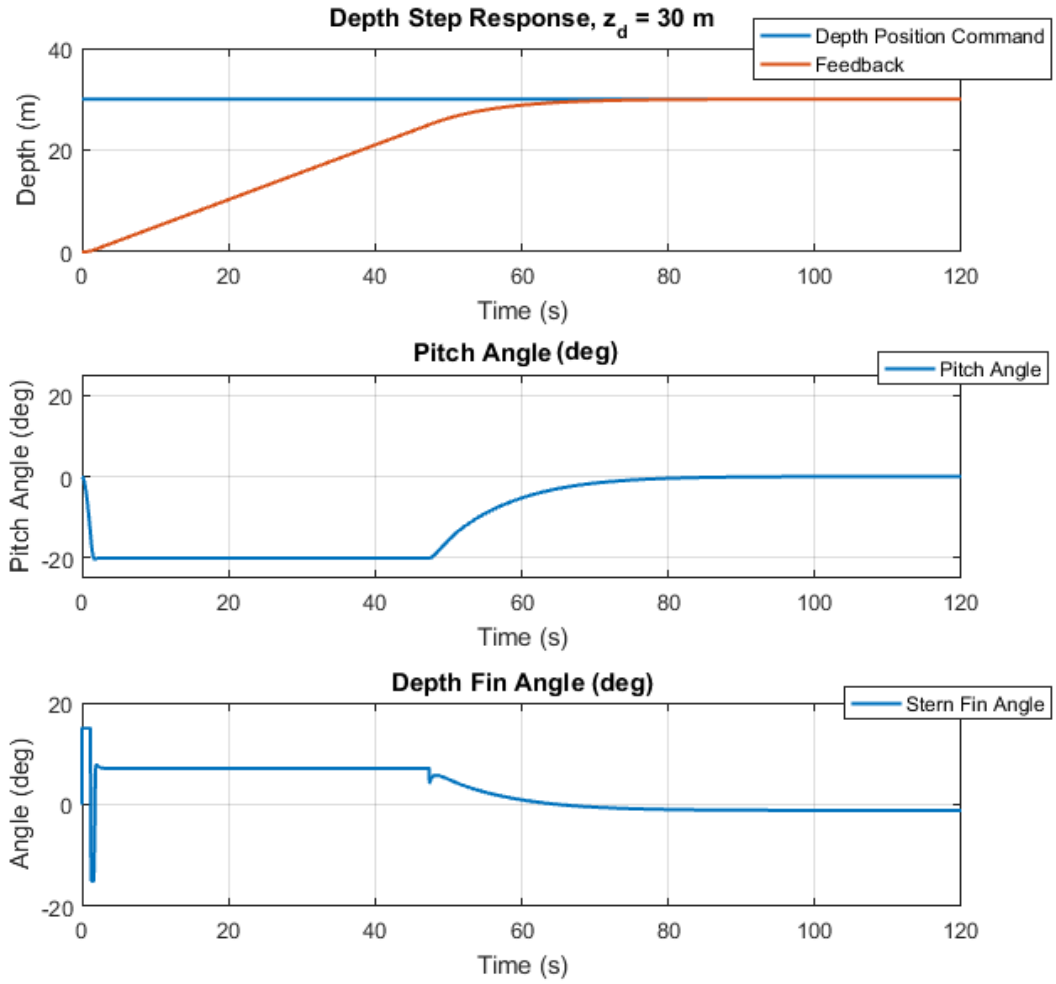

Figure 5.6 Nonlinear switched depth control step response, pitch angle and stern fin angle ($z_d = 30\ m$)

The pitch angle is firstly reached to its maximum value that is defined as 20 degree using the control rule found in (5.24). Then the (5.22) let the vehicle dive to the desired depth position.

In Section 5.2, the linearized equations of motion have been obtained and PD type controller has been designed and implemented. The PD type controller is easy to apply and controller parameters can be calculated using analytical methods. However, linearization and/or negligence of nonlinear terms can cause unpredictable behaviors in real applications.

The nonlinear switched control designed in the section 5.3 has been used to drive the AUV to desired depth as fast as possible on the basis of avoiding the appearance of stall.

The simulation results shows the effectiveness of method. The difficulty in this method is to find the optimal controller parameters. This problem can be achieved using optimization tools and algorithms which are available in literature and actively used in many applications. This method has also advantages in terms of considering nonlinear effects and switching between pitch and depth controls.

Figure 5.7 shows the comparison between linear and nonlinear depth control of AUV. The vehicle's surge velocity u_0 has been changed from 1.54 m/s to 2.5 m/s.

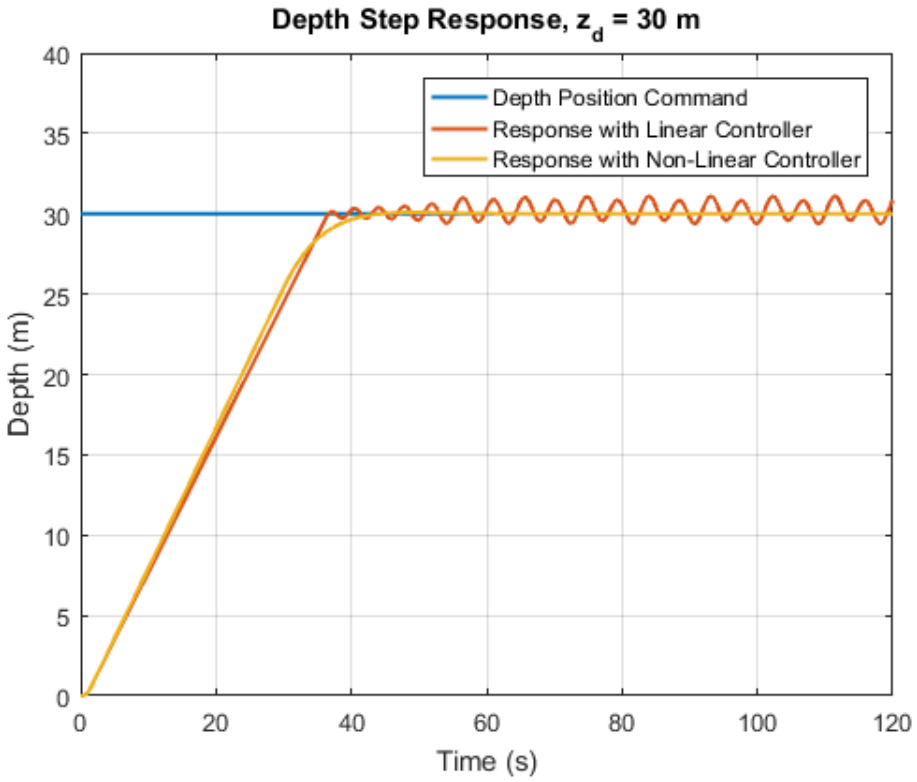

Figure 5.7 Comparison between Linear and Nonlinear Depth Control of AUV

It is clearly seen from the figure that the system shows better performance with nonlinear controller when the velocity of the AUV changes. The nonlinear controller, in other words, is more sensitive to parameter changes in the system when compared to linear controller.

CHAPTER 6

LATITUDINAL DYNAMICS AND HEADING CONTROL

In this section, horizontal plane dynamics of the AUV is derived and nonlinear controllers are applied in order to reach the desired heading (yaw) angle with respect to earth-fixed coordinate frame.

6.1 Horizontal Plane Equations of Motion

The horizontal plane dynamics can be obtained similar to processes given in the previous sections. The linear position and yaw angle equation is found easily by taking $\phi = \theta = w = p = q = 0$.

$$\dot{y} = usin(\psi) + vcos(\psi)$$
$$\dot{\psi} = r \tag{6.1}$$

Linear and angular body velocity equations is written as:

$$\boldsymbol{M}_{lat}\begin{bmatrix}\dot{v}\\ \dot{r}\end{bmatrix} + \boldsymbol{h}_{lat} = \boldsymbol{T}_{lat}\delta_r \tag{6.2}$$

where

$$\boldsymbol{M}_{lat} = \begin{bmatrix} 0 & -my_G \\ m - Y_{\dot{v}} & mx_G - Y_{\dot{r}} \\ 0 & 0 \\ -mz_G & 0 \\ 0 & 0 \\ mx_G - N_{\dot{v}} & I_z - N_{\dot{r}} \end{bmatrix}$$

$$\boldsymbol{h}_{lat} = \begin{bmatrix} r\left(Y_{\dot{r}}r + Y_{\dot{v}}v - m(v + x_G r)\right) - X_{u|u|}u|u| \\ -r\left(X_{\dot{u}}u + Y_{urf}u + Y_{r|r|}|r| - m(u - y_G r)\right) - v\left(Y_{v|v|}|v| + u\left(Y_{uvf} + Y_{uvl}\right)\right) \\ B - W \\ -y_G W - mz_G ur \\ x_G W - mz_G vr \\ -u\left(Y_{\dot{r}}r + Y_{\dot{v}}v - m(v + x_G r)\right) - v\left(N_{v|v|}|v| - X_{\dot{u}}u + u\left(N_{uvf} + N_{uvl}\right) + m(u - y_G r)\right) - r\left(N_{urf}u + N_{r|r|}|r|\right) \end{bmatrix}$$

$$\boldsymbol{T}_{yaw} = \begin{bmatrix} 0 \\ Y_{uu\delta_r}u^2 \\ 0 \\ 0 \\ 0 \\ N_{uu\delta_r}u^2 \end{bmatrix}$$

According to (6.2), the state equations is written as

$$\begin{bmatrix} \dot{v} \\ \dot{r} \end{bmatrix} = (\boldsymbol{M}_{lat}^T \boldsymbol{M}_{lat})^{-1} \boldsymbol{M}_{lat}^T (-\boldsymbol{h}_{lat}) + ((\boldsymbol{M}_{lat}^T \boldsymbol{M}_{lat})^{-1} \boldsymbol{M}_{lat}^T \boldsymbol{T}_{lat})\delta_r \tag{6.3}$$

Since the calculations above include very long terms, the yaw equations is given in following form and values are calculated using MATLAB.

$$\begin{bmatrix} \dot{y} \\ \dot{\psi} \\ \dot{v} \\ \dot{r} \end{bmatrix} = \begin{bmatrix} usin(\psi) + vcos(\psi) \\ r \\ f_v \\ f_r \end{bmatrix} + \begin{bmatrix} 0 \\ 0 \\ b_v \\ b_r \end{bmatrix} \delta_r \tag{6.4}$$

where

$$\begin{bmatrix} f_v \\ f_r \end{bmatrix} = (\boldsymbol{M}_{lat}^T \boldsymbol{M}_{lat})^{-1} \boldsymbol{M}_{lat}^T (-\boldsymbol{h}_{lat})$$

$$\begin{bmatrix} b_v \\ b_r \end{bmatrix} = ((\boldsymbol{M}_{lat}^T \boldsymbol{M}_{lat})^{-1} \boldsymbol{M}_{lat}^T \boldsymbol{T}_{lat})$$

Using the parameter values, which are the parameters of the REMUS vehicle in [25], the dynamics of horizontal plane is obtained.

$$\begin{bmatrix} f_v \\ f_r \end{bmatrix} = \begin{bmatrix} -0.80243v - 20.0v|v| - 0.60456r - 0.32267r|r| \\ -0.50996r - 11.359r|r| - 4.6135v - 5.0125v|v| \end{bmatrix} \text{ and}$$

$$\begin{bmatrix} b_v \\ b_r \end{bmatrix} = \begin{bmatrix} 0.29728 \\ -1.6821 \end{bmatrix}$$

Finally, the total dynamics of the horizontal plane is:

$$\begin{bmatrix} \dot{y} \\ \dot{\psi} \\ \dot{v} \\ \dot{r} \end{bmatrix} = \begin{bmatrix} usin(\psi) + vcos(\psi) \\ r \\ -0.80243v - 20.0v|v| - 0.60456r - 0.32267r|r| \\ -0.50996r - 11.359r|r| - 4.6135v - 5.0125v|v| \end{bmatrix} + \begin{bmatrix} 0 \\ 0 \\ 0.29728 \\ -1.6821 \end{bmatrix} \delta_r \qquad (6.5)$$

6.2 Proportional Yaw Position Control Using Feedback Linearized Angular Velocity

The control of yaw angle can be performed using cascaded position and velocity controllers [42],[47]. It is assumed that the linear velocity of the vehicle is stable while controlling the angular velocity of the AUV. State equations for the angular position ψ amd velocity r can be written from (6.5).

$$\dot{\psi} = r$$

$$\dot{r} = -0.50996r - 11.359r|r| - 4.6135v - 5.0125v|v| - 1.6821\delta_r = f_v + b_v\delta_r$$

The velocity error between de desired velocity and feedback is defined as $e_r = r - r_d$. Differentiating the error and substituting into equation above yields:

$$\begin{aligned} \dot{e}_r &= \dot{r} - \dot{r}_d \\ \dot{e}_r + \dot{r}_d &= f_r + b_r\delta_r \end{aligned} \qquad (6.6)$$

Rudder angle is chosen to obtain the error dynamics that goes to zero with time to infinity.

$$\begin{aligned} \delta_r &= \left(\frac{1}{b_r}\right)(-f_r + \dot{r}_d - K_r e_r) \\ \dot{e}_r + K_r e_r &= 0 \end{aligned} \qquad (6.7)$$

where K_r is positive design parameter.

The control rule in (6.7) will be used in the inner loop of the horizontal plane controller. Velocity command is created from the outer loop controller which is proportional position controller. The general block diagram for the cascaded position and velocity controllers is given below.

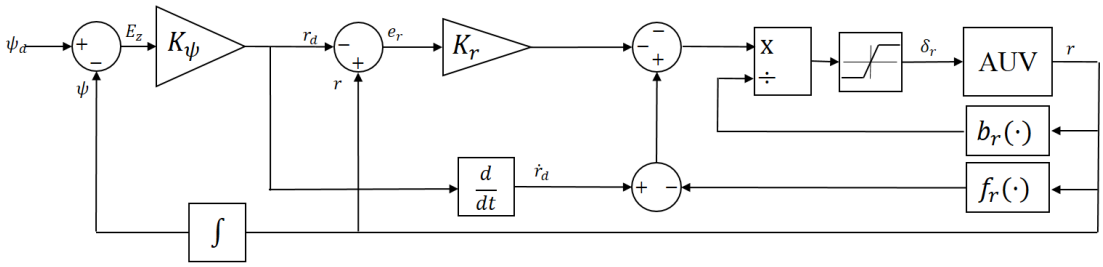

Figure 6.1 Cascaded heading position and velocity controllers

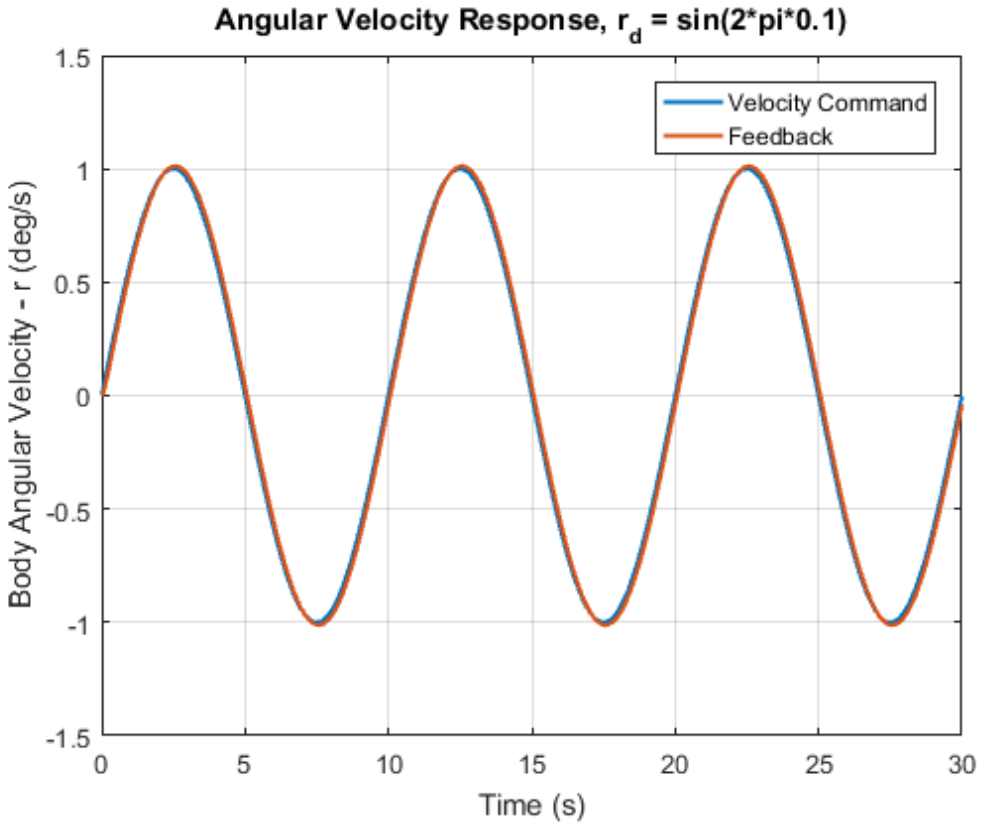

Figure 6.2 Angular velocity tracking response around *z* axis

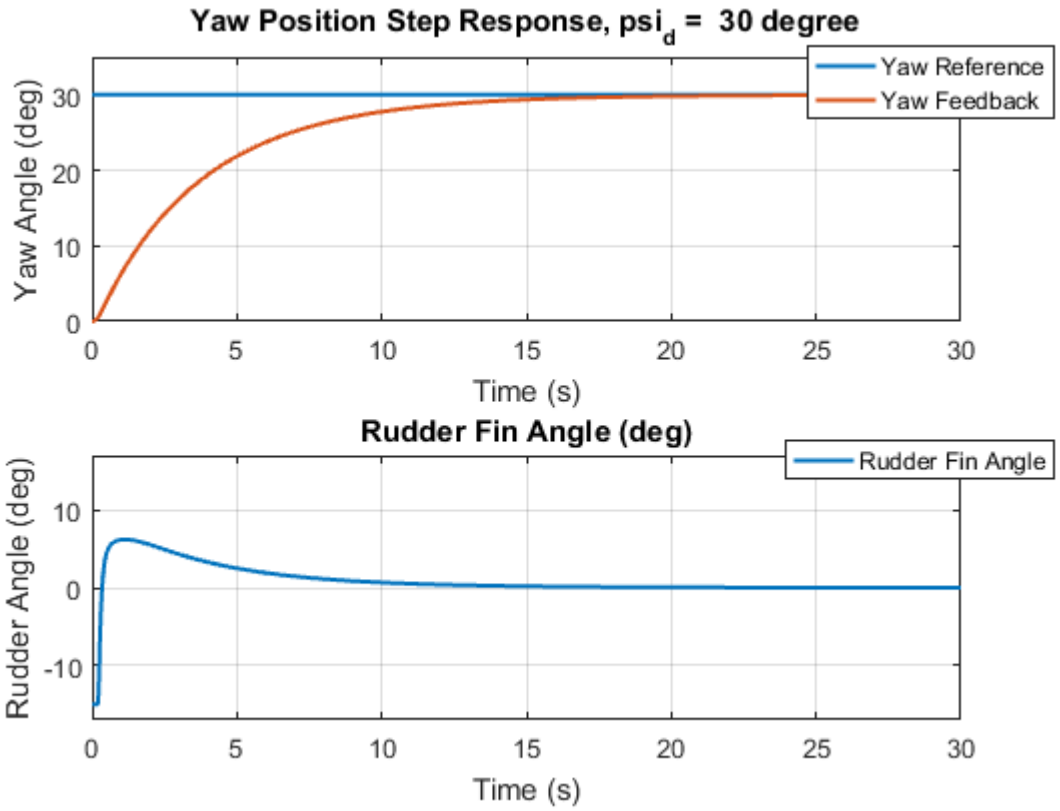

Figure 6.3 Yaw position step response and corresponding rudder fin angle ($\psi_d = 30°$)

Figure 6.2 shows that feedback linearized speed controller is successfully tracking the reference speed values. Proportional yaw position controller is added as outer loop and step response to the constant reference position value is given in Figure 6.3. These figures imply that cascaded position and velocity controllers are working successfully in order to control the yaw angle of the vehicle.

6.3 Single Input Multiple States (SIMS) Sliding Mode Control

In heading control, single input multiple states (SIMS) sliding mode control defined in [21],[38],[46] is used. The nonlinear damping terms are neglected and following linear equations of motion in lateral plane are obtained from the (6.5).

$$\begin{bmatrix} \dot{v} \\ \dot{r} \\ \dot{\psi} \end{bmatrix} = \begin{bmatrix} -0.80243 & -0.60456 & 0 \\ -4.6135 & -0.50996 & 0 \\ 0 & 1 & 0 \end{bmatrix} \begin{bmatrix} v \\ r \\ \psi \end{bmatrix} + \begin{bmatrix} 0.29728 \\ -1.6821 \\ 0 \end{bmatrix} \delta_r \tag{6.8}$$

The linear lateral system can be written as generalized linear system.

$$\dot{\boldsymbol{x}} = \boldsymbol{A}\boldsymbol{x} + \boldsymbol{B}u + \boldsymbol{f}(\boldsymbol{x}) \tag{6.9}$$

where

$$A = \begin{bmatrix} -0.80243 & -0.60456 & 0 \\ -4.6135 & -0.50996 & 0 \\ 0 & 1 & 0 \end{bmatrix} = \begin{bmatrix} A_{11} & A_{12} & 0 \\ A_{21} & A_{22} & 0 \\ 0 & 1 & 0 \end{bmatrix}$$

$$B = \begin{bmatrix} 0.29728 \\ -1.6821 \\ 0 \end{bmatrix} = \begin{bmatrix} B_1 \\ B_2 \\ 0 \end{bmatrix},$$

$\boldsymbol{f}(x)$ is considered as a nonlinear function that describes the deviation from linearity in terms of disturbances and unmodelled dynamics [38].

The set of sliding surfaces based on state variable errors is defined.

$$\sigma(\tilde{\boldsymbol{x}}) = \boldsymbol{h}^T \tilde{\boldsymbol{x}} \tag{6.10}$$

where $\tilde{\boldsymbol{x}} = \boldsymbol{x} - \boldsymbol{x}_d$ is the tracking error and $\boldsymbol{h} \in R^n$ is a vector of known coefficients which are not arbitrary and calculated later. The control law for the heading control system is given below:

$$u = \hat{u} + \bar{u} \tag{6.11}$$

where $\hat{u} = -\boldsymbol{K}\boldsymbol{x}$ and $\bar{u}$ is the sliding controller. Substituting these inputs to (6.9) yields

$$\dot{\boldsymbol{x}} = (\boldsymbol{A} - \boldsymbol{B}\boldsymbol{K})\boldsymbol{x} + \boldsymbol{B}\bar{u} + \boldsymbol{f}(x) = \boldsymbol{A}_c\boldsymbol{x} + \boldsymbol{B}\bar{u} + f(x) \tag{6.12}$$

The gain vector $\boldsymbol{K}$ can be calculated by pole placement specifying the closed loop state matrix $\boldsymbol{A}_c$ [45]. The nonlinear part $\bar{u}$ is selected as:

$$\bar{u} = (\boldsymbol{h}^T\boldsymbol{B})^{-1}\left(\boldsymbol{h}^T\dot{\boldsymbol{x}}_d - \boldsymbol{h}^T\hat{\boldsymbol{f}}(\boldsymbol{x}) - \eta sgn(\sigma)\right), \eta > 0 \tag{6.13}$$

where $\hat{\mathbf{f}}(\mathbf{x})$ is the estimate of $\mathbf{f}(\mathbf{x})$. The vector of $\mathbf{h}$ can be chosen as the right eigenvector of $\mathbf{A}_c^{\mathrm{T}}$ for the eigenvalue $\lambda = 0$. The sliding dynamics finally reduces to

$$\dot{\sigma} = -\eta \mathrm{sgn}(\sigma) + \mathbf{h}^{\mathrm{T}}\tilde{\mathbf{f}}; \quad \tilde{\mathbf{f}} = \mathbf{f} - \hat{\mathbf{f}} \tag{6.14}$$

The Lyapunov function candidate can be chosen as energy like function [46] and differentiation the Lyapunov function yields

$$\begin{aligned} V &= 0.5\sigma^2 \\ \dot{V} &= \sigma\dot{\sigma} = -\eta|\sigma| + \sigma h^T\tilde{f} \end{aligned} \tag{6.15}$$

Selecting the η according to condition $\eta > ||h|| \cdot ||\tilde{f}||$ ensures that $\dot{V} \leq 0$ and σ converges to zero in finite time. In implementation, $sgn(\sigma)$ is replaced with $tanh(\sigma/\phi)$ in order to remove chattering and discontinuities [48],[49]. Here the parameter ϕ is called

the sliding surface boundary layer thickness. Finally, the following control law for heading system is obtained:

$$u = -Kx + (\boldsymbol{h}^T\boldsymbol{B})^{-1}[\boldsymbol{h}^T\dot{\boldsymbol{x}}_d - \boldsymbol{h}^T\hat{\boldsymbol{f}}(\boldsymbol{x}) - \eta\, tanh(\sigma/\phi)] \tag{6.16}$$

The control system block diagram for heading subsystem is given in Figure 6.4.

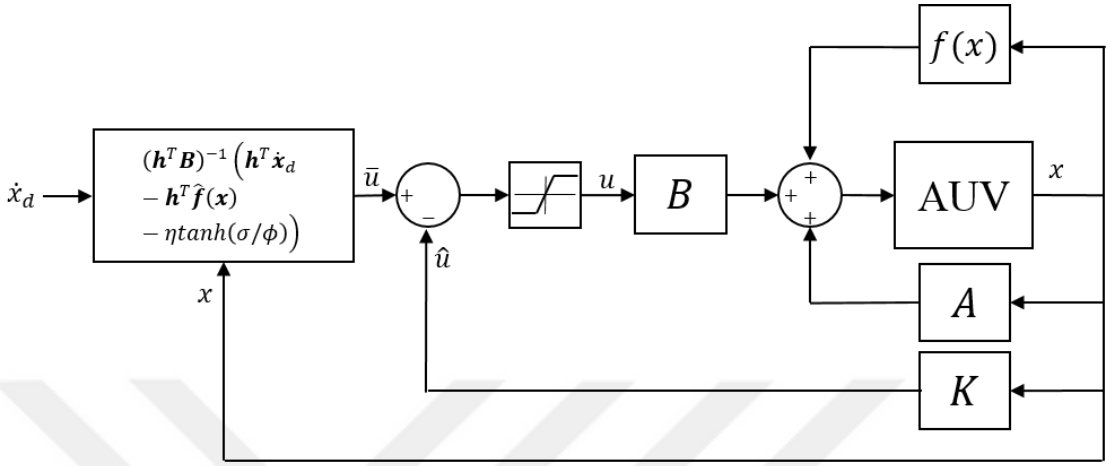

Figure 6.4 Heading Control System Block Diagram

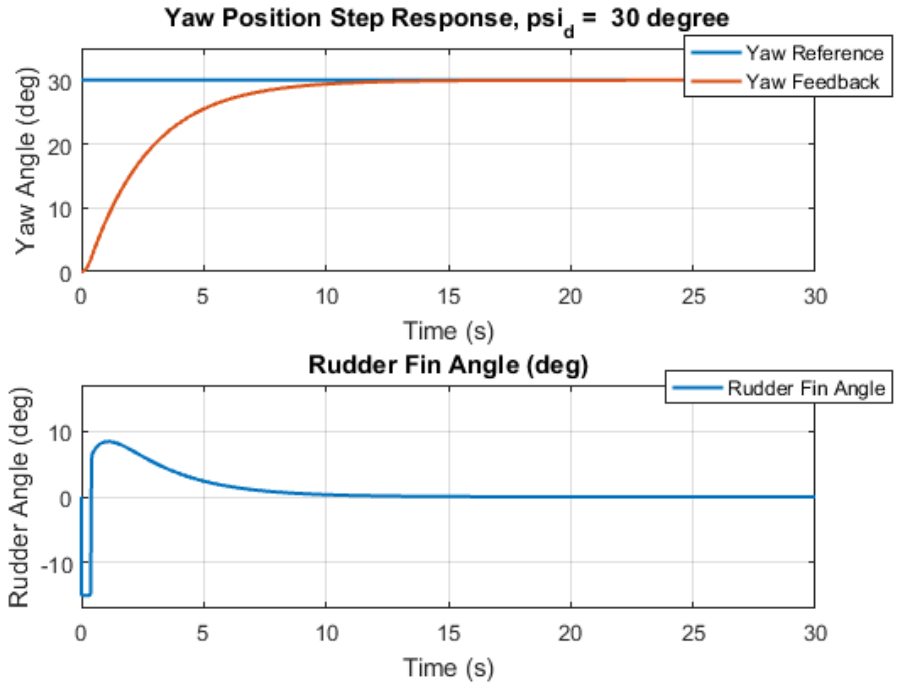

Figure 6.5 SIMS yaw position control step response and corresponding rudder fin angle, ($\psi_d = 30°$)

Figure 6.5 shows the step response of the heading angle to constant reference position value. The single input multiple states sliding mode control has been successfully applied to the decoupled heading dynamics.

In Section 6.2, cascaded proportional yaw position and feedback linearized speed controllers have been performed. The obtained results show that vehicle has reached to the reference values. The implementation of controllers and finding the controller parameters are easy if the parameters are known.

Single Input Multiple States (SIMS) sliding mode controller has been designed in Section 6.3. The sliding mode controller is more difficult to implement compared to previous controller. Controller parameters can be found using simulation results and/or optimization methods similar to the previous sections' controllers. The most important property of the sliding mode controller is robustness with respect to parametric uncertainties and disturbances.

Figure 6.6 shows the comparison between cascaded and sliding mode heading control of AUV. The vehicle's surge velocity u_0 has been changed from 1.54 m/s to 2.5 m/s and unmodelled dynamics $f(x)$ has been added to the system input as $0.2\sin\big((0.2\pi)t\big)$.

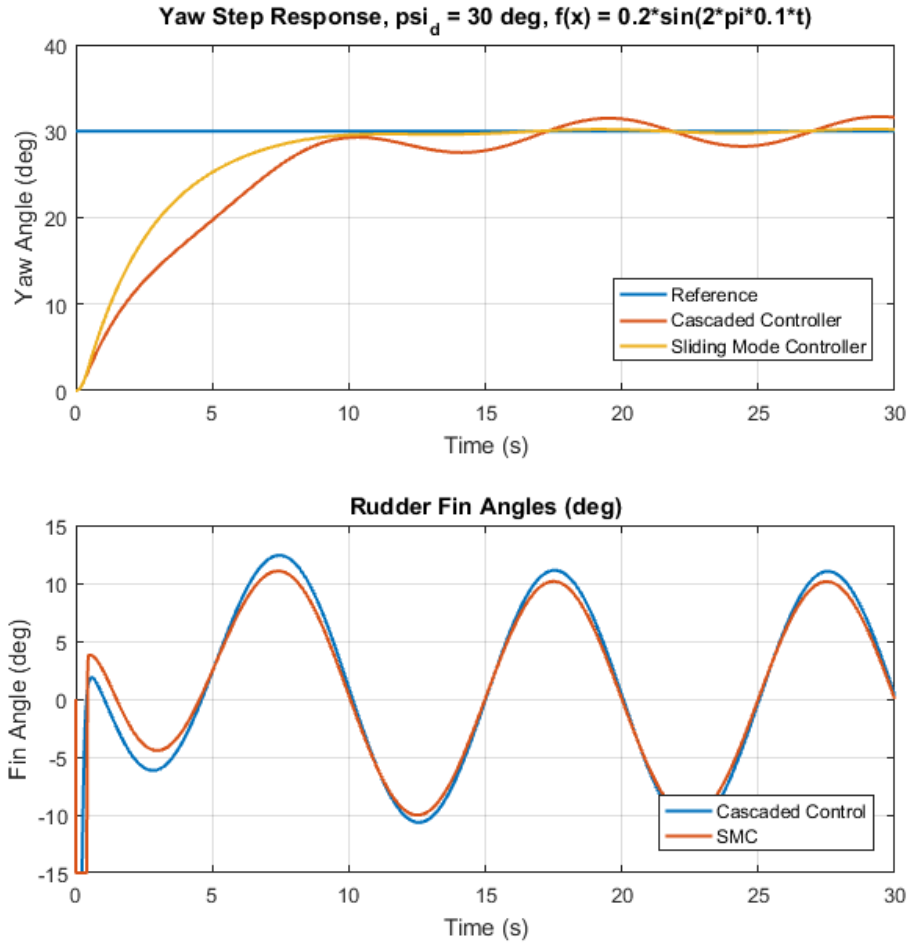

Figure 6.6 Comparison between Cascaded and Sliding Mode Heading Control of AUV

It is inferred from the figure that the system has better performance with sliding mode controller after changing parameters and adding disturbance. The sliding mode controller, in other words, is said to be more robust with respect to parametric uncertainties and disturbances as mentioned before.

CHAPTER 7

6-DOF SIMULATION WITH DECOUPLED CONTROLLERS

In previous chapters, the 6-DOF equations of motion have been obtained and different decoupled controller have been designed and implemented separately. It is expected that the vehicle shows similar behavior when decoupled controllers are applied to the 6-DOF dynamics at the same time.

In this chapter, 6-DOF model in (3.75) is implemented using MATLAB/Simulink and decoupled controllers are applied to the system simultaneously. The block diagram including decoupled controllers for the 6-DOF AUV in Figure 7.1 shows the inputs and outputs of the vehicle and controllers.

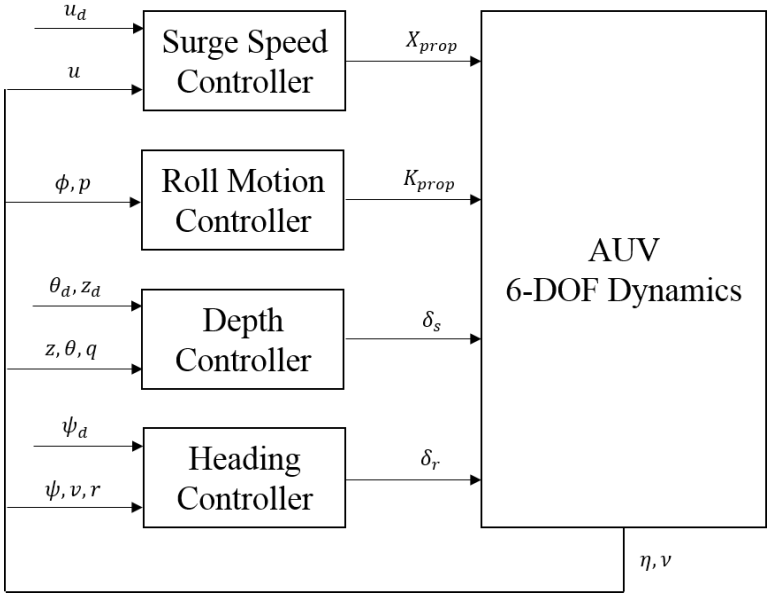

Figure 7.1 6-DOF block diagram including decoupled controllers

In previous chapters, many controllers have been designed and implemented. Table 7.1 shows the selected controllers that are used in 6-DOF simulation.

Table 7.1 Selected Decoupled Controllers

Decoupled System	**Control Method**
Surge Motion	Feedback Linearization
Roll Motion	Backstepping Control
Depth Motion	Nonlinear Switched Control
Heading Motion	SIMS Sliding Mode Control

The reference speed of the vehicle is constant value which is $u = 1.54\ m/s$. The roll motion controller is used to make the roll angle and velocity zero. Other reference values for depth and heading angles are given in Table 7.2.

Table 7.2 Reference Values For Depth And Heading Angle

Time Range (s)	**Depth (m)**	**Heading Angle (deg)**
0-10	0	0
10-40	5	0
40-100	5	60
100-140	5	-30
140-180	1	0

Using the controllers and reference values given in Table 7.1 and Table 7.2, following system responses are obtained from the 6-DOF simulation.

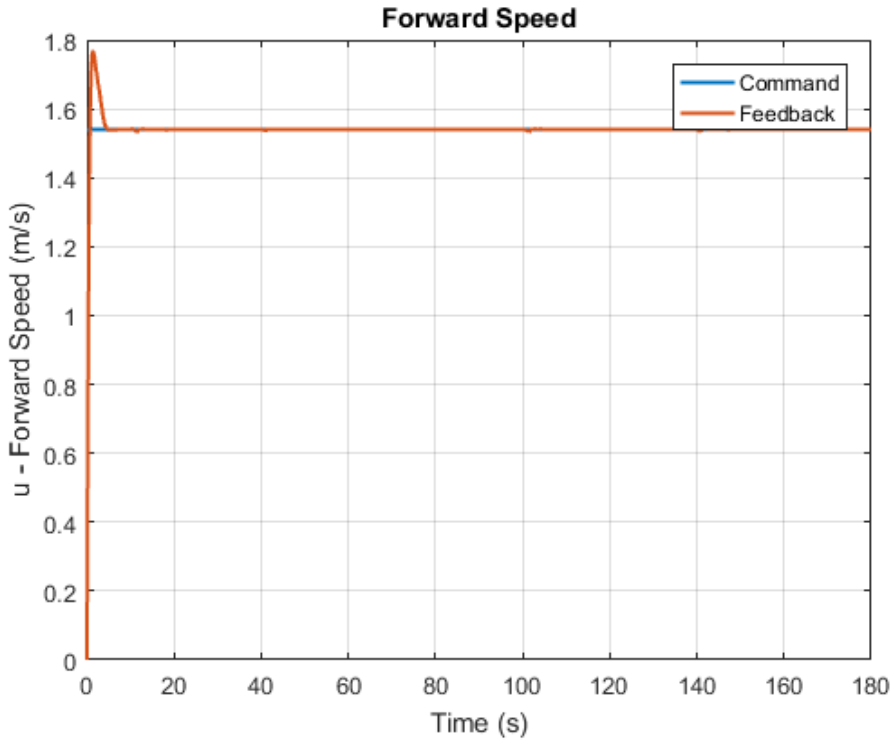

Figure 7.2 Forward speed response in 6-DOF simulation

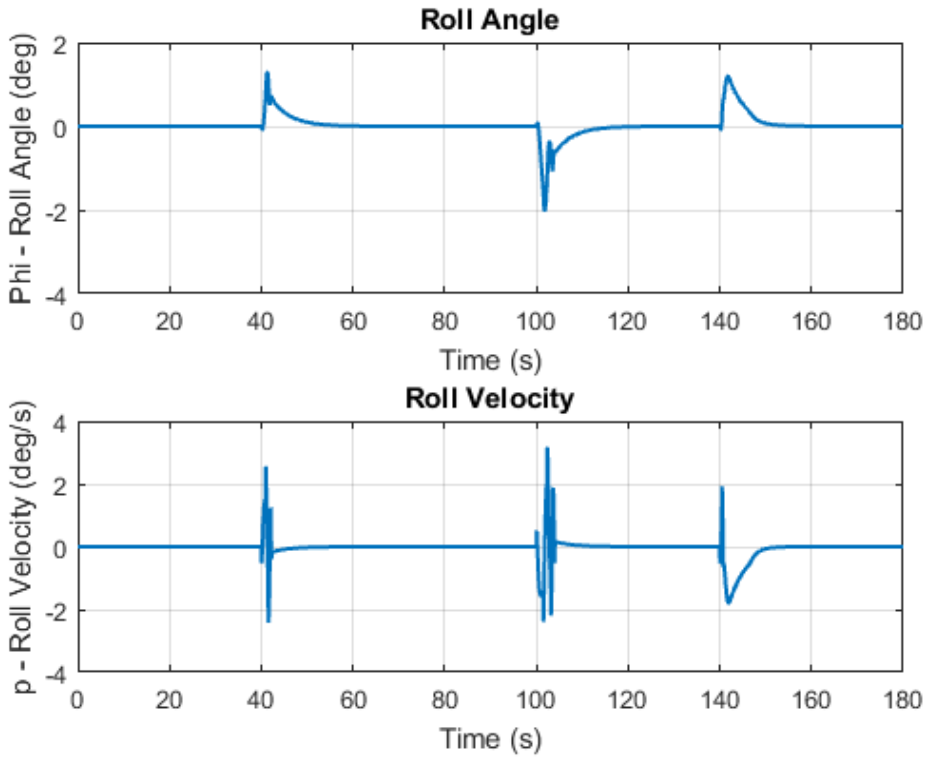

Figure 7.3 Roll position response in 6-DOF simulation

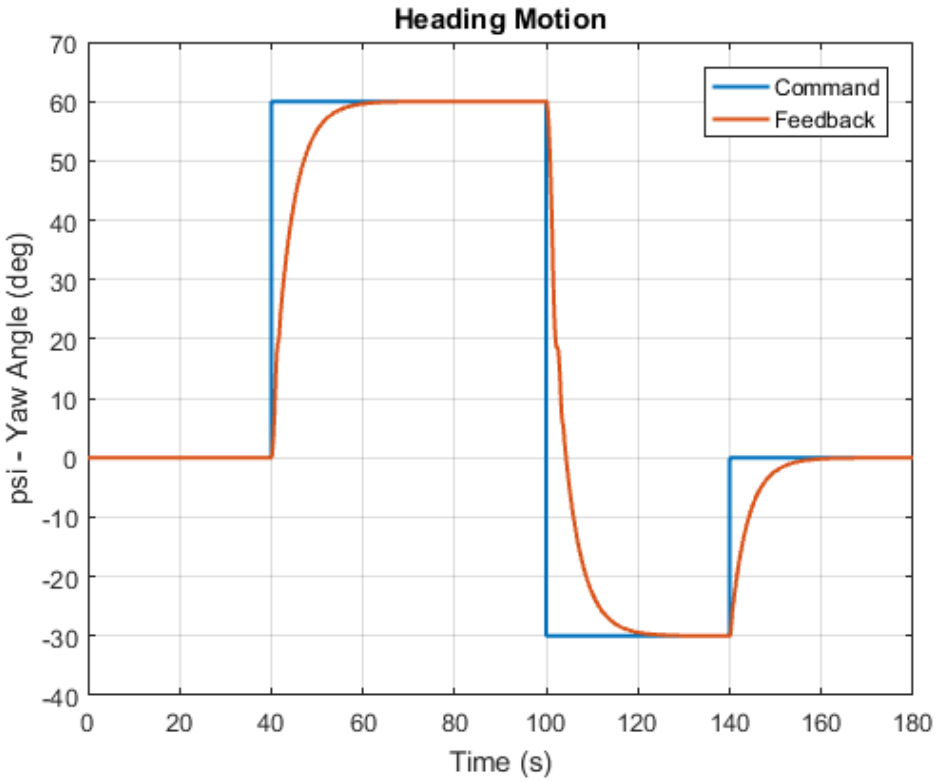

Figure 7.4 Heading angle response in 6-DOF simulation

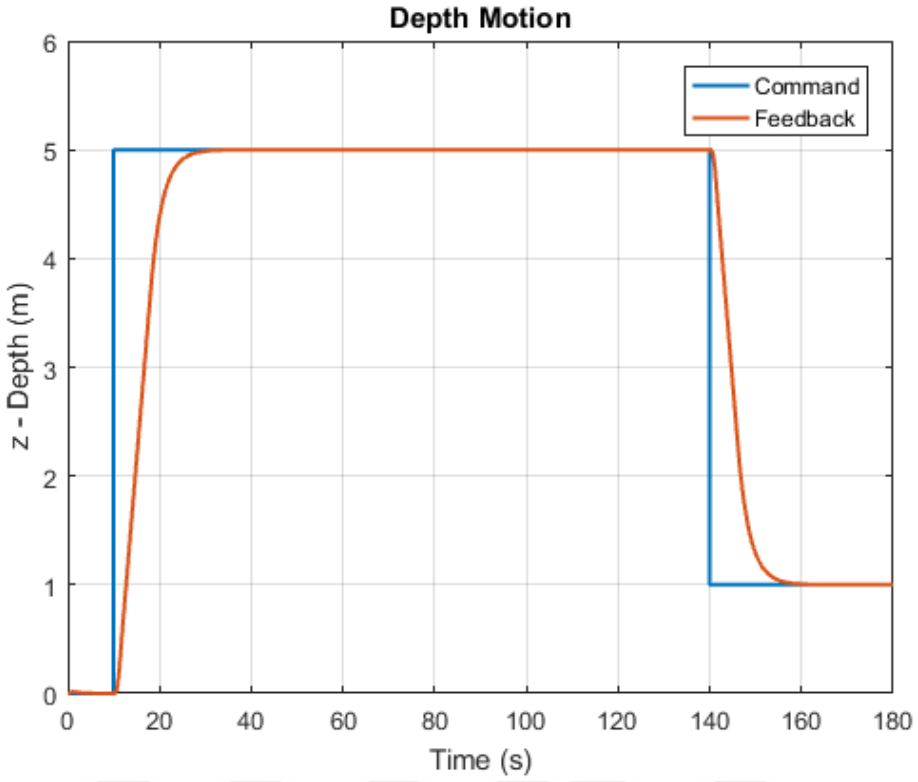

Figure 7.5 Depth position response in 6-DOF simulation

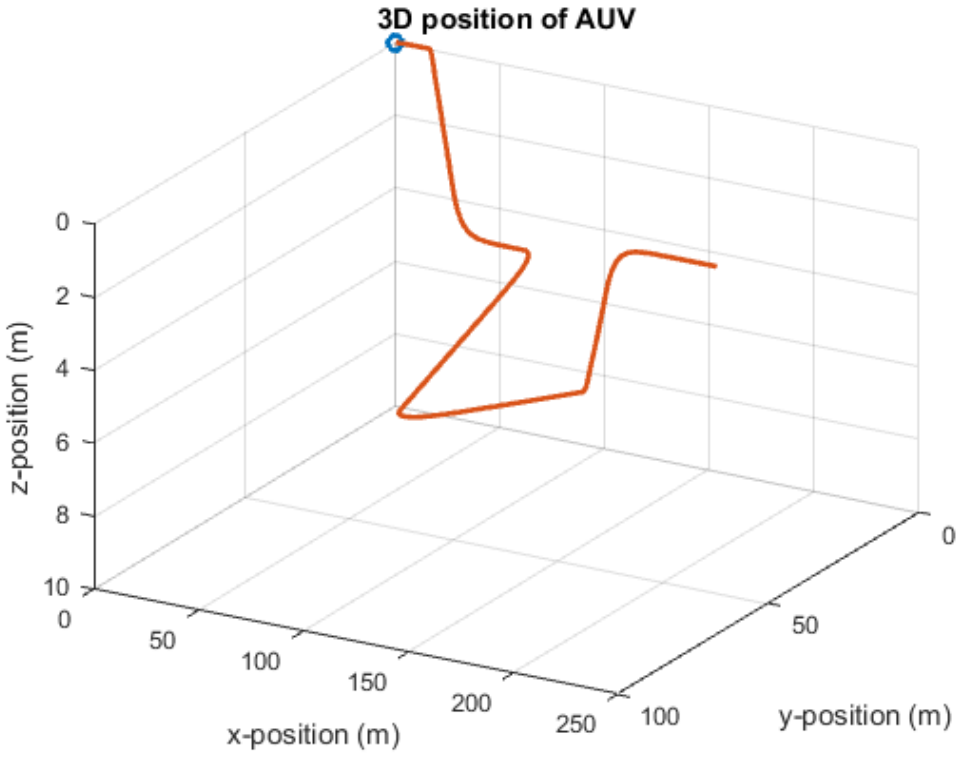

Figure 7.6 6-DOF motion of AUV

Initial conditions are set to the zero for all states in the simulation. Simulation results shows that the system has successfully reached the reference values in forward speed, roll position and velocity, depth position and heading angle. When the heading angle changes, the vehicle starts moving around *x-axis* and then the roll controller makes the roll position and velocity zero in a short time. These results also imply that the equation decoupling is an applicable method in order to design and implement separate controllers for AUVs.

CHAPTER 8

CONCLUSION AND FUTURE WORK

In this study, decoupled control design for dynamically modeled AUVs has been examined. The dynamic equations are decoupled in order to control speed, roll, depth and heading motion of the vehicle. Linear proportional control and feedback linearization methods are used to control the forward speed. The roll effect is not neglected here and backstepping method is applied to stabilize the roll motion. The depth of the vehicle is controlled using cascaded proportional and proportional-derivate control and nonlinear switched control. Single input multiple states (SIMS) sliding mode control and cascaded position and velocity controllers are designed to reach the desired heading angle. Simulation results obtained by MATLAB/Simulink environment have been reported in the corresponding sections. The simulation results show that designing independent controllers for decoupled systems gives successful results.

After designing decoupled controllers, the 6-DOF AUV model is simulated by applying the controllers simultaneously. The obtained results show that the vehicle can reach the desired values using decoupled controllers in forward speed, roll motion, depth position and heading angle. It is also verified that decoupling of equations is an applicable approach in order to design and analyze controllers for the 6-DOF AUVs.

Adaptive and intelligent controllers will be designed and implemented in the next study since the hydrodynamic coefficients are difficult to calculate and measure. State estimators will also be proposed in order to obtain unmeasured states of the vehicle and disturbances due to the subsea environment.

The output of this study is planned to be used in TORK system, an anti-torpedo torpedo system developed by ASELSAN Inc., Turkey.

REFERENCES

[1] Breivik, M. and Fossen, T.I., (2009). Guidance Laws for Autonomous Underwater Vehicles, First Edition, Norwegian University of Science and Technology, Norway.

[2] Ewart, T. E., (1976). "Observations from Straight Line Isobaric Runs of SPURV", Joint Oceanography Assembly, Edinburgh (UK).

[3] Ewart, T. E. and Bender, W. P., (1981). "An Observation of the Horizontal and Vertical Diffusion of a Passive Tracer in the Deep Ocean", Journal of Geophysical Research, 86(11):10,974-10,982.

[4] Michel, J. L. and Le Roux, H., (1981). "Epulard: Deep Bottom Surveys Now with Acoustic Remote Controlled Vehicle, First Operational Experience", OCEANS'81 MTS/IEEE, 16-18 September 1981, Boston, 99-103.

[5] Xu, O., (2004). Autonomous Underwater Vehicles (AUVs), Report, The University of Western Australia.

[6] Blidberg, D.R., (1997). The Development of Autonomous Underwater Vehicles (AUV), First Edition, Autonomous Undersea Systems Institute, Lee New Hampshire.

[7] Autonomous Undersea Vehicle Applications Center, General Information, 10 http://auvac.org/tools-resources/general-information, 10th April 2017.

[8] Geo Prose, Autonomous Underwater Vehicles, http://www.geo-prose.com/ALPS/white papers/alt.pdf, 15th April 2017.

[9] Bluefin Robotics, Autonomy and Behaviors, http://www.bluefinrobotics.com/technology/autonomy-and-behaviors/, 18th April 2017.

[10] NPS Center for AUV Research, Research on Autonomous Underwater Vehicles, http://www.cs.nps.navy.mil/research/auv/, 18th April 2017.

[11] Bellingham, J., Goudey, C., Consi, T. and Chryssostomidis, C., (1992). " A Small Long Range Autonomous Vehicle for Deep Ocean Exploration", 2nd International Offshore and Polar Engineering Conference, 14-19 June 1992, San Francisco, 148-155.

[12] Curtin, T. B., Bellingham, J. G., Catapovic, J. and Webb, D., (1993). "Autonomous Oceanographic Sampling Networks". Oceanographics, 6(3): 86 – 93.

[13] Von Alt, C., Allen, B., Austin, T. and Stokey, R., (1994). "Remote Environmental Measuring Units", IEEE AUV'94 Symposium on Autonomous Underwater Vehicle Technology, 19-20 July 1994, Massachusetts, 13-19.

[14] Nekton Research Ltd., AUVs Applications, http://www.nektonresearch.com/, 20th April 2017.

[15] Desa, E., Madhan, R. and Maurya, P., (2006). "Potential of Autonomous Underwater Vehicles as New Generation Ocean Data Platforms", Current Science, 90(9):1202-1209.

[16] Issac, M. T., Adams, S., He, M., Bose, N., Williams, C. D., Bachmayer, R. and Crees, T., (2007). "Manoeuvring Experiments Using the MUN Explorer AUV", Symposium on Underwater Technology and Workshop on Scientific Use of Submarine Cables and Related Technologies, 17-20 April 2007, Tokyo, 256-262.

[17] Healey, A. J., and Lienard, D., (1993). "Multivariable Sliding Mode Control for Autonomous Diving and Steering of Unmanned Underwater Vehicles", IEEE Journal of Oceanic Engineering, 18(3):327-339.

[18] Song, F. and Smith, S. M., (2000). "Automatic Design and Optimization of Fuzzy Logic Controllers for an Autonomous Underwater Vehicle", OCEANS 2000 MTS/IEEE Conference and Exhibition, 11-14 September 2000, Providence, 829-834.

[19] Fossen, T. I. and Fjellstad, O. E., (1995). "Robust Adaptive Control of Underwater Vehicles: A Comparative Study", IFAC Proceedings Volumes, 28(2):66-74.

[20] Gaskett, C., Wettergreen, D., and Zelinsky, A., (1999). "Autonomous Guidance and Control for an Underwater Robotic Vehicle", International Conference on Field and Service Robotics, 29-31 August 1999, Pittsburgh, 29-31.

[21] Fossen, T.I., (1994). Guidance and Control of Ocean Vehicles, First Edition, John Wiley & Sons, England.

[22] SNAME, (1950). The Society of Naval Architects and Marine Engineers. Nomenclature for Treating the Motion of a Submerged Body Through a Fluid, Technical and Research Bulletin, 1-5.

[23] Fossen, T.I., (2002). Marine Control Systems: Guidance, Navigation and Control of Ships, Rigs and Underwater Vehicles, First Edition, Marine Cybernetics AS, Trondheim.

[24] Fossen, T.I, (1991). Nonlinear Modeling and Control of Underwater Vehicles, Ph.D. Thesis, Department of Engineering Cybernetics, Norwegian University of Science and Technology, Trondheim, Norway.

[25] Prestero, T., (2001). Verification of a Six-Degree of Freedom Simulation Model for the REMUS Autonomous Underwater Vehicle, M.Sc. Thesis, Massachusetts Institute of Technology and Woods Hole Oceanographic Institution, Massachusetts.

[26] Tinker, S.J., (1982). "Identification of Submarine Dynamics From Free-Model Test", DRG Seminar on Advanced Hydrodynamic Testing Facilities, Netherlands.

[27] Salvesen, N., Tuck, E.O. and Faltinsen, O.M., (1970). “Ship Motions and Sea Loads”, Transactions of SNAME, 78:250–287.

[28] Silvestre, C. and Pascoal, A., (2001). “The Infante AUV Dynamic Model, Technical Report”, Dynamical Systems and Ocean Robotics Laboratory, Institute for Systems and Robotics, Lisbon, Portugal.

[29] Nise, N. S., (2011). Control System Engineering, Sixth Edition, John Wiley & Sons. Inc, New York.

[30] Slotine, J. J. E. and Li, W., (1991). Applied Nonlinear Control, First Edition, Prentice-Hall Englewood Cliffs.

[31] Ogata, K., (2009). Modern Control Engineering, Fifth Edition, Pearson, New Jersey.

[32] Silvestre, C. and Pascoal , A., (2004). “Control of the INFANTE AUV Using Gain Scheduled Static Output Feedback”, Control Engineering Practice, 12(12):1501–1509.

[33] Allen, B., Stokey, R., Austin, T., Forrester, N., Goldsborough, R., Purcell, M. and Von Alt, C., (1997). “REMUS: A Small, Low Cost AUV; System Description, Field Trials And Performance Results”, OCEANS '97 MTS/IEEE, 6-9 October 1997, Noca Scotia, 994-1000.

[34] Roberts, G. N. and Sutton, R. (2006). Advances in Unmanned Marine Vehicles, First Edition, IET Digital Library, England.

[35] Pan, L. X., Jin, H. Z., and Wang, L. L., (2011). “Robust Control Based On Feedback Linearization For Roll Stabilizing of Autonomous Underwater Vehicle Under Wave Disturbances”, China Ocean Engineering, 25(2):251-263.

[36] Roberts, G.N., (2008). “Trends In Marine Control Systems”, Annual Reviews In Control, 32(2):263-269.

[37] Krstic, M., Kanellakopoulos, I. and Kokotovic, P.V., (1995). Nonlinear and Adaptive Control Design, First Edition, Wiley, New York.

[38] Healey, A.J. and Lienard, D., (1993). “Multivariable Sliding Mode Control For Autonomous Diving and Steering of Unmanned Underwater Vehicles”, IEEE Journal of Ocean Engineering, 18(3):327–339.

[39] Pascoal, A., Oliveira, P., Silvestre, C., Bjerrum, A., Ishoy, A., Pignon, J. P. and Petzelt, C. (1997). “MARIUS: An Autonomous Underwater Vehicle For Coastal Oceanography”, IEEE Robotics & Automation Magazine, 4(4):46-59.

[40] Wang, J., Song, X., Zhao, Y. and Zhang, G. (2011). “Nonlinear Switched Diving Control for Under-actuated Autonomous Underwater Vehicles”, 29th IEEE Chinese Control Conference (CCC), 29-31 July 2010, Beijing, 705-710.

[41] Khalil, H. K. (2015). “Lyapunov’s Stability Theory”, Encyclopedia of Systems and Control, 685-690.

[42] Skogestad, S. and Postlethwaite, I., (2001). Multivariable Feedback Control: Analysis and Design, Second Edition, Wiley, New York.

[43] Kumar, R. P., Dasgupta, A., and Kumar, C. S., (2007). “Robust Trajectory Control of Underwater Vehicles Using Time Delay Control Law”, Ocean Engineering, 34(5):842-849.

[44] Yoerger, D., and Slotine, J., (1985). “Robust Trajectory Control of Underwater Vehicles”, IEEE Journal of Oceanic Engineering, 10(4):462-470.

[45] Ogata, K., (1995). Discrete-Time Control Systems, Second Edition, Prentice Hall, Englewood Cliffs.

[46] Kwatny, H., Bahar, L. and Pasrija, A., (1985). “Energy-like Lyapunov functions for power system stability analysis”, IEEE Transactions on Circuits and Systems, 32(11):1140-1149.

[47] Maciejowski, J. M., (1989). Multivariable Feedback Design, First Edition, Addison-Wesley, Wokingham.

[48] Shi, J., (2006). “Design of sliding mode autopilot with steady-state error elimination for autonomous underwater vehicles”, IEEE TENCON 2006, 14-17 November 2006, Hong Kong, 1-4.

[49] Rodrigues, L., Tavares, P., and de Sousa Prado, M.G. (1996). “Sliding mode control of an AUV in the diving and steering planes”, OCEANS'96 MTS/IEEE, 23-26 September 1996, Florida, 576-583.

[50] Matlab, M. (2008). Simulink. MathWorks Inc., Version, 7(0).

CURRICULUM VITAE

PERSONAL INFORMATION

Name Surname : Alper YALMAN

Date of birth and place : 26.08.1991, Şahinbey

Foreign Languages : English

E-mail : alperyalman@gmail.com

EDUCATION

Degree	**Department**	**University**	**Date of Graduation**
Undergraduate	Mechatronics Eng.	Yildiz Technical University	27.06.2014
High School	Science and Math	Yavuz Selim High School	12.06.2009

WORK EXPERIENCE

Year	**Corporation/Institute**	**Enrollment**
2015-Present	ASELSAN Inc.	Defense Systems Engineer
2015-2015	BSH Home Appliances Inc.	R&D Project Student
2013-2014	Mercedes-Benz Türk Inc.	PEP Intern
2013-2013	Turkish Technic Inc.	Intern
2012-2012	Petes Machinery Inc.	Intern

PUBLICATIONS

Conference Papers

1. Yalman, A. and Yeşildirek, A., (2017). "Decoupled Nonlinear Control Design and Simulation of Torpedo Shaped Autonomous Underwater Vehicles (AUVs)", ICETAS 2nd International Conference on Engineering Technology and Applied Sciences, 20-21 April 2017, Baia Mare, 32-37.

2. Songül, G., Yalman, A., Ilginoğlu, A., Gökçe, A., Koçulu, Ö. E. C., Kırlı, A. and Tüfekçi, C. S., (2015). "Model Picosatellite Design for Energy Harvesting and Telemetry Data Transmission through RF Communication", IEEE 7th International Conference on Recent Advances in Space Technologies (RAST), 16-19 June 2015, İstanbul, 839-844.

Projects

1. CANSAT Model Satellite Design, Embedded Software – Ground Station Software CANSAT Competition 2015, Texas, USA

2. Design/Implementation of A Micro-Robotic Arm and Non-Contact Manipulation with Visual Servoing (June 2014 – March 2015)

3. Mobile Alcoholmeter, Undergraduate Thesis Supported by TUBITAK 2241-A Industry-Focused Thesis Program

4. CANSAT Model Satellite Design, Mechanics - Electronics - Embedded Software, CANSAT Competition 2014, Texas, USA